Behavior and Control of Mercury in Sewage Sludge Thermal Treatment Process

2020

CHENG YINGCHAO

Behavior and Control of Mercury in Sewage Sludge Thermal Treatment Process

（下水汚泥熱処理プロセスにおける水銀の挙動と排出制御）

2020

CHENG YINGCHAO

ACKNOWLEDGMENTS

I would like to express my deepest appreciation to my supervisor, Prof. Masaki Takaoka, for his guidance, patience and profound belief in my abilities. Ever since my internship at Kyoto University in 2014, I was inspired by Prof. Takaoka and decided to do my Ph.D. with him. After a whole year of Japanese language training and another half-year of being a research student, I finally made my way to be a Ph.D. student of him. However, thinking about the nice discussions with my supervisor and the support I got from him, it was all worth it. I am and will always be proud of my decision upon this journey, and I could not be more grateful to my supervisor for all his help.

I would also like to thank Prof. Kazuyuki Oshita, who always helped and nurtured me during my research. His kind support meant a lot to me, not only for my studies but also for my life.

Special thanks go to lab technician Kenji Shiota. Without him, most of my experiments never would have been possible. I am grateful for his help with utilizing software, advice on data analysis and constructive suggestions for my papers. Even though I leave here, all the skills and good habits he imparted upon me will last for sure.

I am also so grateful to Dr. Sylwia Oleszek for her patience and guidance in revising my paper. Her enthusiasm for research impressed me deeply and inspired me a lot, and it was a great pleasure for me to work with her.

Many thanks to Associate Professors Takashi Fujimori and Taketoshi Kusakabe for their help with my research. Thanks to Mrs. Yamamoto for her kindness in helping me with many procedures.

I very much appreciate the support from the Chief Director, Mr. Akito Matsuyama, and all staff at the National Institute for Minamata Disease during my internship there.

Thanks should also go to Dr. Mengmei Zhang, who inspired and encouraged me a lot in my research, and all young students in our lab for their friendliness and teaching me an

interesting Japanese dialect. I enjoyed the time we spent together and will treasure all those sweet memories I share with all of you.

I also want to thank my family and friends in China for their support and patience.

This work was supported by JSPS KAKENHI Grant Number JP 17H03335. A part of my experiments was conducted in cooperation with Takuma Co. Ltd. and Tsukishima Kikai Co. Ltd. Also, I very much appreciate the support from WWTP A and B in local governments. XAFS analyses at BL01B1 in SPring-8 were conducted with the approval of the Japan Synchrotron Radiation Research Institute (JASRI) (proposal No. 2018A1508), with much help from Dr. Kiyofumi Nitta. Finally, a part of this research was funded by the Environment Research and Technology Development Fund of Japan, grant number (3-1701).

Last but not least, I would like to thank the MEXT scholarship from the Japanese government for financial support.

ABSTRACT

Behavior and Control of Mercury in Sewage Sludge Thermal Treatment Process

Sewage sludge is the inevitable byproduct generated in the wastewater water treatment process. In recent decades worldwide, the amount of SS is dramatically increasing. In order to treat the large amount of SS, a thermal method such as incineration is widely used in densely populated regions like Japan for its advantages in terms of volume reduction, which facilities the smallest space occupation at the landfill. Another thermal process, carbonization, is also a promising method for SS treatment in terms of the recycling of the embedded energy in SS. However, both of these two methods pose the potential risk of Hg emission to the atmosphere. Since the Minamata Convention on Mercury entered into force on August 16, 2017, mercury emission from sewage sludge thermal treatment process is drawing more attention. Therefore, the objectives of this dissertation are: (1) to investigate the Hg emission behavior in SS thermal treatment process; (2) to develop high-performance Hg removal sorbents and clarify the adsorption mechanisms by prepared sorbents.

Firstly, a comprehensive study on the distribution and mass balance of heavy metals in SS mono-incineration was conducted. Different enrichment behavior of semi-volatile elements was found in the incinerated sewage sludge ash (ISSA) between the step grate stoker (GS) and fluidized bed incinerators (F-types). The distinct ash removal procedure in GS and F-types was considered the main reason for this different enrichment behavior. By discharging the bottom ash at a high temperature of 850 ºC at the bottom of the incinerator, GS discharges the main ash with lower concentrations of heavy metals under the regulation of fertilizer production. F-types, however, generates only fly ash at a lower temperature of 250 ºC and almost entirely enriched heavy metals from the SS. Thermodynamic calculations indicate a shift of the dominant phase from the gas to the solid, with the temperature decreasing from 850 to 250 ºC, which compares well with the distinct

enrichment behavior between GS and F-types we found. To conclude, GS has an advantage over F-types in terms of the recycling of the ISSA for fertilizer production.

In all studied incinerators, wastewaters, especially from WS, are the main sink for soluble elements, including Hg. Nevertheless, from the flue gas, only Hg was found to be significantly emitted in all studied incinerators. Since the Hg emission is reported to be associated with species of Hg in the flue gas, speciation Hg continuous emission monitoring was further carried out in both GS and F-types. Another fluidized bed incinerator and a carbonization furnace were also monitored. Results show that, in SS incinerators, the dominant species of Hg in the flue gas was Hg^{2+} before the WS, but the Hg^0 showed higher fraction after being treated at the WS. Different from the incinerators, Hg^0 was always the dominant species both before and after the WS in the carbonization furnace. These tendencies are consistent with the thermodynamic calculations. Therefore, WS can effectively remove the Hg^{2+}, but Hg^0 significantly escaped, and the removal of Hg^0 should be further studied.

During the continuous monitoring at the carbonization furnace, Hg removal experiments were also conducted on the spot. Two sorbent towers, one uses modified activated carbon (MAC) and the other uses the composite polymer, were set in front of the stack in parallel. Both these two kinds of sorbents showed excellent Hg (dominantly Hg^0) removal performance, with the MAC of higher removal efficiencies, although more obstacles in operation.

Since the MAC has proved feasible for Hg^0 removal, a further study on AC modification for Hg^0 removal was conducted through iodine impregnation. By utilizing different measurement methods, including Brunauer-Emmett-Teller (BET) specific surface area analysis, X-ray diffraction (XRD), X-ray photoelectron spectroscopy (XPS), and X-ray absorption near-edge structure analysis (XANES), we confirmed the texture

characteristics of the ACs, as well as the species and chemical state of the compounds impregnated in and adsorbed on the ACs. Based on these experimental results, putative pathways for Hg^0 removal by the prepared ACs were proposed and evaluated according to the Gibbs free energy value.

All sorbents showed excellent removal efficiencies of Hg^0 as 97.2–99.9%. The XANES results showed no metal Hg^0 in all sorbents, including the virgin AC, indicating that the chemisorption dominant in the Hg^0 removal by the prepared ACs. Despite the different precursors used in the impregnation, the main form of Hg^0 adsorbed in the iodine impregnated ACs was HgI_2. The large BET surface area and oxygen functional groups promoted the adsorption, whereas the chemical composition, especially the existence of Cl, S, and I, were essential factors responsible for the high Hg^0 removal efficiencies. Molecular I_2 was identified in ACs impregnated with NH_4I, KIO_3, and a co-impregnation of KI followed by $CuSO_4$, and $Hg + I_2 = HgI_2$ is considered to be the primary mechanism for Hg^0 adsorption by the impregnated ACs. Moreover, I_3^- was also detected in all impregnated ACs and possibly contributed to the adsorption by serving as the I_2 donor.

CONTENTS

LIST OF ABBREVIATIONS

AC	Activated carbon
APCDs	Air pollution control devices
BET	Brunauer-Emmett-Teller
CEM	Continuous emission monitors
E_f	Enrichment factor
ESPs	Electrostatic precipitators
FBC	Fluidized bed
FF	Fabric filter
FGD	Flue gas desulfurization
F-type	Fluidized bed incinerators
GS	Step grate stoker
HTC	hydrothermal carbonization
ISSA	Incinerated sewage sludge ash
LOQ	Limit of quantification
MAC	Modified activated carbon
MeHg	Methylmercury
MHF	Multiple hearth furnace
MSW	Municipal solid waste
SCR	Selective catalytic reduction
SS	Sewage sludge
THg	Total mercury
TS	Total solids content
VTS	Volatile total solids content
WAS	Waste activated sludge
WS	Wet scrubbers
WWTPs	Wastewater treatment plants
XANES	X-ray absorption near edge structure
XPS	X-ray photoelectron spectroscopy
XRD	X-ray diffraction

Chapter 1 General introduction

With the small land area available for sewage sludge disposal, thermal treatment is most widely used in Japan due to its advantage in minimizing the volume of sewage sludge. However, heavy metals are of great concern for the thermal treatment process. Because the Minamata Convention on Mercury entered into force on August 16, 2017, mercury emission from sewage sludge thermal treatment process is drawing attention. In this chapter, firstly, the sewage sludge generation and thermal treatments are introduced, and then mercury removal technologies are also reviewed. Finally, I show the research objectives and research structure in my dissertation.

1.1 Sewage sludge generation

Sewage sludge (SS) is the inevitable byproduct generated in the wastewater treatment process (Chen et al., 2012). It contains inorganic material, plant nutrients, heavy metals, organic micro-pollutants, and pathogens (Epstein, 2002; Christodoulou and Stamatelatou, 2016). With the increase of the global population and the proceeding of the urban and modernization expansion, the waste generation also shows a rapid increase in recent decades worldwide (Manzetti and Spoel, 2015), amongst the amount of sewage sludge is also dramatically increasing (Albero et al., 2012; Hong et al., 2009). In Japan, more than 2 million tons of dry sewage sludge is produced annually (**Fig. 1-1**)(MLIT).

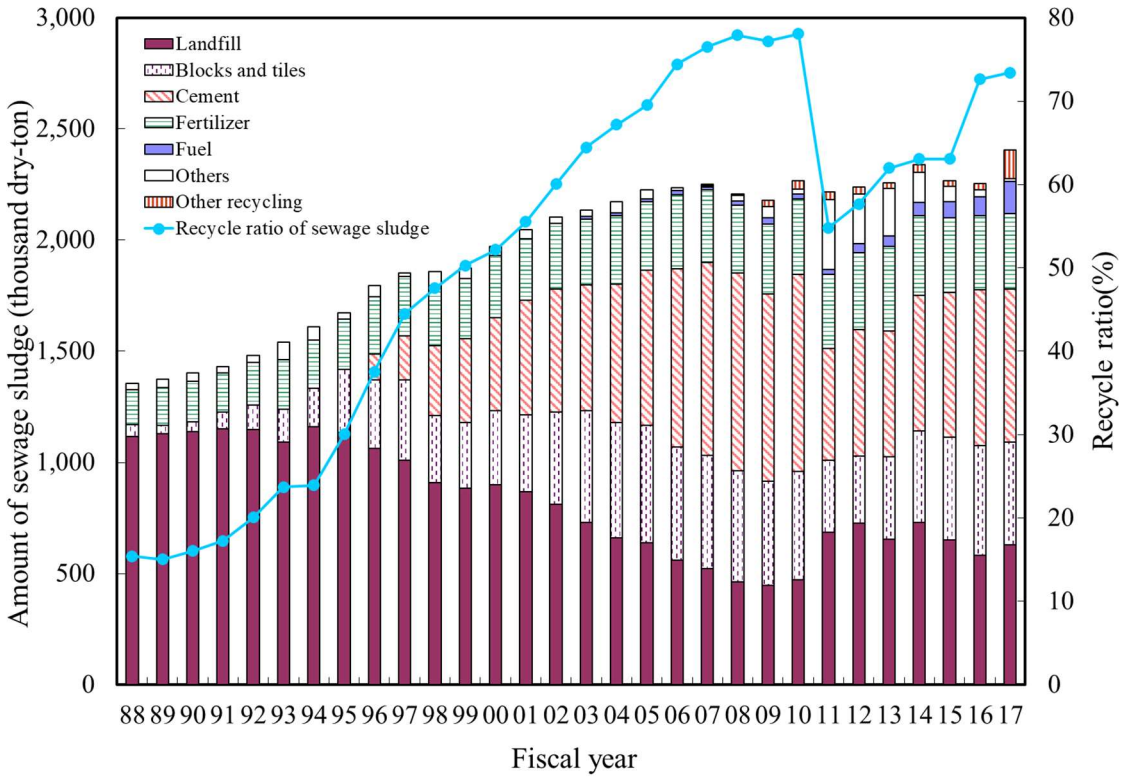

Figure 1-1. Annual sewage sludge production and its management in Japan (MLIT, 2020)

1.2 Sewage sludge disposal

The treatment and disposal of sewage sludge have long been a concern worldwide (Xu et al., 2014), and sludge disposal still represents up to 50% of the managing costs in a WWTP (Bolzonella et al., 2007). Landfill, land application, and incineration are principal disposal methods for SS (Chen et al., 2012). None of these end-used are fundamentally either good or bad; each one is more or less appropriate for a given situation (Campbell, 2000).

1.2.1 Landfill

The landfill method usually mixes the concentrated sludge with solid waste in municipal landfills (O'kelly, 2005). This method is commonly adopted worldwide, especially in developing countries such as China (Chen et al., 2012), due to its low cost.

Sludge handling and landfill construction are most favorable within the water content range of 85~95% water content (O'kelly, 2005). Sewage sludge in a slurry state would increase the construction difficulties of the landfill site and lead to the instability of the landfill slopes, and it is sometimes refused by the landfill operators (O'kelly, 2005). In recent years, due to the stricter waste disposal legislation and economic capacity, the landfill is decreasing worldwide (Chen et al., 2012; O'kelly, 2005). For example, the sewage sludge landfilling is prohibited since 2016 in Poland (Przydatek and Katarzyna, 2020). Moreover, the odor and sanitary problem also make the landfilling of the dewatered sludge less favorable due to the opposition of citizens.

1.2.2 Land application

Since the SS contains considerable amounts of nutrient elements such as N and P, it is often used as the soil amendation materials directly or after the composting, as widely used in the US and some EU countries (Atmospheres, 2016; Cieślik et al., 2015; Lu et al., 2012). At present, 53% of sewage sludge produced in the EU-15 is reused in agricultural application, while 21% is incinerated (Kelessidis and Stasinakis, 2012). Land application of SS can benefit the soil improvement and re-establish vegetation and restoration of degraded ecosystems. However, due to its relatively low N : P ratio (about 3.1-3.4) (Shepherd and Withers, 2001), the application of SS can also result in the build-up of P in soil and subsequent P release into the surface or subsurface waters leading to the eutrophication (Sharpley et al., 1998). Further, even at a low concentration, the accumulation by years of the SS land application may still pose a potential risk in animals and human health (Lu et al., 2012). Besides, similar to the landfill, the land application also has the problem of odors, and this may induce the oppose from the citizens for the land application (Lu et al., 2012).

1.2.3 Incineration

Incineration is an exothermic oxidation process of SS, resulting in the flue gas comprising of CO_2 and H_2O, ash, and a certain amount of heat (Raheem et al., 2018). It can significantly reduce the volume of SS; therefore, it is primarily executed in densely populated regions like Japan for the low land availability (Bolzonella et al., 2007; Cieślik et al., 2015; Takaoka et al., 2012). The heat generated in the incineration process can be recovered to produce steam, which can subsequently be converted into power via steam turbines (Raheem et al., 2018; Tyagi and Lo, 2013). The incinerated sewage sludge ash (ISSA) generated during the combustion can be disposed into the landfills or be utilized for building material production (Wu et al., 2016). Because of the nutrients contained, the ISSA can also be used for the improvement of the arable land for food production (Mailler et al., 2014; Peccia and Westerhoff, 2015). With the consideration of the heavy metals enriched together with the P during the incineration and the low P plant-accessibility, the direct use of the ISSA for agriculture is sometimes not favorable. However, even not suitable for direct land use, the ISSA can still be treated as a potential source of P-fertilizer for agricultural systems with the high content of P (Krüger et al., 2014; Ottosen et al., 2013).

Compared with other disposal methods, incineration has the best volume reduction and pathogen decomposition effect, but the highest cost at the same time (Lundin et al., 2004). The high costs are mainly associated with the drying process, in which the SS is dried to a solid content of 18~35% (Donatello and Cheeseman, 2013). Whenever appropriately designed, this process does not have to generate high additional costs (Winkler et al., 2013). For example, the bio drying and the recycling of the heat generated in the incineration process for SS drying can reduce the cost to a great extent. Therefore, incineration is the primary SS treatment and disposal method in Japan (MLIT).

1.2.4 Recycling

As mentioned above, the SS can be recycled directly for the land application. However, Spreading sludge on agricultural land was the least preferable option from an environmental point of view (Lundin et al., 2004). The land application only solves part of the problem, because with the metals and persistent organic pollutants remain in the sludges, which can induce the release of nutrients and acidifying substances and transfer the content of heavy metals in the sludge to agricultural soil (Lundin et al., 2004; Peccia and Westerhoff, 2015). Besides, energy is required for transportation, spreading, and pasteurization of the sludge, which makes this process economically unfavorable. Moreover, because of new legislation, the disposal of biosolids is difficult since land application and landfilling are becoming almost forbidden (Bolzonella et al., 2007).

On the other hand, the recycling of the ISSA has been receiving considerable attention worldwide. The recovery of high-value metals, as Westerhoff et al. (2015) suggested, e.g., Al, Ca, Fe, Mg, Mn, Cu, Cr, and Ni, could be an economic and environmental win-win scenario (Peccia and Westerhoff, 2015). Besides this, the ISSA can also be recycled as an adsorbent for lead (Wang et al., 2019), cement mortars (J. S. Li et al., 2017), and other construction materials (Chen et al., 2018; Lynn et al., 2015; Smol et al., 2015).

1.3 Sewage sludge incineration

Since incineration can minimize the volume of sewage sludge, decompose organic pollutants, and induce almost no odor problem, it is widely used, especially in countries with the limited land area available for sewage sludge disposal, such as in Japan. Sewage sludge is usually co-combusted with other fuels or mono-combusted, depending on its calorific properties and the incineration technologies.

1.3.1 Co-combustion

Sewage sludge co-combustion with coal, municipal solid waste, wood, and other biomass are applied worldwide (**Table 1-1**). Co-combustion utilizes the existing power plants or wastes treatment facilities; hence it can save the investment for construction. Meanwhile, the co-combusted fuels benefit the energy budget and make the incineration possible for sludge that cannot be self-sustaining combusted due to the low volatiles content and low heating value (Chen et al., 2017). However, a co-combustion of sludge with other fuels may induce problems with SCR systems (Selective Catalytic Reduction) (Cieślik and Konieczka, 2017) and is not favorable for the recycling of ISSA, such as fertilizer production, due to the dilution effect of co-combusted fuels (Peccia and Westerhoff, 2015).

1.3.2 Monocombustion

Monocombustion, on the other hand, can recover the embedded energy in sludge meanwhile reduce the greenhouse gas emission effectively (Liu et al., 2013), and the generated ISSA can be recycled as construction materials or fertilizer, as is implemented in Japan (MAFF). It is also widely used in Germany (Krüger and Adam, 2014), Switzerland (Meier et al., 2016), and other European countries (Donatello and Cheeseman, 2013).

At present, the mono-combustion of sewage sludge is considered as one of the best options because it facilitates the recovery of valuable resources, such as phosphorus (essential plant nutrient with limited availability), from the ash (Escala et al., 2013). Therefore, most of the sewage sludge in Japan is mono-incinerated.

1.3.3 Sewage sludge mono-incinerators

In the last century, the dominant mono-combustion furnaces for sewage sludge were the fluidized bed (FBC) and multiple hearth (MHF) furnaces, although others, e.g., rotary

kiln, cyclone and different types of smelting furnaces were also used (Werther and Ogada, 1999). In recent years, the utilization of FBC and step grate stokers have gained a significant increase.

Fluidized bed incinerator

Fluidized bed technology has been used since 1922; since then, it has received extensive applications (Werther and Ogada, 1999). FBC technology usually uses sand as bed material. Excess amount of air (25~50%) is supplied to the FBC from the bottom of the furnace. The air agitates the bed material into the fluidized state. Thus, the bed material also acts as the agitator resulting in high turbulence inside the incinerator, which enables a stable temperature inside the furnace (Mullen, J.F., 1992). During the combustion, the furnace can be divided into three different sections in the vertical direction. From the bottom to the top, it is the fluidized-bed, the primary combustion chamber, and the secondary combustion chamber, respectively. After combustion, the flue gas is treated at the following APCDs and particles entrained in the flue gas are collected as fly ash. Depending on the concentrations of heavy metals, the disposal of this ISSA goes to the landfill, land application, or cement production. Gaseous pollutants are washed and removed in the wastewater from the APCDs and sent back to the wastewater treatment process.

FBC technology is more popular than the step grate stoker in the SS mono-incineration (**Table 1-1**). Usually, auxiliary fuels are used in this type of incinerator. Thus, the dewatered SS can be combusted without further drying. And some improvements have been made to achieve a higher combustion efficiency (**Fig. 1-2**).

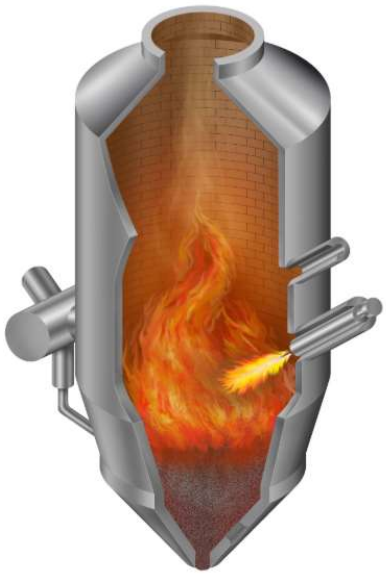

Figure 1-2. Fluidized bed incinerator, Tsukishima Kankyo Engineering Ltd.

Figure 1-2 shows the latest fluidized-bed incineration system developed by the Tsukishima Kankyo Engineering Ltd, Japan. This system can improve combustion efficiency with the air from the bottom of the furnace and leave little unburned materials.

Step grate stoker

Step grate stoker consists of a series of stepped fire grates. By moving back and forth the grates, the SS inside the furnace contacts efficiently with the air. **Figure 1-3** shows the structure of a step grate stoker developed by TAKUMA Co. Ltd., Japan. Compared with the fluidized bed type, the step grate stoker has lower electricity consumption (60% of the fluidized bed), lower N_2O emission, feasible for waste heat recovery by the boiler, and needs no auxiliary fuel.

Step grate stoker is most widely used in the municipal solid waste (MSW) incineration due to its low cost and simple pretreatment needed before the combustion. It is also applicable for the SS incineration and used in Japan. An unfavorable aspect for the step grate stoker is the concern of dioxins generation caused by a lower temperature than 850 ℃

when starting the furnace. Moreover, mechanical agitation also limits the temperature inside the furnace. Besides, MSW, especially household food, often contains high salt, and some plastics also contain Cl, for which studies reveal that the generation of PCDD/Fs is closely related to the Cl content of the fuel (Zhang et al., 2013). Air pollution control devices (**APCDs**) are therefore utilized to remove toxic pollutants such as PCDD/Fs and make the step grate stoker feasible for MSW incineration.

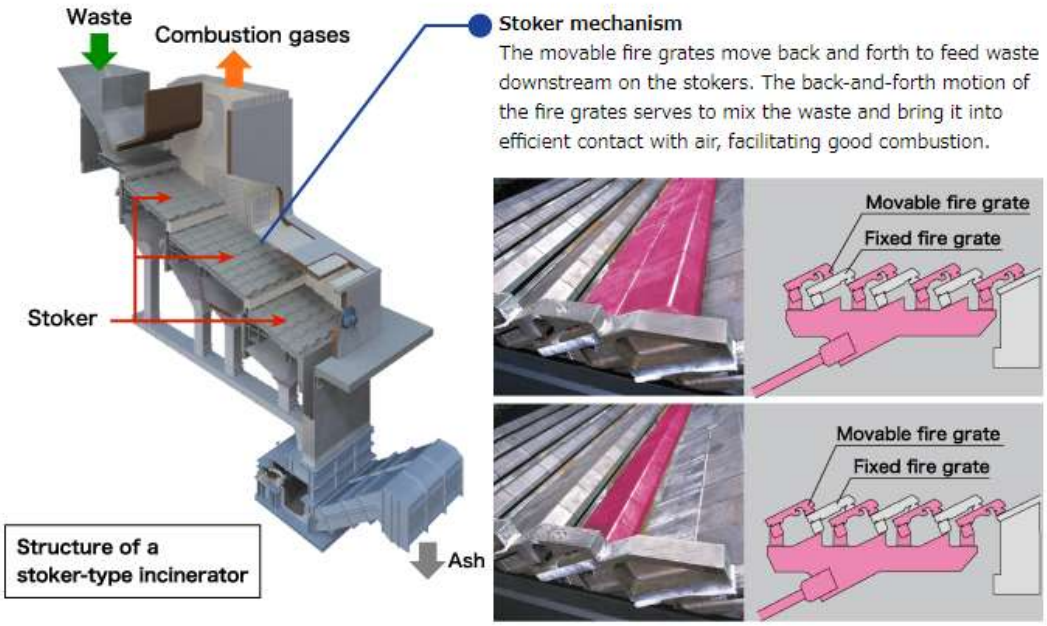

Figure 1-3. Step grate stoker. TAKUMA Co. Ltd., Japan.

The application of the step grate stoker for SS incineration is favorable because the composition of SS is more simple and stable compared with the MSW. With a lower Cl content, the risk of PCDD/Fs generation for SS is also lower than the MSW. Moreover, the APCDs can remove most pollutants such as particles and some heavy metals. Then, the stoker discharges ashes mainly from the bottom as the bottom ash, and fine particles are collected at the APCDs as the dust, which is also classified as fly ash.

Table 1-1. Literature survey of sewage sludge incineration.

Incinerator type	Mono-/co-combustion	Feed	Temperature	Scale	Target elements	Country	Reference
multiple-hearth, fluidized bed	mono-	SS	700~930 ℃	–	As, Cd, Pb, Hg, Ni and Zn	USA	(Gerstle and Albrinck, 1982)
multiple hearths	mono-	SS		full-scale plant	Hg	USA	(Balogh, S. and Liang, L., 1995)
fluidized bed	mono-	SS		pilot	Cd, Cr, Mn, Ni, Pb, and Zn	Italy	(Marani et al., 2003)
fluidized bed	mono-	SS		full-scale plant	Hg	USA	(Balogh and Nollet, 2008)
fluidized bed	mono-	Urban + industrial sludge		full-scale plant	As, Cd, Cu, Pb, Cr, Hg, Ni, and Zn	Belgium	(Van de Velden et al., 2008)
melting chamber	mono-	SS		pilot	Na, Zn, K, Mg, P, Pb, Cu and As	China, Japan	(Han et al., 2008)
tubular-furnace reactor	mono-	SS	500~1100 ℃	laboratory	Cd, Pb, Cr, Cu, Zn, Mn and Ni	China	(Chen and Yan, 2012)
fluidized bed	mono-	SS		full-scale plant	Hg	Japan	(Takaoka et al., 2012)
fluidized bed	mono-	SS	900 ℃	full-scale plant	As, Cd, Cr, Ni, Pb, and Hg	Korea	(Pudasainee et al., 2013)
fluidized bed	mono-	SS (dried)	950 ℃	full-scale plant	32 elements (Al, Ag, As, Ba, Be, Br, Ca, Cd, Cl, Co, Cr, Cu, Fe, Hg, K, Li, Mg, Mn, Mo, N, Na, Ni, P, Pb, S, Sb, Se, Sn, Sr, Ti, V, Zn)	Denmark	(Yoshida et al., 2015)

SS: sewage sludge; mono-: mono-combustion; co-: co-combustion

Table 1-1. Literature review for sewage sludge incineration. (continued)

Incinerator type	Mono-/co-combustion	Feed	Temperature	Scale	Target elements	Country	Reference
tubular-furnace reactor	mono-	SS		laboratory	Pb, Zn, Cr, Cu, Mn and Ni	China	(Liu et al., 2015)
circulating fluidized bed	mono-	SS (dried)		laboratory	–	China	(Zhu et al., 2015)
fluidized bed	mono-	SS		Pilot/bench	Ag nanoparticles	Switzerland, France	(Meier et al., 2016)
fluidized bed	mono-	SS	850 ℃	full-scale plant	Cu, Zn, As, Pb, Ni, and Se	China	(J. shan Li et al., 2017)
circulating fluidized bed	mono-	Household + industrial sludge (1:1)		full-scale plant	Zn, Cu, Cr, Pb, Ni, Ba, Mn, and As	China	(Y. Li et al., 2017)
cylindrical down fired furnace	co-	SS (dry)+bituminous coal		500 kW	Cr, Hg, Mn, Ni, Pb and Zn	Germany, Denmark	(Cenni et al., 1999)
stoker-fired boiler	co-	SS + coal		laboratory	SO_2, NO_x, CO and dust	Poland	(Nadziakiewicz and Kozioł, 2003)
fluidized bed	co-	SS + coal		pilot	As, Cd, Co, Cu, Cr, Hg, Mn, Ni, Pb and Zn	Portugal	(Lopes et al., 2003)
circulating fluidized bed	co-	SS + coal/wood		12 MW_{th}	Hg, Pb, Cd, Cr, Cu, Ni, Mn, Co, As, Sb, V, and Zn	Sweden	(Åmand and Leckner, 2004)
circulating fluidized bed	co-	SS + wood		laboratory	As, Cd, Co, Cr, Cu, Hg, Mn, Ni, Pb, Se, Sb, Tl, V and Zn	Sweden	(Elled et al., 2007)

SS: sewage sludge; mono-: mono-combustion; co-: co-combustion.

Table 1-1. Literature review for sewage sludge incineration. (continued)

Incinerator type	Mono-/co-combustion	Feed	Temperature	Scale	Target elements	Country	Reference
grate furnace	co-	chemical and sewage sludge (3% mass substitution rate) +MSW		full-scale WTE plant	Cr(total), Pb, Ni, Zn, Hg, As, Cd, Cu, Se, soluble Cu and Cr(VI)	Italy	(Biganzoli et al., 2012)
fluidized bed	co-	SS + coal		pilot	Cd, Cr, Cu, Co, Mn, Ni, Pb, Zn, and Hg	Portugal	(Gulyurtlu et al., 2006)
power plants	co-	SS (5%, 10%, 15%, 20%) + coal		pulverized coal power plant	PCDD/Fs and Hg, Cd, Pb, Cr, and Cu	China	(Zhang et al., 2013)
grate boiler	co-	SS + wood sawdust (pelletized fuel)		PF 2000 Kg/h	Pb, Zn, Cu, Cr, Cd, As and Ni	China	(Xiao et al., 2015)
drop tube combustion system	co-	coal + SS (dried) (coal : sludge= 3:1 or 5:1)		laboratory	Hg (unburned carbon, Cl, Cu, and Fe)	Korea, USA	(Lee and Wilcox, 2017)
bubbling fluidized bed	co-	SS + cotton stalk	900 ± 5 ℃	5 kW	As	China	(Zhao et al., 2017)
cement kiln	co-	SS (25%)+raw meal	950~1450 ℃	–	Cu, Ni, Pb, and Zn	China	(Yu et al., 2017)
coal-fired boiler	co-	SS + coal		–	–	China	(Chen et al., 2017)
tubular-furnace reactor	co-	municipal/coal-coking industrial sludge (10~50%)+bituminous coal		laboratory	Cd, Zn, Cr, Ni, Pb, Zn and gas pollutants	China	(Zhao et al., 2019)

SS: sewage sludge; mono-: mono-combustion; co-: co-combustion.

1.4 Sewage sludge carbonization

In recent years, carbonization has attracted extensive attention as a promising SS handling method. Carbonization transforms SS into a carbon-containing product as bio-coal (Sang W. Park and Jang, 2011; Sang Woo Park and Jang, 2011), which is considered as a storable energy carrier (Axelsson et al., 2012; Titirici et al., 2007). With the characteristics of brown coal, the bio-coal can be co-fired with fossil coal to generate electricity in power plants (Sang W. Park and Jang, 2011; Sang Woo Park and Jang, 2011).

Sewage sludge carbonization mainly includes conventional carbonization, hydrothermal carbonization (HTC) and torrefaction. Conventional carbonization is often carried out in an inert atmosphere at temperatures of 277~677 ℃ (Maschio, G., Koufopanos, C., Lucchesi, 1992). Torrefaction also heat the biomass in an inert or nitrogen atmosphere, but at a lower temperature of 200~300 ℃ than conventional carbonization (Prins et al., 2006). HTC is defined as a thermochemical process used to convert organic feedstock into a carbonaceous product (hydrochar) in the presence of water under moderate temperatures (180~350 °C) and pressures (2~10 MPa) (Mumme et al., 2011). During HTC, two distinct phases, i.e., solid and liquid, are formed (He et al., 2013). The evolved gas is small and mainly consists of carbon dioxide (Berge et al., 2011).

During SS carbonization, the heavy metals in the SS may distribute into the biochar, flue gas, or wastewater from the APCDs. Amongst, Hg emission is of great concern because of its high toxicity. However, to date, no report is available about the behavior of Hg in SS carbonization process.

1.5 Gaseous Hg removal technology

1.5.1 Hg emission inventory

Ever since 1956, the breakout of the Minamata disease, mercury has attracted

extensive attention all over the world. Mercury, as a dangerous toxin that harms human health and the environment, it can be emitted to the atmosphere from natural and anthropogenic sources and then transported globally in the atmosphere and impacts areas far away from the source (Pacyna et al., 2010). The global mercury assessment revealed that human activities had increased total atmospheric mercury concentrations by about 450% above natural levels (Global mercury assessment, 2018). Amongst, the majority of emissions occurred in Asia (49%), of which 39% in East and South-east Asia.

Worldwide, the predominant source sector is artisanal and small-scale gold mining (~38%), while the stationary combustion of other fuels, including biomass, accounts for 3% of the anthropogenic mercury emission to air. In Japan, however, waste incineration is the primary source for mercury emission, as shown in **Figure 1-4 (**Ministry of the Environment, 2018). Since the Minamata Convention on mercury (UN environment programme) entered into force on 16 August 2017, in which mercury emission from waste incineration is also under regulation, the control of mercury emission in the waste incineration process, e.g., sewage sludge thermal treatment, is of great importance in Japan.

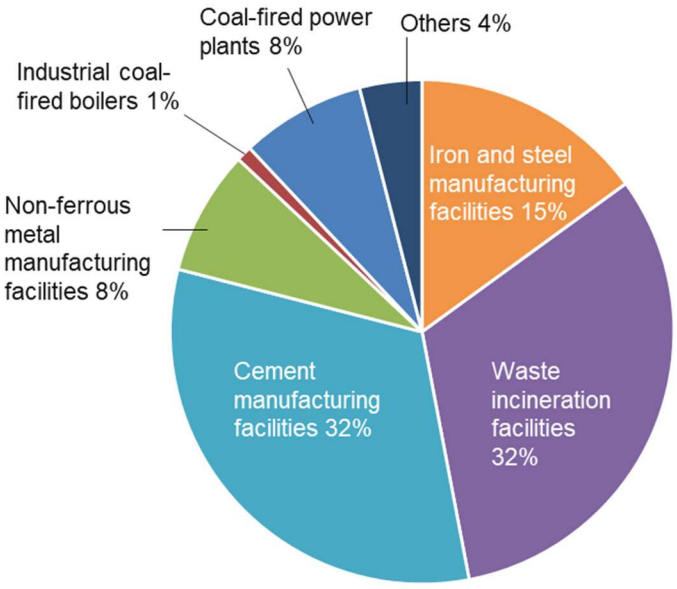

Figure 1-4. Inventory of atmospheric mercury emission in Japan (FY 2014)

1.5.2 Hg removal by air pollution control devices

The flue gas arising from the combustion of SS can be wet or dry, depending on the moisture content of the fuel used (Singh and Shukla, 2014). Also, with different types of fuel and methods used, the composition of the flue gas varies. The flue gas contains particulate matters and toxic gases. The particulate matters can be removed by dry methods with cyclones, electrostatic precipitators, and filters. The toxic gases, in which some components are solvable, can be absorbed and removed by the wet methods such as wet scrubbers and wet electrostatic precipitators. However, insolvable gaseous components, e.g., vapor-phase elemental Hg (Hg^0), may escape from the APCDs.

The APCDs are designed to remove particulates, water-soluble emissions, NO_x, and toxic materials. Alongside, Hg^{2+} can also be removed due to its high solubility.

1.5.2.1 Dry methods

- **Cyclones**

Mainly cyclones are solid-gas separation systems widely used in different industries for cleaning of the waste gas/flue gas. Sometimes cyclones are also used as the primary system to reduce the burden on the expensive secondary system used for further cleaning. For example, studies show that cyclones have been very useful as pre-cleaning devices of particles larger than 10 μm aerodynamic diameter. At high temperature and pressure, cyclones are more efficient even for a fine particle size of 2~3 μm in diameter, which makes them more economical for use in process industries (Singh and Shukla, 2014).

- **Electrostatic precipitator**

Electrostatic precipitators (ESPs) are particle control device utilizing the electrical forces to move particles out of the exhaust gas stream. The pollutant particles are given an electric charge, which led them to pass through a region where gaseous ion flows called the corona. The electrical field provided to particulates comes from electrodes mounted on the surface of the wall and maintains a high voltage in the center of the corona. ESPs are extensively used as capable pollutant control systems. Their major merits of high collection efficiency and a wide range of operating temperatures make them appropriate solutions for various applications in industry.

- **Filters**

One of the major advantages of filters is that their high removal efficiency of particulate is almost independent of the size distribution of particulates in the flue gas. A fabric filter is a very successful option used were not only particulates but gaseous impurities, e.g., SO_2 and HCl need to be removed. However, one major limitation of the fabric filter is that the flue gas must be dry otherwise particulate cannot be removed properly from the flue gas.

1.5.2.2 Wet methods

- **Scrubbers**

Wet scrubbers (WS) have been widely used for the collection of acidic gases, mists, and particles with significantly reducing risks of fire, explosion, and erosion. Many WS operates around the water dew point of the exhaust gas from biomass combustion. One major disadvantage in WS is the water pollution and foul smell due to the deposition of salt as water is frequently used as a scrubbing agent and associated cost in treating the sludge before disposal. Another problem is the freezing of the scrubbing agent, which is usually water, due to the low temperature in cold climates.

- **Wet electrostatic precipitator (Wet ESP)**

In the wet ESP, the dust is absorbed in the liquid and drained off from the collecting plates, which is also a major benefit of the wet ESP with comparison to ESP that dust resistivity does not play a major role in the wet ESP.

1.5.3 Hg removal by various sorbents

Various adsorbents are used for the Hg removal in the flue gas, which can mainly be classified as carbon-based and non-carbon based sorbents.

1.5.3.1 Carbon-based sorbents

Activated carbon (AC) is a typical carbon-based sorbent and has a long history to be used for gaseous phase pollutants removal. For example, AC made from coconut shell is reported excellent Hg^0 removal performance due to the large specific surface area. Also, ACs derived from corn straw, bamboo powder, sawdust (Hong et al., 2019), seaweed (Liu et al., 2019), and SS (Park and Lee, 2018), are studied as the carrier for active sites which

can adsorb Hg chemically. Moreover, ACs modified by halogens showed even higher Hg^0 removal efficiency (Rungnim et al., 2016; Tong et al., 2017; Yang et al., 2018b; Zhou et al., 2017, 2015).

Besides the AC, biochar derived from the biomass such as bamboo (Tan et al., 2012, 2011), seaweed (Park and Lee, 2018; Xu et al., 2019), sargassum (Yang et al., 2018b), wheat straw (Zhang et al., 2019), com straw (Zhang et al., 2019), sunflower seed shells (Zhang et al., 2019), coconut pitch (Johari et al., 2016; Saman et al., 2019), and SS, are also reported excellent Hg removal performance after impregnation or other pretreatments.

Among all these carbon-based sorbents, the AC is most suitable for the Hg removal due to its large specific surface area (Kim et al., 2011). It can, on the one hand, adsorb the Hg^0 physically, on the other hand, it serves as an excellent carrier for modifiers, which can further elevate the Hg removal performance.

1.5.3.2 Noncarbon-based sorbents

In addition to the traditional carbon-based sorbents, some non-carbon based sorbents are also studied by many researchers. For example, red mud (Yang et al., 2018a), clay (Cai et al., 2014; Shen et al., 2016), fly ash (Wang et al., 2016), and bentonite (Shao et al., 2016) are tested for Hg removal after the chemical impregnation of halogens.

Metal oxides, e.g., Fe_2O_3 nanoparticles (Borderieux et al., 2004), V_2O_5-TiO_2 (Borderieux et al., 2004), CeO_2-TiO_2 (Li et al., 2011), Mn-a-Al_2O_3 (Jia, 2010), $CoTiO_2$ (Liu et al., 2011), and MnO_2-CeO_2TiO_2 catalysts (Li et al., 2012), which can oxidize the Hg^0 into Hg^{2+} then adsorb the Hg chemically, are also reported excellent performance. These noncarbon-based sorbents usually have a lower cost than the AC, and therefore are also very promising sorbents for Hg removal.

1.6 Research objectives and the structure of the dissertation

With the small land area available for sewage sludge disposal, thermal treatment, especially sewage sludge mono-incineration, is most widely used in Japan due to its advantage in minimizing the volume of sewage sludge. However, heavy metals are of great concern for the thermal treatment process. The concentrations of heavy metals limit the recycling and disposal of wastewater, ash, and flue gas. Previous research revealed that unless other heavy metals that can be treated by the APCDs, a significant amount of mercury is emitted from flue gas. Moreover, Hg emission from the flue gas is associated with its speciation, for which the Hg^p can be collected in the ashes, Hg^{2+} can be absorbed by water at the WS, while Hg^0 may distribute mainly in the flue gas. Hence, Hg^0 emission in flue gas is a critical issue in sewage sludge incineration that needs further investigation. Besides, carbonization, as an emerging thermal treatment technology, also poses a potential risk in Hg^0 emission, which is rarely studied so far.

Hence, the objectives of this research are, firstly, to investigate the concentrations of heavy metals in each stream generated in the full-scale sewage sludge mono-incinerators; then, use these data, combining with the practical flow rates, to calculate the mass balance and distribution of heavy metals and speculate the specific problem in the sewage sludge mono-incineration process. After that, in an attempt to solve the problem revealed from the above research, which is mainly Hg emission from the flue gas, continuous monitoring of Hg emission and speciation in sewage sludge thermal treatment process was conducted. At last, sorbents for Hg^0 removal were developed and the mechanism for Hg^0 adsorption by prepared sorbents was clarified.

The final goal of this dissertation is to develop effective sorbents for Hg removal in sewage sludge thermal treatment process, which is sewage sludge mono-incineration and carbonization in this study. The dissertation is organized as follows (**Fig. 1-5**):

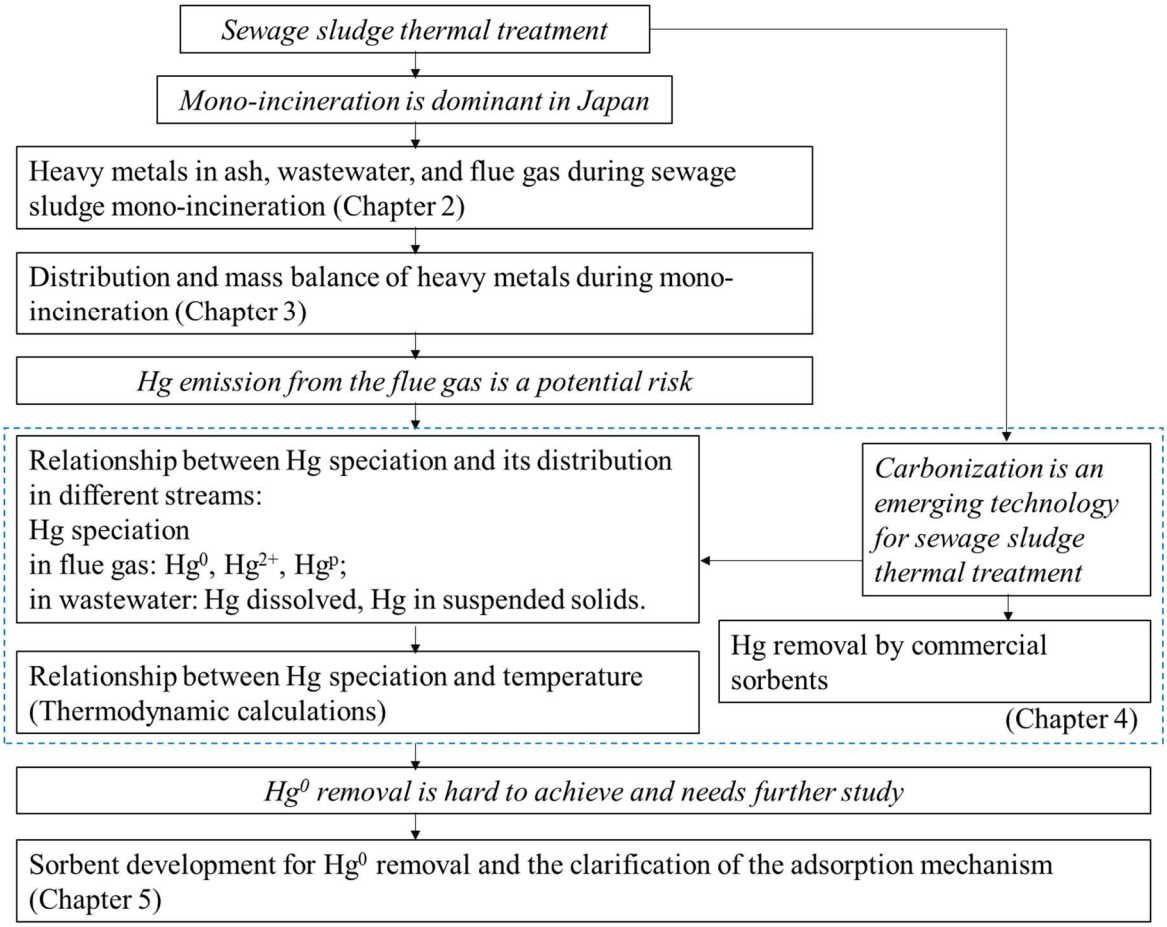

Figure 1-5. Research outline for the behavior and control of mercury in sewage sludge thermal treatment process.

The first chapter generally introduces the background of this dissertation and generally survey literature concerning the studies conducted in the following chapters.

Chapter 2 describes the general concentrations of elements in the input (SS, recycling water) and output (ash, wastewater, and flue gas) in SS mono-incinerators and compares with reported data in Japan and other countries.

Chapter 3 investigates the behavior of elements during the SS mono-incineration. Two types of typical SS mono-incinerators, one step grate stoker and two fluidized bed incinerators, are studied. Use the same sludge as the feed, the differences in the distribution of elements in the output caused by different types of incinerators are clarified. All the

target elements are classified into three groups, and the thermodynamic calculation identifies the phases of incineration products responsible for the different distributions for each group with the *FactSage* software.

Chapter 4 further discusses mercury behavior in the SS treatment process. Mercury continuous emission monitors (Hg-CEM) are used to monitor the Hg emission in SS mono-incinerators and a carbonization plant. Thermodynamic calculations are also conducted and compared with the experiment data.

Chapter 5 is a study on mercury removal by activated carbons (ACs) impregnated with iodine and bromine. The objective of this chapter is to produce adsorbents with high adsorption performance and clarify the mechanisms for Hg removal by the prepared ACs. The form of the precursors which impregnated on the ACs as well as the species of Hg on the used ACs are identified by methods such as XRD, XPS, and XAFS. Possible reactions responsible for the adsorption are assumed and confirmed by the Gibbs free energy, which is calculated by the *FactSage* software.

Chapter 6 concludes the dissertation by discussing the key findings.

References

Albero, B., Pérez, R.A., Sánchez-brunete, C., Tadeo, J.L., 2012. Occurrence and analysis of parabens in municipal sewage sludge from wastewater treatment plants in Madrid (Spain). J. Hazard. Mater. 239–240, 48–55. https://doi.org/10.1016/j.jhazmat.2012.05.017

Åmand, L.E., Leckner, B., 2004. Metal emissions from co-combustion of sewage sludge and coal/wood in fluidized bed. Fuel 83, 1803–1821. https://doi.org/10.1016/j.fuel.2004.01.014

Axelsson, L., Franzén, M., Ostwald, M., Berndes, G., Lakshmi, G., Ravindranath, N.H., 2012. Perspective: Jatropha cultivation in southern India: Assessing farmers' experiences. Biofuels, Bioprod. Biorefining 6, 246–256. https://doi.org/10.1002/bbb

Balogh, S., Liang, L., 1995. Mercury pathways in municipal wastewater treatment plants. In Mercury as a Global Pollutant 1181–1190. Springer, Dordrecht.

Balogh, S.J., Nollet, Y.H., 2008. Mercury mass balance at a wastewater treatment plant employing sludge incineration with offgas mercury control. Sci. Total Environ. 9, 125–131. https://doi.org/10.1016/j.scitotenv.2007.08.021

Berge, N.D., Ro, K.S., Mao, J., Flora, J.R.V., Chappell, M.A., Bae, S., 2011. Hydrothermal carbonization of municipal waste streams. Environ. Sci. Technol. 45, 5696–5703. https://doi.org/10.1021/es2004528

Biganzoli, L., Grosso, M., Giugliano, M., Campolunghi, M., 2012. Chemical and sewage sludge co-incineration in a full-scale MSW incinerator: Toxic trace element mass balance. Waste Manag. Res. 30, 1081–1088. https://doi.org/10.1177/0734242X12441236

Bolzonella, D., Pavan, P., Zanette, M., Cecchi, F., 2007. Two-phase anaerobic digestion of waste activated sludge: Effect of an extreme thermophilic prefermentation. Ind. Eng. Chem. Res. 46, 6650–6655. https://doi.org/10.1021/ie061627e

Borderieux, S., Wu, C.Y., Bonzongo, J.C., Powers, K., 2004. Control of elemental mercury vapor in combustion systems using Fe2O3 nanoparticles. Aerosol Air Qual. Res 4(1), 74–90.

Cai, J., Shen, B., Li, Z., Chen, J., He, C., 2014. Removal of elemental mercury by clays impregnated with KI and KBr. Chem. Eng. J. 241, 19–27. https://doi.org/10.1016/j.cej.2013.11.072

Campbell, H.W., 2000. Sludge management - Future issues and trends. Water Sci. Technol. 41, 1–8. https://doi.org/10.2166/wst.2000.0135

Cenni, R., Frandsen, F., Gerhardt, T., Spliethoff, H., Hein, K.R.G., 1998. Study on trace metal partitioning in pulverized combustion of bituminous coal and dry sewage sludge. Waste Manag. 18(6-8), 433-444.

Chen, H., Yan, S., Ye, Z., Meng, H., Zhu, Y., 2012. Utilization of urban sewage sludge: Chinese perspectives. Environ. Sci. Pollut. Res. 19, 1454–1463. https://doi.org/10.1007/s11356-012-0760-0

Chen, T., Yan, B., 2012. Fixation and partitioning of heavy metals in slag after incineration of sewage sludge. Waste Manag. 32, 957–964. https://doi.org/10.1016/j.wasman.2011.12.003

Chen, W., Wang, F., Kanhar, A.H., 2017. Sludge acts as a catalyst for coal during the co-combustion process investigated by thermogravimetric analysis. Energies 10(12), 1993.

Chen, Z., Li, J.S., Poon, C.S., 2018. Combined use of sewage sludge ash and recycled glass cullet for the production of concrete blocks. J. Clean. Prod. 171, 1447–1459. https://doi.org/10.1016/j.jclepro.2017.10.140

Christodoulou, A., Stamatelatou, K., 2016. Overview of legislation on sewage sludge management in developed countries worldwide. Water Sci. Technol. 73, 453–462. https://doi.org/10.2166/wst.2015.521

Cieślik, B., Konieczka, P., 2017. A review of phosphorus recovery methods at various steps of wastewater treatment and sewage sludge management. The concept of “no solid waste generation” and analytical methods. J. Clean. Prod. 142, 1728–1740. https://doi.org/10.1016/j.jclepro.2016.11.116

Cieślik, B.M., Namieśnik, J., Konieczka, P., 2015. Review of sewage sludge management: Standards, regulations and analytical methods. J. Clean. Prod. 90, 1–15. https://doi.org/10.1016/j.jclepro.2014.11.031

Donatello, S., Cheeseman, C.R., 2013. Recycling and recovery routes for incinerated sewage sludge ash (ISSA): A review. Waste Manag. 33, 2328–2340. https://doi.org/10.1016/j.wasman.2013.05.024

Elled, A.L., Åmand, L.E., Leckner, B., Andersson, B.Å., 2007. The fate of trace elements in fluidised bed combustion of sewage sludge and wood. Fuel 86, 843–852. https://doi.org/10.1016/j.fuel.2006.08.014

Escala, M., Zumbühl, T., Koller, C., Junge, R., Krebs, R., 2013. Hydrothermal carbonization as an energy-efficient alternative to established drying technologies for sewage sludge: A feasibility study on a laboratory scale. Energy and Fuels 27, 454–460. https://doi.org/10.1021/ef3015266

Epstein, E., 2002. Land application of sewage sludge and biosolids. CRC Press.

Gerstle, R.W., Albrinck, D.N., 1982. Atmospheric Emissions of Metals from Sewage Sludge Incineration. J. Air Pollut. Control Assoc. 32, 1119–1123. https://doi.org/10.1080/00022470.1982.10465519

Global mercury assessment 2018. UN environment programme. (Accessed on 26 December 2019)

https://www.unenvironment.org/resources/publication/global-mercury-assessment-2018

Gulyurtlu, I., Lopes, M.H., Abelha, P., Cabrita, I., Oliveira, J.S., 2006. The study of partitioning of heavy metals during fluidized bed combustion of sewage sludge and coal. J. Energy Resour. Technol. 128, 104–110.

Han, J., Xu, M., Yao, H., Furuuchi, M., Sakano, T., Kim, H.J., 2008. Influence of calcium chloride on the thermal behavior of heavy and alkali metals in sewage sludge incineration. Waste Manag. 28, 833–839. https://doi.org/10.1016/j.wasman.2007.01.015

He, C., Giannis, A., Wang, J.Y., 2013. Conversion of sewage sludge to clean solid fuel using hydrothermal carbonization: Hydrochar fuel characteristics and combustion behavior. Appl. Energy 111, 257–266. https://doi.org/10.1016/j.apenergy.2013.04.084

Hong, D., Zhou, J., Hu, C., Zhou, Q., Mao, J., Qin, Q., 2019. Mercury removal mechanism of AC prepared by one-step activation with. Fuel 235, 326–335. https://doi.org/10.1016/j.fuel.2018.07.103

Hong, J., Hong, J., Otaki, M., Jolliet, O., 2009. Environmental and economic life cycle assessment for sewage sludge treatment processes in Japan. Waste Manag. 29(2), 696–703.

Li, J., Yan, N., Qu, Z., Qiao, S., Yang, S., Guo, Y., Liu, P., Jia, J., 2010. Catalytic oxidation of elemental mercury over the modified catalyst Mn/α-Al2O3 at lower temperatures. Environ. Sci. Technol. 44(1), 426–431.

Johari, K., Saman, N., Song, S.T., Chin, C.S., Kong, H., Mat, H., 2016. Adsorption enhancement of elemental mercury by various surface modified coconut husk as eco-friendly low-cost adsorbents. Int. Biodeterior. Biodegrad. 109, 45–52.

Kelessidis, A., Stasinakis, A.S., 2012. Comparative study of the methods used for treatment and final disposal of sewage sludge in European countries. Waste Manag. 32, 1186–1195. https://doi.org/10.1016/j.wasman.2012.01.012

Kim, B.J., Bae, K.M., Park, S.J., 2011. A study of the optimum pore structure for mercury vapor adsorption. Bull. Korean Chem. Soc. 32(5), 1507–1510.

Krüger, O., Adam, C., 2014. Recovery potential of German sewage sludge ash. Waste Manag. 45, 400–406. https://doi.org/10.1016/j.wasman.2015.01.025

Krüger, O., Grabner, A., Adam, C., 2014. Complete survey of German sewage sludge ash. Environ. Sci. Technol. 48, 11811–11818. https://doi.org/10.1021/es502766x

Lee, S.S., Wilcox, J., 2017. Behavior of mercury emitted from the combustion of coal and dried sewage sludge: The effect of unburned carbon, Cl, Cu and Fe. Fuel 203, 749–756. https://doi.org/10.1016/j.fuel.2017.04.104

Li, H., Wu, C.Y., Li, Y., Zhang, J., 2012. Superior activity of MnOx-CeO2/TiO2 catalyst for catalytic oxidation of elemental mercury at low flue gas temperatures. Appl. Catal.,

B 111, 381–388.

Li, H., Wu, C.Y., Li, Y., Zhang, J., 2011. CeO2–TiO2 catalysts for catalytic oxidation of elemental mercury in low-rank coal combustion flue gas. Environ. Sci. Technol. 45(17), 7394–7400.

Li, J. shan, Xue, Q., Fang, L., Poon, C.S., 2017. Characteristics and metal leachability of incinerated sewage sludge ash and air pollution control residues from Hong Kong evaluated by different methods. Waste Manag. 64, 161–170. https://doi.org/10.1016/j.wasman.2017.03.033

Li, J.S., Guo, M.Z., Xue, Q., Poon, C.S., 2017. Recycling of incinerated sewage sludge ash and cathode ray tube funnel glass in cement mortars. J. Clean. Prod. 152, 142–149. https://doi.org/10.1016/j.jclepro.2017.03.116

Li, Y., Cui, R., Yang, T., Zhai, Z., Li, R., 2017. Distribution characteristics of heavy metals in different size fly ash from a sewage sludge circulating fluidized bed incinerator. Energy and Fuels 31(2), 2044–2051.

Liu, B., Wei, Q., Zhang, B., Bi, J., 2013. Life cycle GHG emissions of sewage sludge treatment and disposal options in Tai Lake Watershed, China. Sci. Total Environ. 447, 361–369.

Liu, J., Fu, J., Ning, X., Sun, S., Wang, Y., Xie, W., Huang, S., Zhong, S., 2015. An experimental and thermodynamic equilibrium investigation of the Pb, Zn, Cr, Cu, Mn and Ni partitioning during sewage sludge incineration. J. Environ. Sci. (China) 35, 43–54. https://doi.org/10.1016/j.jes.2015.01.027

Liu, Y., Wang, Y., Wang, H., Wu, Z., 2011. Catalytic oxidation of gas-phase mercury over Co/TiO2 catalysts prepared by sol–gel method. Catal. Commun. 12(14), 1291–1294.

Liu, Z., Adewuyi, Y.G., Shi, S., Chen, H., Li, Y., Liu, D., Liu, Y., 2019. Removal of gaseous Hg 0 using novel seaweed biomass-based activated carbon. Chem. Eng. J. 366, 41–49. https://doi.org/10.1016/j.cej.2019.02.025

Lopes, M.H., Abelha, P., Lapa, N., Oliveira, J.S., Cabrita, I., Gulyurtlu, I., 2003. The behaviour of ashes and heavy metals during the co-combustion of sewage sludges in a fluidised bed. Waste Manag. 23, 859–870. https://doi.org/10.1016/S0956-053X(03)00025-4

Lu, Q., He, Z.L., Stoffella, P.J., 2012. Land application of biosolids in the USA: A review. Appl. Environ. Soil Sci. 2012. https://doi.org/10.1155/2012/201462

Lundin, M., Olofsson, M., Pettersson, G.J., Zetterlund, H., 2004. Environmental and economic assessment of sewage sludge handling options. Resour. Conserv. Recycl. 41, 255–278. https://doi.org/10.1016/j.resconrec.2003.10.006

Lynn, C.J., Dhir, R.K., Ghataora, G.S., West, R.P., 2015. Sewage sludge ash characteristics and potential for use in concrete. Constr. Build. Mater. 98, 767–779. https://doi.org/10.1016/j.conbuildmat.2015.08.122

Mailler, R., Gasperi, J., Chebbo, G., Rocher, V., 2014. Priority and emerging pollutants in sewage sludge and fate during sludge treatment. Waste Manag. 34, 1217–1226. https://doi.org/10.1016/j.wasman.2014.03.028

Manzetti, S., Spoel, D. Van Der, 2015. Impact of sludge deposition on biodiversity. Ecotoxicology 24, 1799–1814. https://doi.org/10.1007/s10646-015-1530-9

Marani, D., Braguglia, C.M., Mininni, G., Maccioni, F., 2003. Behaviour of Cd, Cr, Mn, Ni, Pb, and Zn in sewage sludge incineration by fluidised bed furnace. Waste manag. 23(2), 117–124.

Maschio, G., Koufopanos, C.,Lucchesi, A., 1992. Pyrolysis, a promising route for biomass utilization. Bioresour. Technol. 42(3), 219–231.

Meier, C., Voegelin, A., Pradas del Real, A., Sarret, G., Mueller, C.R., Kaegi, R., 2016. Transformation of silver nanoparticles in sewage sludge during incineration. Environ. Sci. Technol. 50(7), 3503–3510.

Ministry of Agriculture, Forestry and Fisheries (MAFF) (22 November, 2019 accessed) Fertilizers Regulation Act. http://www.maff.go.jp/j/syouan/nouan/kome/k_hiryo/tebikiso.html

Ministry of the Environment, Regulations on Mercury in Japan, 2018. (13 February, 2020 accessed) https://report.nat.gov.tw/ReportFront/PageSystem/reportFileDownload/C10701749/004

Ministry of Land, Infrastructure, Transport and Tourism(MLIT) (22 November, 2019 accessed) http://www.mlit.go.jp/mizukokudo/sewerage/crd_sewerage_tk_000124.html

Mullen, J.F., 1992. Consider fluid-bed incineration for hazardous waste destruction. Chem. Eng. Prog. 88(6).

Mumme, J., Eckervogt, L., Pielert, J., Diakité, M., Rupp, F., Kern, J., 2011. Hydrothermal carbonization of anaerobically digested maize silage. Bioresour. Technol. 102, 9255–9260. https://doi.org/10.1016/j.biortech.2011.06.099

Nadziakiewicz, J., Kozioł, M., 2003. Co-combustion of sludge with coal. Appl. Energy 75, 239–248. https://doi.org/10.1016/S0306-2619(03)00037-0

O'kelly, B.C., 2005. Sewage sludge to landfill: Some pertinent engineering properties. J. Air Waste Manag. Assoc. 55, 765–771. https://doi.org/10.1080/10473289.2005.10464670

Ottosen, L.M., Kirkelund, G.M., Jensen, P.E., 2013. Extracting phosphorous from incinerated sewage sludge ash rich in iron or aluminum. Chemosphere 91, 963–969. https://doi.org/10.1016/j.chemosphere.2013.01.101

Pacyna, E.G., Pacyna, J.M., Sundseth, K., Munthe, J., Kindbom, K., Wilson, S., Steenhuisen, F., Maxson, P., 2010. Global emission of mercury to the atmosphere from

anthropogenic sources in 2005 and projections to 2020. Atmos. Environ. 44, 2487–2499. https://doi.org/10.1016/j.atmosenv.2009.06.009

Park, J., Lee, S.S., 2018. Adsorption of mercury by activated carbon prepared from dried sewage sludge in simulated flue gas. J. Air Waste Manag. Assoc. 68(10), 1077–1084.

Park, Sang W., Jang, C.H., 2011. Characteristics of carbonized sludge for co-combustion in pulverized coal power plants. Waste Manag. 31, 523–529. https://doi.org/10.1016/j.wasman.2010.10.009

Park, Sang Woo, Jang, C.H., 2011. Effects of carbonization and solvent-extraction on change in fuel characteristics of sewage sludge. Bioresour. Technol. 102, 8205–8210. https://doi.org/10.1016/j.biortech.2011.05.072

Peccia, J., Westerhoff, P., 2015. We Should Expect More out of Our Sewage Sludge. Environ. Sci. Technol. 49, 8271–8276. https://doi.org/10.1021/acs.est.5b01931

Prins, M.J., Ptasinski, K.J., Janssen, F.J.J.G., 2006. Torrefaction of wood Part 2. Analysis of products 77, 35–40. https://doi.org/10.1016/j.jaap.2006.01.001

Przydatek, G., Katarzyna, A., 2020. Analysis of the comprehensive management of sewage sludge in Poland. J. Mater. Cycles Waste Manag. 22, 80–88. https://doi.org/10.1007/s10163-019-00937-y

Pudasainee, D., Seo, Y.C., Kim, J.H., Jang, H.N., 2013. Fate and behavior of selected heavy metals with mercury mass distribution in a fluidized bed sewage sludge incinerator. J. Mater. Cycles Waste Manag. 15, 202–209. https://doi.org/10.1007/s10163-013-0115-z

Pacyna, E.G., Pacyna, J.M., Sundseth, K., Munthe, J., Kindbom, K., Wilson, S., Steenhuisen, F., Maxson, P., 2010. Global emission of mercury to the atmosphere from anthropogenic sources in 2005 and projections to 2020. Atmos. Environ. 44(20), 2487–2499.

Raheem, A., Sikarwar, V.S., He, J., Dastyar, W., Dionysiou, D.D., Wang, W., Zhao, M., 2018. Opportunities and challenges in sustainable treatment and resource reuse of sewage sludge: A review. Chem. Eng. J. 337, 616–641. https://doi.org/10.1016/j.cej.2017.12.149

Rungnim, C., Promarak, V., Hannongbua, S., Kungwan, N., Namuangruk, S., 2016. Complete reaction mechanisms of mercury oxidation on halogenated activated carbon. J. Hazard. Mater. 310, 253–260. https://doi.org/10.1016/j.jhazmat.2016.02.033

Saman, N., Johari, K., Kong, H., Mohtar, S.S., Hassan, O., Ali, N., Mat, H., 2019. Enhanced elemental mercury removal by facile sulfurization of agrowaste chars. Chem. Eng. Res. Des. 144, 198–208.

Shao, H., Liu, X., Zhou, Z., Zhao, B., Chen, Z., Xu, M., 2016. Elemental mercury removal using a novel KI modified bentonite supported by starch sorbent. Chem. Eng. J. 291, 306–316. https://doi.org/10.1016/j.cej.2016.01.090

Sharpley, A., Meisinger, J.J., Breeuwsma, A., Sims, J.T., Daniel, T.C., Schepers, J.S., 1998. Impacts of animal manure management on ground and surface water quality. Animal waste utilization: effective use of manure as a soil resource, 173–242.

Shen, B., Chen, J., Cai, J., 2016. Removal of elemental mercury by KI-impregnated clay. Front. Environ. Sci. Eng. China 10(2), 236–243.

Shepherd, M.A., Withers, P.J., 2001. Phosphorus leaching from liquid digested sewage sludge applied to sandy soils. J. Agric. Sci. 136, 433–441. https://doi.org/10.1017/S0021859601008875

Singh, R., Shukla, A., 2014. A review on methods of flue gas cleaning from combustion of biomass. Renewable Sustainable Energy Rev. 29, 854–864.

Smol, M., Kulczycka, J., Henclik, A., Gorazda, K., Wzorek, Z., 2015. The possible use of sewage sludge ash (SSA) in the construction industry as a way towards a circular economy. J. Clean. Prod. 95, 45–54. https://doi.org/10.1016/j.jclepro.2015.02.051

Takaoka, M., Domoto, S., Oshita, K., Takeda, N., Morisawa, S., 2012. Mercury emission from sewage sludge incineration in Japan. J. Mater. Cycles Waste Manag. 14, 113–119. https://doi.org/10.1007/s10163-012-0044-2

Tan, Z., Sun, L., Xiang, J., Zeng, H., Liu, Z., Hu, S., Qiu, J., 2012. Gas-phase elemental mercury removal by novel carbon-based sorbents. Carbon 50(2), 362–371.

Tan, Z., Xiang, J., Su, S., Zeng, H., Zhou, C., Sun, L., Hu, S., Qiu, J., 2012. Enhanced capture of elemental mercury by bamboo-based sorbents. J. Hazard. Mater. 239–240, 160–166. https://doi.org/10.1016/j.jhazmat.2012.08.053

Titirici, M.M., Thomas, A., Antonietti, M., 2007. Back in the black: Hydrothermal carbonization of plant material as an efficient chemical process to treat the CO2 problem? New J. Chem. 31, 787–789. https://doi.org/10.1039/b616045j

Tong, L., Yue, T., Zuo, P., Zhang, X., Wang, C., Gao, J., Wang, K., 2017. Effect of characteristics of KI-impregnated activated carbon and flue gas components on Hg 0 removal. Fuel 197, 1–7. https://doi.org/10.1016/j.fuel.2016.12.083

Tyagi, V.K., Lo, S.L., 2013. Sludge: A waste or renewable source for energy and resources recovery? Renew. Sustain. Energy Rev. 25, 708–728. https://doi.org/10.1016/j.rser.2013.05.029

UN environment programme, Minamata Convention on mercury. (Accessed on 26 December 2019) http://www.mercuryconvention.org/Convention/Text/tabid/3426/language/en-US/Default.aspx

Van de Velden, M., Dewil, R., Baeyens, J., Josson, L., Lanssens, P., 2008. The distribution of heavy metals during fluidized bed combustion of sludge (FBSC). J. Hazard. Mater. 151, 96–102. https://doi.org/10.1016/j.jhazmat.2007.05.056

Wang, Q., Li, J. shan, Poon, C.S., 2019. Recycling of incinerated sewage sludge ash as an

adsorbent for heavy metals removal from aqueous solutions. J. Environ. Manage. 247, 509–517. https://doi.org/10.1016/j.jenvman.2019.06.115

Wang, S., Zhang, Yongsheng, Gu, Y., Wang, J., Zhang, You, Cao, Y., Romero, C.E., Pan, W., 2016. Using modified fly ash for mercury emissions control for coal-fired power plant applications in China. Fuel 181, 1230–1237. https://doi.org/10.1016/j.fuel.2016.02.043

Werther, J., Ogada, T., 1999. Sewage sludge combustion. Prog. Energy Combust. Sci. 25(1), 55–116.

Westerhoff, P., Lee, S., Yang, Y., Gordon, G.W., Hristovski, K., Halden, R.U., Herckes, P., 2015. Characterization, recovery opportunities, and valuation of metals in municipal sludges from US wastewater treatment plants nationwide. Environ. Sci. Technol. 49(16), 9479–9488.

Winkler, M.K.H., Bennenbroek, M.H., Horstink, F.H., van Loosdrecht, M.C.M., van de Pol, G.J., 2013. The biodrying concept: An innovative technology creating energy from sewage sludge. Bioresour. Technol. 147, 124–129. https://doi.org/10.1016/j.biortech.2013.07.138

Wu, M.H., Lin, C.L., Huang, W.C., Chen, J.W., 2016. Characteristics of pervious concrete using incineration bottom ash in place of sandstone graded material. Constr. Build. Mater. 111, 618–624. https://doi.org/10.1016/j.conbuildmat.2016.02.146

Xiao, Z., Yuan, X., Li, H., Jiang, L., Leng, L., Chen, X., Zeng, G., Li, F., Cao, L., 2015. Chemical speciation, mobility and phyto-accessibility of heavy metals in fly ash and slag from combustion of pelletized municipal sewage sludge. Sci. Total Environ. 536, 774–783. https://doi.org/10.1016/j.scitotenv.2015.07.126

Xu, C., Chen, W., Hong, J., 2014. Life-cycle environmental and economic assessment of sewage sludge treatment in China. J. Clean. Prod. 67, 79–87. https://doi.org/10.1016/j.jclepro.2013.12.002

Xu, W., Pan, J., Fan, B., Liu, Y., 2019. Removal of gaseous elemental mercury using seaweed chars impregnated by NH4Cl and NH4Br. J. Cleaner Prod. 216, 277–287.

Yang, W., Hussain, A., Zhang, J., Liu, Y., 2018a. Removal of elemental mercury from flue gas using red mud impregnated by KBr and KI reagent. Chem. Eng. J. 341, 483–494. https://doi.org/10.1016/j.cej.2018.02.023

Yang, W., Liu, Z., Xu, W., Liu, Y., 2018b. Removal of elemental mercury from flue gas using sargassum chars modified by NH4Br reagent. Fuel 214, 196–206. https://doi.org/10.1016/j.fuel.2017.11.004

Yoshida, H., Christensen, T.H., Guildal, T., Scheutz, C., 2015. A comprehensive substance flow analysis of a municipal wastewater and sludge treatment plant. Chemosphere 138, 874–882. https://doi.org/10.1016/j.chemosphere.2013.09.045

Yu, S., Zhang, B., Wei, J., Zhang, T., Yu, Q., Zhang, W., 2017. Effects of chlorine on the

volatilization of heavy metals during the co-combustion of sewage sludge. Waste Manag. 62, 204–210. https://doi.org/10.1016/j.wasman.2017.02.029

Zhang, G., Hai, J., Ren, M., Zhang, S., Cheng, J., Yang, Z., 2013. Emission, mass balance, and distribution characteristics of PCDD/Fs and heavy metals during cocombustion of sewage sludge and coal in power plants. Environ. Sci. Technol. 47, 2123–2130. https://doi.org/10.1021/es304127k

Zhang, S., Yang, X., Ju, M., Liu, L., Zheng, K., 2019. Mercury adsorption to aged biochar and its management in China. Environ. Sci. Pollut. Res. 26(5), 4867–4877.

Zhao, Y., Ren, Q., Na, Y., 2017. Speciation transformation of arsenic during municipal sewage sludge incineration with cotton stalk as additive. Fuel 202, 541–546. https://doi.org/10.1016/j.fuel.2017.04.074

Zhao, Z., Wang, R., Wu, J., Yin, Q., Wang, C., 2019. Bottom ash characteristics and pollutant emission during the co-combustion of pulverized coal with high mass-percentage sewage sludge. Energy 171, 809–818. https://doi.org/10.1016/j.energy.2019.01.082

Zhou, Q., Duan, Y., Chen, M., Liu, M., Lu, P., 2017. Studies on mercury adsorption species and equilibrium on activated carbon surface. Energy and fuels 31(12), 14211–14218.

Zhou, Q., Duan, Y., Hong, Y., Zhu, C., She, M., Zhang, J., Wei, H., 2015. Experimental and kinetic studies of gas-phase mercury adsorption by raw and bromine modi fi ed activated carbon. Fuel Process. Technol. 134, 325–332. https://doi.org/10.1016/j.fuproc.2014.12.052

Zhu, J.G., Yao, Y., Lu, Q.G., Gao, M., Ouyang, Z.Q., 2015. Experimental investigation of gasification and incineration characteristics of dried sewage sludge in a circulating fluidized bed. Fuel 150, 441–447. https://doi.org/10.1016/j.fuel.2015.02.031

Chapter 2 Concentrations of elements in sludge, recycling water, wastewater, and ash

2.1 Introduction

An unfavorable aspect of the sludge combustion is the partitioning of the heavy metals in ash, wastewater, and flue gas. Various research has been conducted on heavy metals distribution in sewage sludge fluidized bed incinerators. In the wastewater treatment process, both organic and inorganic pollutants were found to be accumulated in sewage sludge (Hargreaves et al., 2016; Karvelas et al., 2003; Goldstone et al., 1990), and the majority of metals and metalloids further accumulated in the incineration ash (Yoshida et al., 2015). Heavy metals (e.g. As, Cd, Cr, Cu, Ni, Pb, and Zn) were efficiently captured in fly ash except for Hg. Hg, Pb, and Cd were also significantly present in the stack emission for their high volatility (Van de Velden et al., 2008). Cd, Cr, Ni, and Pb were found to be mainly enriched in coarse particles, while As content was higher in fine particles (< PM2.5). All these elements were effectively removed in ash, whereas Hg was mainly distributed in flue gas and removed in wastewater (Pudasainee et al., 2013).

Pilot tests results (Marani et al., 2003) indicated higher enrichment of Cd and Pb in fly ash (recovered in the final bag filter) than in ashes from the cyclone immediately following the fluidized bed incinerator, and this was mainly affected by chlorine concentration in the feed sludge (0.2~0.3%). Chlorides and operational conditions were also reported to affect the distribution and speciation of heavy metals (Liu et al., 2015). Combined experimental results from simulated laboratory tubular furnace reactor with calculation results using the FactSage software showed that the volatility of heavy metals (Pb, Zn, Cr, Cu, Mn, and Ni) was enhanced as the chlorine concentration increased. Inorganic Cl influenced the volatilization of heavy metals in the following order of Pb > Zn > Cr > Cu > Mn >Ni. However, the effect of increased retention time was insignificant (Liu et al., 2015).

A few researchers also studied the role of spent water from the flue gas treatment process and paradoxical results were reported (Balogh and Nollet, 2008; Van de Velden et al., 2008; Yoshida et al., 2015). Approximately 14.4~14.9% of Hg partitioned into spent scrubber water and returned to the wastewater treatment process as it was reported by Balogh (Balogh and Nollet, 2008) and Van de Velden (2008) and Yoshida et al. (2015) found that only negligible amounts of elements (0.023% for Cd and 0.0024% for Hg) in wastewater from the flue gas treatment process were back to the inlet of wastewater treatment.

Since the concentrations of elements in sludge, ash, wastewater, and flue gas are associated with the recycling and disposal of these streams during sewage sludge incineration and reflect the effectiveness of the whole wastewater treatment process, the purpose of this chapter is to survey the elemental concentrations in sludge, ash, wastewater, and flue gas during SS mono-incineration. A wastewater treatment plant (WWTP) located in western Japan is selected, and a comprehensive survey of elemental concentrations, especially heavy metals, in SS mono-incinerators was conducted.

2.2 Methodology

2.2.1 Basic information about the wastewater treatment plant

The WWTP selected in this study treats mainly domestic wastewater from about 871,900 population equivalent in western Japan with a capacity of 1,031,000 m^3/day. The incoming wastewater is physically treated by the primary sedimentation process and biologically treated in parallel by activated sludge process, anaerobic-anoxic aerobic process, anaerobic-aerobic activated sludge process and step-feed multistage nitrification/denitrification, respectively. Additionally, a small amount of sludge from water purification plant is also transported to WWTP by pipeline and treated together.

Primary sludge is gravity thickened and anaerobically digested. Waste activated sludge (WAS) is mechanically concentrated with belt-type concentrator. Anaerobically digested primary sludge and concentrated WAS are dewatered with screw press dehydrator to a moisture content of about 80%.

2.2.2 The incineration of dewatered sludge

Two types of incinerators, a step grate stoker (**GS**) and two fluidized bed (**F-type**) incinerators with different dust collectors, are operated in the WWTP. The schematics are shown in **Figure 2-1**. Since all three incinerators treat the same sewage sludge, the characterization of feed is identical, as shown in **Table 2-1**.

The capacity of the **GS** is 150 tons/day for dewatered sludge at a moisture content of 80%. In this incinerator, dewatered sludge is first dried within the indirect heating sludge dryer, using steam derived from the waste-heat boiler, to achieve a moisture content of ~40%. Then, this dried sludge is combusted at temperatures of 850–950°C without auxiliary fuel.

After combustion, residues are discharged mainly as bottom ash (also called main ash) and riddling ash (small quantities that drop between the grates of the **GS**). The heat of the flue gas is recovered at the boiler to produce the steam used in the sludge drier. At the boiler, the fine particles are removed from the flue gas and collected as boiler dust. Then, the particulate matter is removed by a multi-cyclone. Meanwhile, the flue gas is cooled to ~250°C and then directed to a wet scrubber (WS) and a wet electrostatic precipitator (ESP), where acid gas (mainly SO_2 and SO_3) is absorbed by caustic soda solution and the dust is removed. Finally, the treated flue gas is emitted through the stack to the atmosphere.

The F-types are operated in parallel, with a capacity of 150 tons/day each. These incinerators are equipped with similar air pollution control devices (APCDs) except for their dust collectors; one utilizes a bag filter (denoted as **FB**), and the other uses a ceramic

filter (denoted as **FC**). In contrast to the **GS**, in **FB** and **FC**, the dewatered sludge is directly combusted at 850–950°C, with no pre-drying. Instead, auxiliary fuel (heavy oil) is used. Moreover, **FB** and **FC** generate only fly ash.

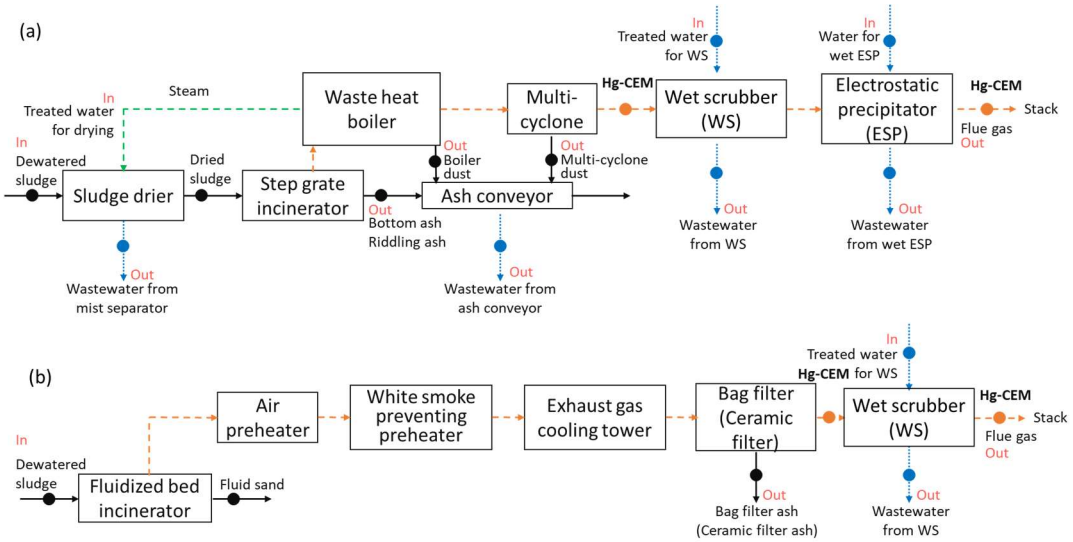

Figure 2-1. Schematic of sample collection from the (a) step grate incinerator (**GS**) and (b) fluidized bed incinerators (**F-types**) equipped with bag (**FB**) and ceramic (**FC**) filters. The green arrow shows the flow of steam. The black, blue, and orange arrows (dots) show the mass flows (sampling points) of solids, water, and flue gas, respectively. Hg-CEM: mercury continuous emission monitor. In GS: ash samples included bottom ash (main ash, dominant among all types of ash generated in the GS), riddling ash (dropped from the gap between grates, minor component), boiler dust, and multi-cyclone dust. The boiler and multi-cyclone dust are also classified as fly ash in the GS.

2.2.3 The sampling process

The sampling event took place between December 2016 and February 2017, including batch sampling and continuous sampling. For the batch samples, dewatered or dried sludge, ash, and drainage, in total 227 samples, from the step grate stoker and the fluidized bed incinerators (**Fig. 2-1**).

For the incinerator **GS**, batch sampling was applied on December 22, 2016, and February 15, 2017. During the sampling, 1000 g of dewatered sludge, 1000 g of dried

sludge, and 1000 g of ash samples, including bottom ash, riddling ash, boiler dust, and multi-cyclone dust, were collected. These solid samples were stored in double zip-lock bags and kept refrigerated (4 °C) and lightproof until analysis. For water samples, including secondary treated water for drying, secondary treated water for wet scrubber (WS), the water of wet ESP, wastewater from mist separator, wastewater from WS, wastewater from wet ESP and wastewater from ash conveyor, 2 L of each were collected with polypropylene bottles. And the storage of these samples was the same as sludge and ash samples.

In order to confirm the reliability and representativeness of the batch samples, which were used in the later calculation of mass balance, continuous sampling was performed as well. A two-week continuous sampling was conducted in December 14~27, 2016. Sludge, ash and water samples were collected daily. As other ashes were minor in the hourly amount, only bottom ash was sampled to represent the ash samples. All continuous samples were collected for 500 g (for solid samples) or 500 ml (for water samples) with 500-ml polypropylene bottles. A total number of 150 samples, including 24 samples for batch (twice) and 126 samples for continuous sampling, were collected in incinerator **GS**.

For incinerators **FB** and **FC**, batch and continuous sampling were also conducted. For incinerator **FB**, batch sampling was performed on December 21, 2016, and February 14, 2017. Solid samples including 1000 g of dewatered sludge, 1000 g of bag filter ash, and 1000 g of fluidized sand were collected. Two liters of drainage water, such as secondary treated water for wet scrubber and wastewater from wet scrubber were sampled at the same time. A one-week continuous sampling was conducted in February 15~21, 2017. All continuous samples were collected for 500 g or 500 ml with 500-ml polypropylene bottles and kept refrigerated and lightproof until analysis. A total of 35 samples (10 for batch sampling and 25 for continuous sampling), were collected in incinerator **FB**.

Similar batch sampling for incinerator **FC** (December 21, 2016, and January 23, 2017) and continuous sampling (January 16~24, 2017) were conducted. Different from

incinerator **FB**, ash sample here was ceramic filter ash. A total of 42 samples, including 10 samples for batch and 32 for continuous sampling, were collected in incinerator **FC**.

All of the collected solid samples were stored in double Ziplock bags and kept refrigerated (4 ℃) in the dark until analysis. The liquid samples were collected in 2-L polypropylene bottles and were also stored at 4 ℃ in the dark until analysis.

During the continuous sampling event, two sets of speciation mercury continuous emission monitors (Hg-CEM; SGM-8T for Hg^{2+} and SGM-8E for Hg^{0}; Nippon Instruments) were also set on the spot. The outlet of multi-cyclone/ bag filter/ ceramic filter and the front of the stack were continuously monitored (**Fig.2-1**). Concentrations of O_2 were measured by a continuous analyzer (CGT-7000, Shimadzu, Kyoto, Japan). The flue-gas temperature was measured by a thermocouple. The emission concentrations of heavy metals in flue gas were corrected for 12% oxygen concentration. The stability and repeatability were ensured by twice samplings and double or triple measurements for each sample. **Fig.2-1** summarizes the schematic and sampling points of incinerators **GS, FB** and **FC**.

Table 2-1. General characterization of dewatered and dried sludge. Contents of C, H, and N were measured with CHN analyzer, and contents of other elements were measured with XRF.

sludge	Category	Incinerator	Date	TS	VTS	C	H	N	S	O	Si	Al	P	Ca	Fe	K	Mg	Cl
				%	%TS	%TS	%TS	%TS	%TS	%TS	%TS	%TS	%TS	%TS	%TS	%TS	%TS	%TS
Dewatered	Batch	S	12/22/2016	20.3	79.9	39.7	6.2	4.9	0.9	28.4	2.7	2.6	2.2	0.9	0.9	0.4	0.4	0.06
			2/15/2017	19.8	82.5	41.9	6.7	4.7	0.8	28.8	2.1	2.0	2.0	0.9	0.7	0.4	0.3	0.06
		FB	12/21/2016	18.8	80.6	41.2	6.5	4.6	0.9	27.8	2.6	2.3	2.1	1.0	0.9	0.4	0.4	0.06
			2/14/2017	16.7	82.4	41.9	6.6	4.6	0.8	28.7	2.3	2.0	2.0	1.0	0.7	0.4	0.4	0.06
		FC	12/21/2016	18.5	80.8	41.6	6.5	4.6	0.8	27.6	2.7	2.2	2.1	0.8	0.8	0.4	0.4	0.06
			1/23/2017	14.3	79.3	40.3	6.1	3.6	0.9	28.8	2.8	2.5	2.2	1.0	0.8	0.4	0.4	0.07
	Continuous	S	12/14/2016	21.1	79.1	40.0	6.0	4.5	0.9	28.1	2.9	2.4	2.0	0.9	1.0	0.4	0.4	0.06
			12/15/2016	21.7	77.6	39.2	5.8	3.6	0.7	28.5	3.5	2.4	1.7	0.8	0.9	0.4	0.3	0.05
			12/16/2016	19.6	78.2	39.3	5.9	4.3	0.9	28.1	3.1	2.6	2.0	0.8	1.0	0.4	0.3	0.06
			12/17/2016	17.0	75.1	37.8	5.7	4.8	1.0	26.1	3.6	3.2	2.3	0.9	1.1	0.5	0.4	0.07
			12/18/2016	19.4	76.9	38.6	5.8	4.6	0.9	27.3	3.3	2.9	2.3	1.0	1.0	0.5	0.4	0.06
			12/19/2016	18.8	76.5	38.7	6.0	4.8	0.9	26.4	3.2	2.9	2.3	1.0	1.0	0.5	0.4	0.06
			12/20/2016	20.2	79.2	39.8	6.2	4.8	0.9	27.9	2.7	2.6	2.1	1.0	0.9	0.4	0.4	0.06
			12/21/2016	18.6	77.0	38.7	6.0	4.8	0.9	27.0	3.2	2.9	2.3	1.1	0.9	0.4	0.4	0.07
			12/22/2016	19.4	79.5	39.8	6.1	5.1	0.9	27.8	2.7	2.6	2.3	1.0	0.9	0.4	0.4	0.07
			12/23/2016	22.2	78.8	39.6	6.0	4.7	0.9	27.8	3.0	2.5	2.1	1.0	0.9	0.4	0.4	0.06
			12/24/2016	20.9	80.4	40.2	6.2	4.7	0.8	28.8	2.7	2.4	2.0	0.9	0.8	0.4	0.3	0.06
			12/25/2016	20.7	80.7	40.3	6.1	4.7	0.8	29.0	2.7	2.4	2.0	0.8	0.8	0.4	0.3	0.06
			12/26/2016	20.7	81.1	40.7	6.2	5.1	0.8	28.6	2.5	2.4	2.1	0.8	0.8	0.4	0.3	0.06
			12/27/2016	20.8	81.2	40.8	6.2	5.1	0.8	28.6	2.4	2.4	2.1	0.8	0.7	0.4	0.3	0.06
		FC	1/16/2017	19.7	79.5	40.8	6.5	4.4	0.9	27.2	2.5	2.7	2.1	1.0	0.8	0.4	0.4	0.06
			1/17/2017	20.5	81.0	41.0	6.4	4.2	0.8	28.8	2.4	2.4	2.1	1.0	0.7	0.4	0.4	0.06
			1/18/2017	20.4	83.2	40.8	6.4	4.0	0.8	31.5	2.6	2.4	2.0	1.0	0.8	0.4	0.4	0.06
			1/19/2017	19.1	81.6	40.9	6.4	4.0	0.7	29.8	2.5	2.2	2.0	1.0	ND	ND	0.3	0.05
			1/20/2017	20.4	82.4	41.4	6.5	4.1	0.9	29.8	2.5	1.8	2.0	1.0	0.8	0.4	0.4	0.06
			1/21/2017	20.3	81.2	40.9	6.5	4.0	0.9	29.2	2.6	2.1	2.1	1.0	0.8	0.4	0.4	0.06
			1/22/2017	19.6	80.0	40.3	6.4	4.2	0.8	28.5	2.7	2.6	2.1	1.0	0.8	0.4	0.4	0.06
			1/23/2017	18.9	80.3	40.5	6.4	4.3	0.9	28.5	2.5	2.6	2.2	1.0	0.8	0.4	0.4	0.07
			1/24/2017	19.3	82.8	41.1	6.5	4.2	0.8	30.4	2.2	2.2	2.1	0.9	0.7	0.4	0.3	0.06
		FB	2/15/2017	20.3	83.9	42.0	6.2	4.8	0.8	30.3	2.2	1.9	2.1	1.0	0.7	0.4	0.4	0.06
			2/16/2017	20.4	82.4	41.6	6.1	4.7	0.8	29.5	2.3	2.3	2.0	0.9	0.7	0.4	0.4	0.06
			2/17/2017	19.8	83.5	42.3	6.2	4.9	0.8	29.6	2.2	1.8	2.0	1.0	0.7	0.4	0.4	0.06
			2/18/2017	20.3	84.6	43.2	6.2	4.8	0.8	29.9	2.0	1.7	1.9	0.9	0.6	0.4	0.3	0.06
			2/19/2017	20.6	84.4	43.3	6.1	4.7	0.8	29.7	2.0	1.8	1.9	0.9	0.6	0.4	0.3	0.06
			2/20/2017	20.2	83.9	43.0	6.1	5.0	0.9	29.1	2.0	1.9	2.0	1.0	0.7	0.4	0.4	0.06
			2/21/2017	22.3	83.9	42.8	6.2	4.7	0.8	29.6	2.2	1.7	1.8	1.0	0.6	0.4	0.3	0.05
Dried	Batch	S	12/22/2016	55.4	81.1	40.7	6.5	5.5	0.9	27.8	2.5	2.2	2.2	0.9	0.9	0.4	0.4	0.06
			2/15/2017	59.5	84.6	43.2	6.9	5.3	0.7	28.8	1.9	1.6	1.8	0.8	0.6	0.3	0.3	0.05
	Continuous	S	12/14/2016	61.5	80.3	40.8	6.4	4.9	0.9	27.6	2.7	2.4	2.0	0.8	0.8	0.4	0.3	0.05
			12/15/2016	64.0	79.7	40.3	6.1	3.9	0.8	28.9	3.0	2.1	1.6	0.8	0.9	0.4	0.3	0.06
			12/16/2016	58.9	79.7	40.5	6.3	4.6	0.8	27.9	2.9	2.2	1.8	0.8	0.9	0.4	0.3	0.05
			12/17/2016	58.7	79.2	40.1	6.3	5.1	0.9	27.1	3.0	2.3	2.1	0.8	0.9	0.4	0.4	0.06
			12/18/2016	56.1	77.8	39.2	6.2	5.1	0.9	26.8	3.2	2.7	2.2	0.9	0.9	0.4	0.4	0.06
			12/19/2016	57.1	78.7	39.6	6.2	5.2	0.9	27.1	2.9	2.5	2.2	0.9	0.9	0.4	0.4	0.06
			12/20/2016	58.6	80.2	40.4	6.3	5.0	0.8	28.0	2.5	2.4	2.1	0.9	0.9	0.4	0.4	0.05
			12/21/2016	60.0	79.6	40.6	6.4	5.3	0.9	26.7	2.5	2.2	2.2	1.0	0.9	0.4	0.4	0.06
			12/22/2016	58.5	80.9	41.0	6.5	5.4	0.9	27.4	2.4	2.2	2.1	0.9	0.8	0.4	0.4	0.06
			12/23/2016	61.4	80.8	41.3	6.5	5.1	0.8	27.3	2.5	2.2	2.0	0.9	0.8	0.4	0.3	0.05
			12/24/2016	59.5	81.4	41.4	6.5	4.9	0.8	28.1	2.5	2.0	1.9	0.8	0.8	0.4	0.3	0.06
			12/25/2016	61.8	81.6	41.3	6.4	4.7	0.8	28.7	2.5	2.1	1.9	0.8	0.7	0.4	0.3	0.06
			12/26/2016	60.9	81.6	41.2	6.5	5.0	0.8	28.4	2.5	2.3	2.0	0.8	0.8	0.4	0.3	0.06
			12/27/2016	58.8	82.7	41.8	6.6	5.1	0.7	28.7	2.1	2.1	1.9	0.7	ND	ND	0.3	0.05

2.2.4 The general characterization of sludge

The total solids content (*TS*) of dewatered sludge was measured from the difference between the weight of the sludge before and after baking at 105 °C for 24 hours. The volatile total solids content (*VTS*) was measured by weighing of the sludge after baking at 625 °C for four hours with a muffle furnace. The contents of C, H, and N were analyzed with the CHN analyzer (CHN, Micro Corder JM10) and the elemental contents (S, O, Si, Al, P, Ca, Fe, K, Mg, Cl, and so forth) were determined with the X-ray fluorescence analysis (XRF, Lab Center XRF-1800, Shimadzu Corp. Kyoto, Japan). All these data are shown in **Table 2-1**.

2.2.5 Analytical methods

Solid (dewatered sludge, dried sludge, ash) and water samples were digested with concentrated hydrochloric acid and nitric acid using the hot plate method (Japan Sewage Works Association, 2012) (JIS K 0102). The mass of samples used for digestion was 10 g for dewatered sludge, 5 g for dried sludge, 0.5 g for ash, and 100 mL for water. After filtration with paper filter (5B, Kiriyama glass corp., Tokyo, Japan), the digested solution was analyzed with inductively coupled plasma atomic emission spectroscopy (ICP-AES, Thermo Fisher Scientific Waltham, USA) for contents of Al, P, Ca, S, Fe, Mg, K, Mn, Zn, Cu, Na, Pb and Ni, and with the inductively coupled plasma mass spectrometry (ICP-MS, Thermo Fisher Scientific Waltham, USA) for contents of Cr, Ag, As and Cd. Reference material BCR176 (Takaoka et al., 2000) was used to confirm the reliability of the procedure (**Table 2-2**).

Table 2-2. Analytical results of elements in reference material BCR No. 176 (n = 4).

Element	Certified value (mg/kg)	AV (mg/kg)	SD (mg/kg)	RSD (%)	Recovery (%)
Al	94,000	68,411	3,657	5.3	73
P	5,540	3,831	353	9.2	69
Ca	81,000	86,450	1,781	2.1	107
S	34,900	32,507	1,682	5.2	93
Fe	21,300	19,434	761	3.9	91
Mg	20,000	15,428	1,117	7.2	77
K	41,000	31,622	1,159	3.7	77
Mn	1,400	1,474	42.3	2.9	105
Zn	25,770	27,171	676	2.5	105
Cu	1,302	1,300	33.2	2.6	100
Na	31,000	26,412	885	3.4	85
Cr	863	633	56.0	8.8	73
Pb	10,870	10,354	402	3.9	95
Ni	123.5	118.2	5.6	4.7	96
Ag	65	N.A.	–	–	–
As	93.3	N.A.	–	–	–
Cd	470	511	9.0	1.8	109

AV: Average; SD: Standard deviation; RSD: Relative standard deviation; N.A.: Not analyzed.

Total Hg concentrations in sludge, ash, and water samples were determined quantitatively by the heat-vaporizing method using an MA-2000 (Nippon Instruments Corp., Osaka, Japan) without acid digestion or heat pretreatment of the samples.

In total, eighteen elements (Al, Cu, Fe, Mn, Ni, Pb, Zn, Ca, K, Mg, Na, Cd, Cr, As, Ag, P, S, and Hg) were measured. All analyzed results are shown in **Tables 2-1 and 2-3**, and concentrations in solid samples (sludge and ash) are based on dry materials. While concentrations in recycling water and wastewater, fluid sand, and flue gas, are shown in **Table 2-5~2-8**.

2.3 Results and Discussion

2.3.1 Sludge

The proximate properties of dewatered sewage sludge are summarized in **Table 2-3**.

The dewatered sewage sludge had high *VTS* content, which usually means high calorific value; therefore it is feasible for mono-incineration.

Table 2-3. General characteristics of dewatered and dried sludges in **GS**, **FB**, and **FC**. Data are based on average results from batch sampling between December 2016 and February 2017.

Incinerator	GS		FB	FC	Average	Yahya (2018)
Sludge	Dewatered	Dried	Dewatered	Dewatered	Dewatered	Dewatered
TS (wt %)	20.1 ± 0.3	57.5 ± 2.1	15.5 ± 1.3	18.6 ± 0.2	18.1 ± 2.1	20.2 ± 3.4
VTS (wt %)	81.2 ± 1.3	82.9 ± 1.8	80.8 ± 1.5	80.7 ± 0.2	80.9 ± 1.2	79.9 ± 6.6
Elemental analysis (wt %)						
C	40.8 ± 1.1	41.9 ± 1.2	41.5 ± 0.4	40.9 ± 0.7	41.1 ± 0.9	39.8 ± 3.5
H	6.4 ± 0.2	6.7 ± 0.2	6.6 ± 0.1	6.3 ± 0.2	6.4 ± 0.2	6.5 ± 0.5
N	4.8 ± 0.1	5.4 ± 0.1	4.6 ± 0.03	4.1 ± 0.5	4.5 ± 0.4	5.7 ± 1.1
S	0.9 ± 0.1	0.8 ± 0.1	0.8 ± 0.02	0.8 ± 0.01	0.8 ± 0.05	1.3 ± 0.4
O	37.3 ± 0.3	36.3 ± 0.1	36.7 ± 0.1	37.6 ± 1.0	37.2 ± 0.7	27.1 ± 3.1
Si	2.4 ± 0.3	2.2 ± 0.3	2.5 ± 0.2	2.8 ± 0.1	2.6 ± 0.3	2.2 ± 0.8
Al	2.3 ± 0.3	1.9 ± 0.3	2.2 ± 0.2	2.4 ± 0.1	2.3 ± 0.2	1.2 ± 0.6
P	2.1 ± 0.1	2.0 ± 0.2	2.0 ± 0.04	2.1 ± 0.04	2.1 ± 0.1	2.8 ± 0.7
Ca	0.9 ± 0.002	0.9 ± 0.1	1.0 ± 0.01	0.9 ± 0.1	0.9 ± 0.1	1.3 ± 0.5
Fe	0.8 ± 0.1	0.7 ± 0.1	0.8 ± 0.1	0.8 ± 0.03	0.8 ± 0.1	2.2 ± 1.5
K	0.4 ± 0.02	0.4 ± 0.04	0.4 ± 0.01	0.4 ± 0.01	0.4 ± 0.02	0.4 ± 0.1
Mg	0.4 ± 0.02	0.3 ± 0.03	0.4 ± 0.02	0.4 ± 0.01	0.4 ± 0.02	0.6 ± 0.3
Cl	0.06 ± 0.004	0.06 ± 0.01	0.06 ± 0.002	0.07 ± 0.01	0.06 ± 0.01	N.D.

TS: total solids contents; *VTS*: total volatile solids content; N.D.: No data.

In average, the dewatered sludge had a high *VTS* content of 80.9 ± 1.2%, with the contents of C, H, N, S and O as 41.1 ± 0.9%, 6.4 ± 0.2%, 4.5 ± 0.4%, 0.8 ± 0.05% and 37.2 ± 0.7%, respectively. Other elements (P, Ca, K and Mg) showed comparable contents to the average value reported in Japan (Yahya, M.,2018) and were lower than previous investigations conducted elsewhere (Cieślik and Konieczka, 2017; Ronda et al., 2019; Thomsen et al., 2017). The content of Al, however, was 2.3 ± 0.2%, higher than the average content (1.2%) in Japan (Yahya, M., 2018). The high Al is caused by the mixed sludge from the water treatment plant, in which polychlorinated aluminum is used as flocculants. The

Cl content in SS was 0.06%, being lower than 0.2–0.3% that reported to affect the speciation of heavy metals in SS combustion (Marani et al., 2003).

Table 2-4. Elemental concentrations in sludges in **GS**, **FB**, and **FC**. All concentrations are based on dry matter.

Incinerator	**GS**		**FB**	**FC**
Sample	Dewatered sludge	Dried sludge	Dewatered sludge	Dewatered sludge
Element	*c* (mg/kg)			
Al	23200 ± 2190	17600 ± 2430	21800 ± 2210	20800 ± 2090
P	18700 ± 957	16000 ± 1220	18300 ± 1810	15600 ± 2090
Ca	7650 ± 292	6780 ± 542	8370 ± 1030	7060 ± 212
S	7820 ± 413	6660 ± 479	7740 ± 710	7030 ± 630
Fe	8140 ± 853	7060 ± 1140	7670 ± 696	6420 ± 278
Mg	2590 ± 92	2300 ± 195	2580 ± 271	2320 ± 185
K	2370 ± 64	2240 ± 255	2500 ± 183	2160 ± 190
Mn	783 ± 39	671 ± 87	747 ± 63.9	627 ± 89.1
Zn	426 ± 9	382 ± 32	458 ± 50.8	470 ± 41.5
Cu	219 ± 7	204 ± 17	235 ± 29.7	227 ± 20
Na	225 ± 19	238 ± 41	210 ± 57.3	240 ± 104
Cr	29.5 ± 1.5	30.5 ± 2.5	25.5 ± 7.5	27.0 ± 6.0
Pb	27.1 ± 3.3	24.3 ± 1.6	27.1 ± 2.8	28.6 ± 3.7
Ni	17.4 ± 2.7	16.6 ± 2.2	19.1 ± 5.8	17.6 ± 1.6
Ag	6.5 ± 0.5	6.0 ± 0	5.5 ± 0.5	9.0 ± 1.0
As	4.5 ± 1.5	5.5 ± 0.5	5.5 ± 1.5	5.0 ± 1.0
Hg	1.6 ± 0.1	1.4 ± 0.1	1.4 ± 0.2	2.0 ± 0.3
Cd	1.0 ± 0	1.0 ± 0	1.0 ± 0	1.0 ± 0

The concentrations of elements in the ISSA are directly affected by the composition of the sludge. **Table 2-4** illustrates the composition of the sludge that fed to incinerators **GS**, **FB,** and **FC**, and elemental analyses showed consistent trends with the proximate analysis results in **Table 2-3**. Besides, some heavy metals were also detected in dewatered sludge under the regulation for fertilizer production. In **GS**, for example, the concentrations of Cr, Pb, Ni, As, Hg and Cd in sludge were 29.5 ± 1.5, 27.1 ± 3.3, 17.4 ± 2.7, 4.5 ± 1.5, 1.6 ± 0.1, 1.0 ± 0 mg/kg, respectively (**Table 2-4**). Concentrations of Cr, Pb, Ni, and Hg

were generally lower than reported data in China (Chen et al., 2012), Korea (Pudasainee et al., 2013), and Italy (Marani et al., 2003); while As, and Cd showed comparable concentrations to sludge reported in Korea (Pudasainee et al., 2013). All these values were higher than the data reported in Sweden (Bhasin, 2017).

To conclude, the SS had major elements as Si, Al, P, Ca, Fe, K, Mg, with comparable value with the average content in Japan. For heavy metals, Cr, Pb, Ni, and Hg had relatively lower concentrations than reported data in other countries like China, Korea, and Italy. Moreover, even fluctuated to some extent for the different sampling periods, concentrations of target elements in sludge were of the same range.

2.3.2 Recycling water and wastewater

During the combustion of the SS, recycling water was used for generating the steam for SS drying, flue gas washing, and cooling down the temperature of ashes. Studies show that, the recycling water may bring a significant amount of heavy metals to the total mass balance for the SS incineration process due to the large volume used (Balogh and Nollet, 2008). The concentrations of elements in the recycling water and wastewater in **GS**, **FB**, and **FC** are summarized in **Table 2-5**.

The element concentrations, including heavy metals (**Table 2-5**) measured in the recycling water were low, and even below the standards for tap water (MHLW) or sewage effluent (Ministry of the Environment).

Table 2-5. Elemental concentrations (*c*[mg/L]) in recycling water in **GS**, **FB**, and **FC**.

Incinerator	**GS**			**FB**	**FC**
Sample	Treated water for drying	Treated water for WS	Water for wet ESP	Treated water for WS	Treated water for WS
Element	*c* (mg/L)				
Al	0.07 ± 0.04	0.07 ± 0.04	0.001 ± 0.03	0.06 ± 0.05	0.08 ± 0.06
P	1.0 ± 0.1	1.0 ± 0.1	N.D	0.8 ± 0.04	0.7 ± 0.03
Ca	17.6 ± 0.3	17.6 ± 0.3	14.3 ± 0.4	18.3 ± 0.4	18.4 ± 0.2
S	15.8 ± 2	15.8 ± 2	4.5 ± 0.5	13.8 ± 2.5	13.3 ± 3.5
Fe	0.29 ± 0.14	0.29 ± 0.14	0.7 ± 0.21	0.15 ± 0.07	0.08 ± 0.02
Mg	4.1 ± 0.1	4.1 ± 0.1	2.4 ± 0.02	4.1 ± 0.1	4.1 ± 0.1
K	7.7 ± 0.4	7.7 ± 0.4	1.3 ± 0.03	7.1 ± 0.5	7.0 ± 0.8
Mn	0.04 ± 0.02	0.04 ± 0.02	0.004 ± 0	0.08 ± 0.003	0.06 ± 0
Zn	0.03 ± 0.002	0.03 ± 0.002	0.01 ± 0.01	0.05 ± 0.01	0.04 ± 0.01
Cu	0.01 ± 0.001	0.01 ± 0.001	0.001 ± 0.001	0.01 ± 0.002	0.01 ± 0.001
Na	36.2 ± 1.6	36.2 ± 1.6	8.2 ± 0.3	36.8 ± 5.3	34.8 ± 7
Cr	0.1 ± 0	0.1 ± 0	0.1 ± 0	<0.2	<0.2
Pb	0.006 ± 0.003	0.006 ± 0.003	N.D.	0.001 ± 0.01	N.D.
Ni	N.D.	N.D.	0.006 ± 0.005	0.002 ± 0.009	0.008 ± 0.009
Ag	0.01 ± 0	0.01 ± 0	0.01 ± 0	<0.01	<0.01
As	0.01 ± 0	0.01 ± 0	0.01 ± 0	<0.01	<0.01
Hg	0.004 ± 0.003	0.004 ± 0.003	0.003 ± 0.002	0.00004 ± 0	0.004 ± 0
Cd	0.002 ± 0	0.002 ± 0	0.002 ± 0	<0.003	<0.003

In wastewater, however, significant increases in concentrations of S and Na were observed from WS in **F-types** (**Table 2-6**). The increase in S concentration in wastewaters may be related to the accumulation of S in the slurry at WS and the possible inhomogeneity that can hardly be avoided by the one-spot sampling of wastewater from WS. The increase in Na concentrations in wastewaters is by large caused by the addition of caustic soda that used for acid gas (SO_2 and SO_3) removal at WS. Since no specific Na removal procedures were adopted in SS mono-incineration process, the concentration of Na was accumulated and elevated in wastewaters from WS.

Table 2-6. Elemental concentrations (*c*[mg/L]) in wastewater in **GS**, **FB**, and **FC**.

Incinerator	**GS**				**FB**	**FC**
Sample	Wastewater from mist separator	Wastewater from WS	Wastewater from wet ESP	Wastewater from ash conveyor	Wastewater from WS	Wastewater from WS
Element	*c* (mg/L)					
Al	0.09 ± 0.05	0.13 ± 0.05	0.02 ± 0.05	21.9 ± 0.5	0.1 ± 0.04	0.17 ± 0.07
P	1.0 ± 0.02	1.5 ± 0.3	6.1 ± 1.4	20.1 ± 2.0	0.8 ± 0.2	0.9 ± 0.3
Ca	16.6 ± 0.9	18.3 ± 0.5	17.2 ± 0.3	32.5 ± 1.1	17.6 ± 0.5	17.8 ± 0.2
S	14.2 ± 1.7	59.8 ± 2.7	27.4 ± 1.5	20.7 ± 0.8	48.5 ± 8	56.6 ± 8.2
Fe	0.09 ± 0.01	0.21 ± 0.17	0.07 ± 0.01	9.6 ± 0.3	0.13 ± 0.09	0.23 ± 0.17
Mg	3.9 ± 0.2	4.3 ± 0.1	4.1 ± 0.1	7.6 ± 0.3	4 ± 0.1	4.0 ± 0.1
K	7.0 ± 0.4	7.9 ± 0.4	8.4 ± 0.2	12.0 ± 0.3	8.1 ± 0.7	7.9 ± 0.9
Mn	0.02 ± 0.0004	0.02 ± 0.001	0.02 ± 0.001	1.0 ± 0.04	0.06 ± 0.01	0.07 ± 0.01
Zn	0.04 ± 0.01	0.52 ± 0.07	10.7 ± 1.5	0.4 ± 0.08	0.04 ± 0.004	0.05 ± 0.02
Cu	0.01 ± 0	0.02 ± 0.003	0.12 ± 0.01	0.27 ± 0.03	0.01 ± 0.002	0.01 ± 0.004
Na	34.9 ± 5.0	34.2 ± 1.7	34.9 ± 3.2	36.9 ± 3.2	100.7 ± 9.4	99.1 ± 12.5
Cr	0.1 ± 0	0.1 ± 0	0.1 ± 0	0.1 ± 0	<0.2	<0.2
Pb	0.003 ± 0.005	0.046 ± 0.003	1.1 ± 0.2	0.04 ± 0.004	0.003 ± 0.002	N.D.
Ni	0.005 ± 0.002	0.006 ± 0.007	N.D.	0.04 ± 0.004	0.005 ± 0.002	0.005 ± 0.004
Ag	0.01 ± 0	0.01 ± 0	0 ± 0	0.01 ± 0	<0.01	<0.01
As	0.01 ± 0	0.01 ± 0	0.2 ± 0.02	0.01 ± 0	<0.01	<0.01
Hg	0.002 ± 0.002	0.01 ± 0.001	0.01 ± 0.001	0.003 ± 0.0005	0.003 ± 0.003	0.01 ± 0.003
Cd	0.002 ± 0	0.002 ± 0	0.04 ± 0.005	0.002 ± 0	<0.003	<0.003

ESP: electrostatic precipitator; WS: wet scrubber; N.D.: not detected; < 0.01: concentration lower than the limit of quantification.

2.3.3 Ash

After the combustion, the residues generated, namely the ISSA, are of great concern. On the one hand, nutrients such as P enriches in the ISSA and can be recycled for fertilizer production; on the other hand, heavy metals also condensed in the ISSA. Therefore, a comprehensive survey of elemental concentrations in the generated ISSA from the incinerator **GS**, **FB**, and **FC** were conducted, as shown in **Table 2-7**. Compared with the SS, the ISSA showed significant enrichment in concentrations of most elements. The major elements in the ISSA were Al, P, Ca, and Fe, being consistent with that reported in the

literature (Donatello and Cheeseman, 2013). Amongst, P showed high concentrations as 86,400~92,000 mg/kg-dry, higher than the reported data from Germany (Krüger et al., 2014), but comparable with the average value worldwide (Donatello and Cheeseman, 2013). Meanwhile, some elements, e.g., Hg, showed even lower concentrations in the ISSA than in the SS. With higher P content but lower concentrations of heavy metals, the ISSA has the potential to be recycled in the fertilizer production.

Moreover, different tendencies in concentrations of heavy metals such as Zn, Pb, Ag, As, and Cd were found among ISSA in GS, FB, and FC. These differences associated with the incinerator type may significantly affect the recycling and disposal of the ISSA in these incinerators, and therefore, should be further clarified.

Table 2-7. Elemental concentrations (*c*[mg/kg-dry]) in ashes **GS**, **FB**, and **FC**.

Incinerator	GS				FB	FC
Sample	Bottom ash	Riddling ash	Boiler dust	Multi-cyclone dust	Bag filter ash	Ceramic filter ash
Element	*c* (mg/kg-dry)					
Al	99,300 ± 8,840	108,000 ± 3,480	102,000 ± 4,400	106,000 ± 3,020	110,000 ± 7,160	123,000 ± 4,880
P	92,000 ± 13,400	94,800 ± 3,480	87,700 ± 6,120	92,700 ± 4,300	87,700 ± 6,560	86,400 ± 609
Ca	41,900 ± 7,220	42,700 ± 3,070	40,300 ± 4,180	44,100 ± 3,130	39,500 ± 3,520	36,900 ± 3,750
S	1,610 ± 374	1,570 ± 180	3,410 ± 711	3,510 ± 129	3,900 ± 352	4,110 ± 269
Fe	39,800 ± 2,730	41,500 ± 2,820	42,700 ± 2,510	43,700 ± 2,180	41,600 ± 3,190	42,700 ± 3,280
Mg	15,800 ± 2,600	16,200 ± 1,160	15,000 ± 1,520	16,300 ± 1,160	14,400 ± 1,320	13,700 ± 435
K	14,000 ± 2,320	14,500 ± 512	13,000 ± 978	13,700 ± 713	13,700 ± 1,030	13,600 ± 378
Mn	4,110 ± 488	4,300 ± 46	3,950 ± 192	4,200 ± 56	3,880 ± 230	3,680 ± 228
Zn	1,270 ± 293	1,380 ± 171	4,330 ± 369	4,520 ± 1,020	2,430 ± 294	2,430 ± 87.3
Cu	1,200 ± 246	1,240 ± 145	944 ± 115	994 ± 97	1,130 ± 117	1,070 ± 41.8
Na	4,000 ± 377	4,090 ± 236	3,620 ± 195	3,780 ± 65	3,020 ± 264	2,840 ± 162
Cr	190 ± 10	220 ± 0	345 ± 15	210 ± 10	185 ± 5	175 ± 5
Pb	53 ± 31	63 ± 31	399 ± 51	445 ± 97	163 ± 31	167 ± 19
Ni	122 ± 18	112 ± 9	200 ± 14	129 ± 4	110 ± 9	112 ± 8
Ag	23.5 ± 3.5	24.0 ± 4.0	49.0 ± 9.0	52.5 ± 6.5	30.5 ± 0.5	32.5 ± 4.5
As	10.0 ± 1.0	15.5 ± 3.5	80.5 ± 29.5	40.0 ± 4.0	32.5 ± 0.5	33.5 ± 3.5
Hg	0.1 ± 0.1	0.1 ± 0.1	0.1 ± 0.1	0.2 ± 0.1	0.5 ± 0.1	0.018 ± 0.002
Cd	1.1 ± 0.9	1.1 ± 0.9	12.0 ± 2.0	10.5 ± 0.5	4.5 ± 1.5	3.5 ± 0.5

2.3.4 Flue gas

Apart from the ISSA, a small fractions of heavy metals are considered to be emitted

from the flue gas. The monitoring results of concentrations of heavy metals are shown in **Table 2-8**. Concentrations of all monitored elements, except for Hg, were under the limit of quantification (LOQ). The concentrations of these heavy metals are associated with their species during the combustion. The speciations of Pb and Cd are reported to be affected by the Cl content (Marani et al., 2003; Yu et al., 2017), for which the higher Cl enables higher volatilization of these elements. However, Pb and Cd were unable to be detected in the flue gas, which may be related to the relatively lower Cl content of ~0.06% in the SS (**Table 2-3**).

Table 2-8. Elemental concentrations (c[μg/Nm^3]) in flue gases in **GS**, **FB**, and **FC**.

Element (μg/Nm^3)	Incinerator		
	GS	**FB**	**FC**
Cr	<0.01	<0.01	<0.01
Pb	<0.01	<0.01	<0.01
Ag	<0.01	<0.01	<0.01
As	<0.01	<0.01	<0.01
Hg	0.014 ± 0.003	0.018 ± 0.002	0.005 ± 0.003
Cd	<0.01	<0.01	<0.01

2.4 Summary

The concentrations of elements in sludge, water, ash, and flue gas were monitored in all three SS mono-incinerators. Since the same dewatered sludge was used as the feed, the composition of SS was found to be comparable. In SS, major elements are C > O > H > N > Si > Al > P > Ca > S > Fe in the decreasing order. In the recycling water, the concentrations of all the elements were below the standards for tap water (MHLW) or sewage effluent (Ministry of the Environment). In ashes, concentrations of almost all the elements, e.g., P, showed significant increases. However, the concentration of Hg was lower in the ashes than in the SS. Moreover, different enrichment behaviors of heavy metals in

the ISSA were found in incinerators **GS**, **FB**, and **FC**, which may also affect the recycling and disposal of the ISSA. In flue gas, only Hg was detected and concentrations of other elements were lower than the limit of quantification.

References

Balogh, S.J., Nollet, Y.H., 2008. Mercury mass balance at a wastewater treatment plant employing sludge incineration with offgas mercury control. Sci. Total Environ. 9, 125–131. https://doi.org/10.1016/j.scitotenv.2007.08.021

Bhasin, A., 2017. Recovery of phosphorus from incineration of sewage sludge study at Fortum Värme. (KTH institute of technology, School of chemical and engineering)

Chen, H., Yan, S., Ye, Z., Meng, H., Zhu, Y., 2012. Utilization of urban sewage sludge: Chinese perspectives. Environ. Sci. Pollut. Res. 19, 1454–1463. https://doi.org/10.1007/s11356-012-0760-0

Cieślik, B., Konieczka, P., 2017. A review of phosphorus recovery methods at various steps of wastewater treatment and sewage sludge management. The concept of "no solid waste generation" and analytical methods. J. Clean. Prod. 142, 1728–1740. https://doi.org/10.1016/j.jclepro.2016.11.116

Donatello, S., Cheeseman, C.R., 2013. Recycling and recovery routes for incinerated sewage sludge ash (ISSA): a review. Waste Manage. 33(11), 2328–40. https://doi.org/10.1016/j.wasman.2013.05.024

Goldstone, M. E., P. W. W. Kirk, J. N. Lester., 1990. The behaviour of heavy metals during wastewater treatment II. Lead, nickel and zinc. Sci. Total Environ. 253–270.

Hargreaves, A.J., Vale, P., Whelan, J., Constantino, C., Dotro, G., Cartmell, E., 2016. Mercury and antimony in wastewater: Fate and treatment. Water. Air. Soil Pollut. 227. https://doi.org/10.1007/s11270-016-2756-8

Karvelas, M., Katsoyiannis, A., Samara, C., 2003. Occurrence and fate of heavy metals in the wastewater treatment process. Chemosphere 53, 1201–1210. https://doi.org/10.1016/S0045-6535(03)00591-5

Krüger, O., Grabner, A., Adam, C., 2014. Complete survey of German sewage sludge ash. Environ. Sci. Technol. 48, 11811–11818. https://doi.org/10.1021/es502766x

Liu, J., Fu, J., Ning, X., Sun, S., Wang, Y., Xie, W., Huang, S., Zhong, S., 2015. An experimental and thermodynamic equilibrium investigation of the Pb, Zn, Cr, Cu, Mn and Ni partitioning during sewage sludge incineration. J. Environ. Sci. (China) 35, 43–54. https://doi.org/10.1016/j.jes.2015.01.027

Marani, D., Braguglia, C.M., Mininni, G., Maccioni, F., 2003. Behaviour of Cd, Cr, Mn, Ni, Pb, and Zn in sewage sludge incineration by fluidised bed furnace. Waste manag. 23(2), 117–124.

Ministry of Health, Labour and Welfare (22 July, 2019 accessed) Tap water quality standard. https://www.mhlw.go.jp/stf/seisakunitsuite/bunya/topics/bukyoku/kenkou/suido/kijun/kijunchi.html

Ministry of the Environment (22 July, 2019 accessed) National Effluent Standard. https://www.env.go.jp/en/water/wq/nes.html

Pudasainee, D., Seo, Y.C., Kim, J.H., Jang, H.N., 2013. Fate and behavior of selected heavy metals with mercury mass distribution in a fluidized bed sewage sludge incinerator. J. Mater. Cycles Waste Manag. 15, 202–209. https://doi.org/10.1007/s10163-013-0115-z

Ronda, A., Gómez-Barea, A., Haro, P., de Almeida, V.F., Salinero, J., 2019. Elements partitioning during thermal conversion of sewage sludge. Fuel Process. Technol. 186, 156–166. https://doi.org/10.1016/j.fuproc.2019.01.001

Takaoka, M., Nakatsuka, D., Takeda, N., Fujiwara, T., 2000. Application of X-ray fluorescence analysis to determination of elements in fly ash. J. Jpn. Soc. Waste Manage. 11(6), 333-342. (in Japanese)

Thomsen, T.P., Sárossy, Z., Ahrenfeldt, J., Henriksen, U.B., Frandsen, F.J., Müller-Stöver, D.S., 2017. Changes imposed by pyrolysis, thermal gasification and incineration on composition and phosphorus fertilizer quality of municipal sewage sludge. J. Environ. Manage. 198, 308–318. https://doi.org/10.1016/j.jenvman.2017.04.072

Van de Velden, M., Dewil, R., Baeyens, J., Josson, L., Lanssens, P., 2008. The distribution of heavy metals during fluidized bed combustion of sludge (FBSC). J. Hazard. Mater. 151, 96–102. https://doi.org/10.1016/j.jhazmat.2007.05.056

Yahya, M., 2018. Heating value and energy recovery potential of sewage sludge and suspended solids in municipal wastewater treatment plant (Dissertation, Kyoto University, Japan).

Yoshida, H., Christensen, T.H., Guildal, T., Scheutz, C., 2015. A comprehensive substance flow analysis of a municipal wastewater and sludge treatment plant. Chemosphere 138, 874–882. https://doi.org/10.1016/j.chemosphere.2013.09.045

Yu, S., Zhang, B., Wei, J., Zhang, T., Yu, Q., Zhang, W., 2017. Effects of chlorine on the volatilization of heavy metals during the co-combustion of sewage sludge. Waste Manag. 62, 204–210. https://doi.org/10.1016/j.wasman.2017.02.029

Chapter 3 Mass balance and distribution of elements in incinerators

3.1 Introduction

Understanding the environmental fate of metals, including their transformation and distribution pathways, is essential for improving the operating conditions of incineration plants to control behavior and emission of the pollutants. Previous studies mostly focused on co-combustion of sewage sludge with municipal solid wastes (MSW), coal (Lee and Wilcox, 2017; Nadziakiewicz and Kozioł, 2003; Niu et al., 2018; Spliethoff et al., 2000; Zhang et al., 2013; Zhao et al., 2019) or wood (Åmand and Leckner, 2004; Elled et al., 2007). Few researchers investigated heavy metals during incineration of sewage sludge (Balogh and Nollet, 2008; Kasina et al., 2017; Pudasainee et al., 2013; Takaoka et al., 2012; Van de Velden et al., 2008; Yoshida et al., 2015) and mostly concentrated on behavior of heavy metals in fluidized bed incinerators as they are applied widely. However, step grate incinerators also have advantages associated with the lower construction investment, lower exploitation cost, and simple operation. Therefore, investigation of the behavior of heavy metals in such stokers should be of high significance including differences between fluidized bed and step grate incinerators.

Moreover, **Chapter 2** demonstrated different enrichment behaviors of heavy metals in ISSA from the step grate stoker and fluidized bed incinerators, which may further affect the recycling and disposal of the ISSA. Therefore, the purposes of this chapter are: (1) to investigate the distribution of heavy metals in the ISSA; (2) to compare the differences in the behavior of heavy metals between the step grate stoker and fluidized bed incinerator; and (3) to evaluate the potential of the ISSA for fertilizer production.

3.2 Methodology

3.2.1 The calculation of enrichment factor and mass balance

Based on experimental data in **Tables 2-4** and **3-1**, we calculated the enrichment factor in ashes and the mass balance in incinerators **GS**, **FB**, and **FC**.

During combustion, elements in sludge were either concentrated in the solid phase (e.g., particles or adsorbed on particles then collected as ash) or emitted into the gas phase and treated by the APCDs. The enrichment factor (E_f) of elements in ash was therefore defined as in equation (1):

$$E_f = \frac{c_{ash}}{c_{sludge}} \quad (1)$$

Where c_{ash} (mg/kg) and c_{sludge} (mg/kg) represent the concentrations of elements in the ash and sludge, respectively.

The recycling water contains significant amounts of heavy metals (Balogh and Nollet, 2008; Van de Velden et al., 2008); therefore, it was also included as the input for mass balance calculation in both sludge drying unit in **GS** and the whole combustion process in each incinerator.

The input to incinerator **GS** included four streams: dewatered sludge, treated water for drying, treated water for WS, and water for wet ESP. The output included eight streams in three kinds: ash (bottom ash, riddling ash, boiler dust, and multi-cyclone dust), wastewater (wastewater from mist separator, WS, and wet ESP) and flue gas.

For the drying process in **GS**, the input included dewatered sludge and treated water for drying, while the output consisted of dried sludge and wastewater from mist separator.

The input to **FB** (**FC**) included two streams: dewatered sludge and treated water for WS. The output consisted of three streams: bag filter ash (ceramic filter ash), wastewater from WS, and flue gas.

The fraction of each stream (sludge and recycling water) to the total input for each

element was calculated by equation (2):

$$\text{Mass fraction (\%)} = \frac{Q_i}{Q_{in}} \quad (Q_{in} = \sum Q_i \, , Q_i = c_i \cdot q_i) \tag{2}$$

where Q_i represents the quantity of each stream (mg/h), Q_{in} represents the quantity of total input (mg/h), with c_i (mg/kg or mg/L) and q_i (kg/h or L/h) denotes the concentration and flow rate of elements in each stream of input, respectively.

The mass balance of each element during combustion was assessed by the recovery rate. The recovery rate was defined as the ratio of the total output of each element to the input, as shown in equation (3):

$$\text{Recovery rate (\%)} = \frac{Q_{out}}{Q_{in}} \quad (Q_{out} = \sum Q_k \, , Q_k = c_k \cdot q_k) \tag{3}$$

where Q_{out} denotes the output quantity (mg/h); c_k (mg/kg or mg/L) and q_k (kg/h or L/h) represents the concentration and flow rate of elements in each stream of output, respectively.

In the flue gas, elements with concentrations under the limit of quantification (LOQ), namely Cr, Pb, Ag, As, and Cd (**Table 2-8**), were not included in the calculations of recovery rates in all incinerators. Only Hg in the flue gas was involved in the mass balance.

3.2.2 Thermodynamic calculation

Thermodynamic equilibriums across the **GS**, **FB**, and **FC** were estimated using *FactSage* software (version 6.1) under Equilib mode (Bale et al., 2016). This mode assumes that chemical equilibrium is achieved in the combustion chamber.

All parameters were set according to the operating conditions in each incinerator. The input mass of each element was calculated based on concentrations and flow rates of sludge using the data collected in **Tables 2-4 and 3-1**. Calculations were conducted at 850 °C (combustion) and 250 °C (secondary interactions at dust collectors: multi-cyclone, bag, and ceramic filters in the **GS**, **FB**, and **FC**, respectively) at atmospheric pressures of 100.485, 100.805, and 100.915 Pa in the **GS**, **FB**, and **FC**, respectively.

Table 3-1. Flow rates (q) of sludge, water, wastewater, ash, and flue gas in a step grate stoker (**GS**) and fluidized bed incinerators equipped with the bag (**FB**) and ceramic (**FC**) filters.

Input							**Output**								
Sample	Dewatered sludge	Dried sludge	Air	Treated water for drying	Treated water for WS	Water for wet ESP	Wastewater from mist separator	Wastewater from WS	Wastewater from wet ESP	Wastewater from ash conveyor	Main ash[a]	Riddling ash	Boiler dust	Multi-cyclone dust	Flue gas
Flow rate (q)	(t/h wet basis)		(Nm^3/h)		(m^3/h)			(m^3/h)			(kg/h)				(Nm^3/h)
GS	5.5 ± 0.2	2.1 ± 0.04	5810	72.5 ± 0.5	130 ± 0	5.8 ± 0.3	75.9 ± 0.7	131 ± 0	6 ± 0	44.3 ± 0.3	212 ± 23	2.9 ± 0.8	0.05 ± 0.004	0.6 ± 0.2	11200 ± 250
FB	2.4 ± 0.8		10869		140.5 ± 8.5			145.6 ± 10.6			88.3 ± 33.0				13200 ± 250
FC	3.7 ± 0.6		11259		149.5 ± 0.5			151.2 ± 0.8			120 ± 34				16000 ± 1250
TS/*SS* %	(wt %)			(mg/L)			(mg/L)				(wt %)				
GS	20.1 ± 0.3	57.5 ± 2.1		2 ± 0	2 ± 0	0.5 ± 0	18.5 ± 1.5	3.5 ± 0.5	35 ± 0	205 ± 25					
FB	15.5 ± 1.3				4.1 ± 0.7			25.4 ± 21.9			99.7 ± 0.02				
FC	18.6 ± 0.2				3 ± 0.5			25.5 ± 22.2			99.9 ± 0				
VTS/*VSS* %	(wt %)			(mg/L)			(mg/L)				(wt %)				
GS	81.2 ± 1.3	82.9 ± 1.8													
FB	80.8 ± 1.5				3.2 ± 0.4			7.7 ± 0			0.6 ± 0.02				
FC	80.7 ± 0.2				0.8 ± 0.3			2.3 ± 1.5			0.5 ± 0.1				

[a]Main ash refers to bottom ash in the **GS**, bag filter ash in **FB**, and ceramic filter ash in **FC**.

Different input data were used for the simulation at 250 °C. In the **GS**, since the bottom and riddling ashes are removed at the combustion unit, only combustion components in the gas phase from 850 °C were used in the simulation at 250 °C, while in **FB** and **FC**, the simulations at the dust collectors (250 °C) were performed using the same input data as for combustion. The input data for the thermodynamic calculations are summarized in **Tables 3-2**, **3-3**, and **3-4**. Equilibriums are summarized in **Table 3-5**.

Table 3-2. Input data to the *FactSage* software for **GS**. In the **GS**, since the bottom and riddling ashes are removed at the combustion unit, only combustion components in the gas phase from 850 °C were used in the simulation at 250 °C for the secondary reactions of the combustion components at the APCDs.

Combustion condition					
Temperature	850 °C				
Pressure	100.485 kPa				
Flow rate (kg/h)					
Dried sludge				Combustion air	
Combustible component		Incombustible component			
C	525.9	H_2O	887.7	N_2	7,872
O	483.5	Si	34.1	O_2	2,408
H	82.2	Al	29.3	H_2O	83
N	64.3	P	26.1		
S	10.9	Fe	11.0		
		Ca	10.8		
		K	5.1		
		Mg	4.3		
		Mn	0.8		
		Cl	0.7		
		Zn	0.5		
		Na	0.3		
		Cu	0.2		
		Cr	0.04		
		Pb	0.03		
		Ni	0.03		
		Ag	0.01		
		As	0.01		
		Hg	0.002		
		Cd	0.001		

Table 3-3. Input data to the FactSage software for **FB**. The combustion components were calculated at 850 °C, and the secondary reactions of combustion components at the APCDs were estimated at 250 °C, with other conditions consistent with the combustion at 850°C.

Combustion condition					
Temperature	850 °C				
Pressure	100.805 kPa				
Flow rate (kg/h)					
Dewatered sludge				Combustion air	
Combustible component		Incombustible component			
C	251.0	H_2O	2,650	N_2	10,517
O	223.8	Si	16.1	O_2	3,217
H	39.6	Al	14.3	H_2O	77
N	27.9	P	12.6		
S	5.2	Ca	5.9		
		Fe	5.2		
		K	2.5		
		Mg	2.4		
		Mn	0.43		
		Cl	0.39		
		Zn	0.25		
		Na	0.15		
		Cu	0.13		
		Pb	0.015		
		Pb	0.014		
		Ni	0.013		
		Cr	0.011		
		As	0.004		
		Ag	0.004		
		Hg	0.001		
		Cd	0.0006		

Table 3-4. Input data to the FactSage software for **FC**. The combustion components were calculated at 850 °C, and the secondary reactions of combustion components at the APCDs were estimated at 250 °C, with other conditions consistent with the combustion at 850 °C.

Combustion condition					
Temperature	850 °C				
Pressure	100.915 kPa				
Flow rate (kg/h)					
Dewatered sludge				Combustion air	
Combustible component		Incombustible component			
C	322.7	H_2O	3,454	N_2	10,895
O	284.1	Si	21.0	O_2	3,332
H	50.2	Al	17.4	H_2O	80
N	35.8	P	16.3		
S	6.5	Ca	6.3		
		Fe	5.9		
		K	3.0		
		Mg	2.7		
		Mn	0.56		
		Cl	0.48		
		Zn	0.40		
		Cu	0.19		
		Na	0.11		
		Pb	0.023		
		Cr	0.016		
		Ni	0.013		
		Ag	0.008		
		As	0.005		
		Hg	0.001		
		Cd	0.001		

3.3 Results and Discussion

3.3.1 Enrichment factor

During the incineration of dewatered sludge, organic matter, characterized as *VTS*, turned into the flue gas. Inorganic matter, on the other hand, is expected to remain in the solid phase as the ash. Thus, after combustion, the mass of solid phase (turned into ash) decreased to the same as the inorganic matter contained, which would be 19.1% (*VTS*: 80.9%) as the original amount of sludge on a dry matter basis. Assume that compounds formed by inorganic elements during the incineration were in the solid phase, then

concentrations of these elements in the incineration ash would consequently be elevated to about 5-fold compared with their concentrations in the sludge (dry matter basis).

However, depending on the thermodynamic characteristics of elements contained, a certain fraction of inorganic matter may also distribute into the gaseous phase. To discuss the enrichment behavior of elements clearly in the incineration ash, we classified all target elements into three groups according to their dominant species and practical partitioning in ashes as non-volatile elements (Al, P, Ca, Fe, Mg, K, Mn, Cu, Na, Cr, and Ni), semi-volatile elements (Zn, Pb, Ag, As and Cd), and volatile elements (Hg and S). It should be born in mind that, due to the different feed and type of incinerators used, the definition of each group varies (Elled et al., 2007; Gerstle and Albrinck, 1982; Marani et al., 2003; Yang et al., 1994).

3.3.1.1 Enrichment of elements in ashes in the step grate stoker

In **GS**, non-volatile elements, except for Na, showed E_f as about 5.0 (**Fig.3-1**), which is in agreement with the previous hypothesis. Sodium, however, enriched 16~18 folds in all ashes, indicating extra input of Na. This extra input is considered to be introduced by the recycling water, in which significant concentrations of Na detected (**Table 2-5**), used for cooling down the flue gas temperature.

Moreover, Cr and Ni enriched more than 5-fold in all ashes, with unusually high E_f of 12 present in the boiler dust. Since only a low concentration of Cr and no Ni were detected in the recycling water (**Table 2-5**), the high E_f (> 5.0) may be caused by the underestimated amount of Cr and Ni in the dewatered sludge for the fluctuation and heterogeneity. The high enrichment in the boiler dust, however, is contradictory to the thermodynamic results, from which all generated compounds of Cr and Ni are in the solid-phase. Therefore, it is expected to distribute comparably in different ashes. Nevertheless, similar high concentrations of Cr and Ni were also reported in ashes with smaller particle sizes in a fluidized bed incinerator for sewage sludge and wood co-combustion, although Cr and Ni were also predicted to be non-volatile (Elled et al., 2007).

Semi-volatile elements, such as Zn, Pb, Ag, As, and Cd, featured unique enrichment behavior among ashes. Compared with the bottom and riddling ashes (E_f < 4), these elements enriched greater in the boiler and multi-cyclone dust (E_f: 8~18). Previous research (Huang et al., 2004; Meij and te Winkel, 2007; Zhang et al., 2008) on coal-fired plants and municipal solid waste incinerators, in which similar APCDs and ash removal procedures to the step grate stoker were used, reported similar tendency that Zn, Pb, As, and Cd enriched greater in fly ashes than the bottom ash. The different enrichment in various ashes may be caused by the combined effect of temperature and particle size, which would be discussed later in this section.

Volatile elements, namely S and Hg, almost not enriched in ashes, which is in agreement with the thermodynamic results both at 850 and 250 °C (**Table 3-5**). The extremely low enrichment (E_f <0.1) of Hg, was comparable to the previous research (Pudasainee et al., 2013; Takaoka et al., 2012), even we used different sludge and incinerators. The detected enrichment of S, which was very low in all ashes (E_f<0.4), could be ascribed to the inorganic S (Sommers et al., 1977) contained in the sludge which is expected to settle in the ash rather than gas phase (Pilch and Grill, 1995). While the higher enrichment of S in boiler and multi-cyclone dust may be caused by the secondary interactions of SO_2 and SO_3 with metals in the flue gas, enabling the formation of fine particles. Moreover, ash particles also adsorbed some S compounds, and smaller-sized fly ash (boiler and multi-cyclone dust) having larger surface area are consequently more favorable for the adsorption.

In GS, bottom and riddling ashes, which were mainly coarse particles **(Table 3-6**), were discharged at the combustion temperature of 850 °C. At this temperature, semi-volatile elements such as Pb, Ag, As and Cd in combustion products were present in the gas phase (**Table 3-5**). Only a small amount of these gaseous components were adsorbed on coarse particles and discharged right after combustion, leading to a low enrichment of these elements in the bottom and riddling ashes. The remaining of these elements, subsequently, were entrained in the flue gas.

During the treatment of the flue gas, the temperature decreased from 850 to 250 °C. With the decrease of temperature, the vapor pressures of semi-volatile elements and their salts also drop drastically (Van de Velden et al., 2008), which favor the transition of phase from gas to the solid. Consequently, at 250 °C, combustion products of semi-volatile elements tend to exist in their solid phase. Besides, secondary interactions may also occur among combustion products due to the decrease in temperature. At 250 °C, new combustion products for Pb, Ag, As, and Cd was formed, of which are the solid phase (**Table 3-5**).

Furthermore, the boiler and multi-cyclone dust also have smaller particle sizes than the bottom and riddling ashes (**Table 3-6**). These smaller-sized fly ash particles themselves may, on the one hand, be composed of small heavy metal particles, representing a condensation of the heavy metal atmosphere (Y. Li et al., 2017); on the other hand, it enables a larger surface area that favorable for adsorption (Elled et al., 2007). As a result, semi-volatile elements enriched higher in fly ash (boiler and multi-cyclone dust) in **GS**.

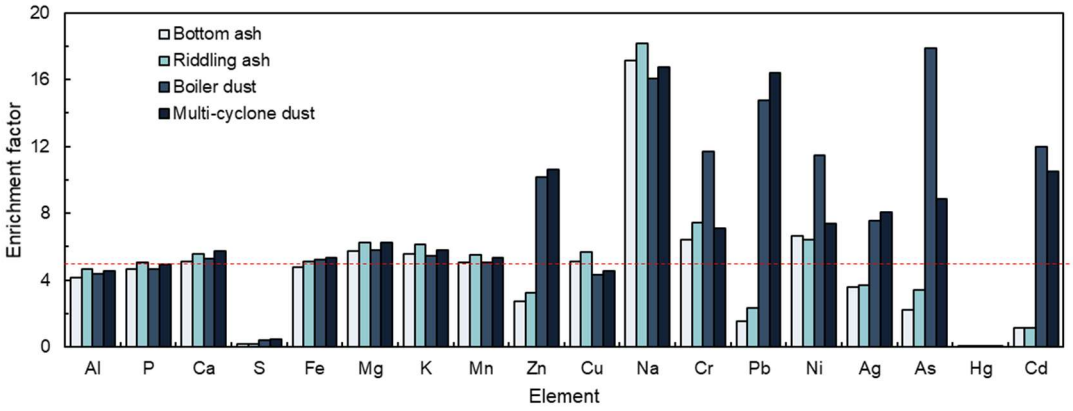

Figure 3-1. Enrichment factors of elements in ashes from the **GS**.

Table 3-5. Thermodynamic equilibriums of elements in **GS**, **FB**, and **FC**. The combustion temperature was 850 °C; the temperature at dust collectors was 250 °C.

	Temperature	850° C			250° C		
	Incinerator	GS	FB	FC	GS	FB	FC
Element	Compound	Mass fraction (%)					
Al	$AlPO_4$ (s)	58	55	61	0	64	71
	Al_2SiO_5 (s)	0	0	0	0	11	28
	$KAl_3Si_3O_{10}(OH)_2$ (s)	0	0	0	0	23	0
	$ZnAl_2O_4$ (s)	0	0	0	0	1	2
	$Mg_2Al_4Si_5O_{18}$ (s)	24	27	21	0	0	0
	KAlSi2O6 (s)	12	12	12	0	0	0
	$Mn_2Al_4Si_5O_{18}$ (s)	3	3	3	0	0	0
	NaAlSi3O8 (s)	1	1	1	0	0	0
	$ZnAl_2O_4$ (s)	1	1	2	0	0	0
	$KAl(SO_4)_2$ (s)	0	0	0	100	0	0
P	$AlPO_4$ (s)	75	72	75	0	84	87
	$Mg_3P_2O_8$ (s)	4	4	5	0	16	13
	$Ca_3(PO_4)_2$ (s)	21	24	20	0	0	0
	$FePO_4$ (s)	0	0	0	100	0	0
Ca	$CaSO_4$ (s)	0	0	0	100	100	100
	$Ca_3(PO_4)_2$ (s)	100	100	100	0	0	0
S	SO_2 (g)	98	85	86	0	0	0
	SO_3 (g)	2	15	14	2	0	0
	$CaSO_4$ (s)	0	0	0	0	91	78
	K_2SO_4 (s)	0	0	0	0	1	15
	$K_3Na(SO_4)_2$ (s)	0	0	0	0	8	5
	$MgSO_4(H_2O)$ (s)	0	0	0	0	0	2
	$O_2S(OH)_2$ (g)	0	0	0	97	0	0
Fe	Fe_2O_3 (s)	98	95	94	0	100	100
	$(CuO)(Fe_2O_3)$ (s)	0	4	6	0	0	0
	$(Cu_2O)(Fe_2O_3)$ (s)	2	0	0	0	0	0
	$Fe_2(SO_4)_3$ (s)	0	0	0	100	0	0
Mg	$Mg_3P_2O_8$ (s)	25	27	38	0	100	96
	Mg2Al4Si5O18 (s)	75	73	62	0	0	0
	$MgSO_4(H_2O)$ (s)	0	0	0	100	0	4
K	K_2SO_4 (s)	0	0	0	0	5	82
	$K_3Na(SO_4)_2$ (s)	0	0	0	100	32	18
	$KAl_3Si_3O_{10}(OH)_2$ (s)	0	0	0	0	64	0
	$KAlSi_2O_6$ (s)	100	100	100	0	0	0
Mn	MnO_2 (s)	0	0	0	0	100	100
	$Mn_2Al_4Si_5O_{18}$ (s)	100	100	100	0	0	0
	$MnSO_4$ (s)	0	0	0	100	0	0
Zn	$ZnAl_2O_4$ (s)	100	100	100	0	100	100
	$ZnSO_4$ (s)	0	0	0	100	0	0
Cu	CuCl (g)	4	2	1	0	0	0
	CuO (s)	0	0	0	0	100	100
	$(CuO)(Fe_2O_3)$ (s)	0	98	99	0	0	0
	$(Cu_2O)(Fe_2O_3)$ (s)	96	0	0	0	0	0
	$CuSO_4$ (s)	0	0	0	100	0	0
Na	$K_3Na(SO_4)_2$ (s)	0	0	0	10	100	100
	$NaAlSi_3O_8$ (s)	100	100	100	0	0	0
	Na_2SO_4 (s)	0	0	0	90	0	0
Cr	Cr_2O_3 (s)	0	0	0	0	100	100
	$(MgO)(Cr_2O_3)$ (s)	100	100	100	0	0	0
	$Cr_2(SO_4)_3$ (s)	0	0	0	100	0	0
Pb	PbO (g)	79	97	97	0	0	0
	$PbCl_2$ (g)	19	2	2	0	0	0
	PbCl (g)	2	0	0	0	0	0
	$(PbO)(Al_2O_3)_6$ (s)	0	0	0	0	100	0
	$PbSO_4$ (s)	0	0	0	100	0	100
Ni	$(NiO)(Fe_2O_3)$ (s)	100	100	100	0	100	100
	$NiSO_4$ (s)	0	0	0	100	0	0
Ag	Ag (g)	2	2	2	0	0	0
	AgCl (g)	98	98	98	0	0	0
	AgCl (s)	0	0	0	0	100	100
	Ag_2SO_4 (s)	0	0	0	100	0	0
As	As_4O_6 (g)	100	100	100	0	0	0
	As_2O_5 (s)	0	0	0	100	100	100
Hg	Hg (g)	100	98	98	0	0	0
	HgO (g)	0	2	2	0	0	0
	$HgCl_2$ (g)	0	0	0	100	100	100
Cd	$Cd(OH)_2$ (g)	62	87	88	0	0	0
	Cd (g)	33	6	6	0	0	0
	CdO (g)	5	7	6	0	0	0
	$CdSO_4$ (s)	0	0	0	100	100	100

(g): gas-phase; (s): solid-phase.

Table 3-6. Particle sizes of various ash.

Incinerator	Sample	$d_{average}$ (μm)			
GS	Boiler dust	141.0			
	Multi-cyclone dust	157.5			
FB	Fluidized sand	843.5			
	Bag filter ash	67.1			
FC	Fluidized sand	947.4			
	Ceramic filter ash	62.1			
		>44 mm	31.7–44 mm	16–31.7 mm	<16 mm
GS	Riddling ash	0%	2%	6%	94%
	Bottom ash	23%	0%	21%	56%

3.3.1.2 Enrichment of elements in ashes from the fluidized bed incinerators

In incinerators **FB** and **FC**, both non-volatile (except for Na) and semi-volatile elements primarily enriched in ashes, with E_f of about 5.0 (**Fig. 3-2**). This enrichment behavior agrees well with the thermodynamic results (**Table 3-5**), in which all combustion products of non-volatile and semi-volatile elements were in the solid phase at both 850 and 250 °C. The same tendency of these elements was also reported in previous research on sewage sludge incineration using the fluidized bed incinerator (Van de Velden et al., 2008). Sodium (Na), as an exception, enriched 14 folds in bag filter and 12 folds in ceramic ash. The high enrichment of Na in **FB** and **FC** were also caused by the use of recycling water in the cooling process of flue gas temperature.

Generally, ceramic filter ash has higher E_f for most elements than that in bag filter ash. The higher enrichment in **FC** was in agreement with the overall enrichment factor calculated by the ratio of ash and sludge in amount (**Table 3-1**), for which the theoretical E_f was 4.9 for **FB** and 5.1 for **FC**. However, slight fluctuations also appeared in some trace elements like Pb, Ag, and Cd, which may be caused by the inhomogeneity of the feed sludge.

Volatile elements (S and Hg) showed low enrichment ($E_f < 0.6$) in ashes in **FB** and **FC**.

For Hg, the main combustion component was Hg(g) at 850 °C and $HgCl_2$(g) at 250 °C, respectively. Both of these two components exist in the gas phase at 250 °C. Therefore, instead of ash, Hg was mainly entrained in the flue gas, which is in agreement with previous research (Pudasainee et al., 2013; Van de Velden et al., 2008).

For S, the main phase of the combustion components at 250 °C was in the solid phase. However, due to the short retention time of the flue gas, secondary interactions of combustion products at 250 °C can hardly proceed to the equilibrium. Thus, only a part of S transformed into the solid phase, while the remaining were still in the form of SO_2(g) and SO_3(g). Hence, even a bit higher than Hg (E_f <0.4), low E_f of 0.5~0.6 was found in ashes from **FB** and **FC**.

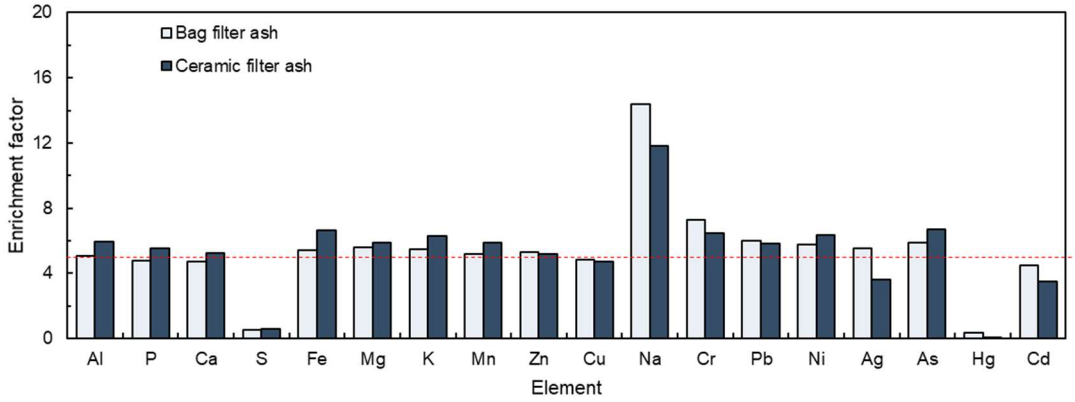

Figure 3-2. Enrichment factors of elements in ashes from **FB** (bag filter ash) and **FC** (ceramic filter ash).

3.3.1.3 Comparison of the enrichment of elements in incinerator GS, FB, and FC

Enrichment behavior of non-volatile and volatile elements was comparable between **GS** and **F-types**, while that of semi-volatile showed differences. In **GS**, semi-volatile elements enriched greater in boiler and multi-cyclone dust than the bottom and riddling ashes. In contrast, semi-volatile elements also enriched to 5-fold as the non-volatile elements in **FB** and **FC**.

According to the thermodynamic equilibriums, the incineration can be divided into two stages. Stage 1: combustion stage, which is at 850 °C, non-volatile exist in the solid phase while semi-volatile and volatile elements present in the gas phase; stage 2:

condensation stage, which is at about 250 °C. In this stage, both the non-volatile and semi-volatile elements generally exist in the solid phase and the volatile elements still in the gas phase. Meanwhile, the adsorption occurs in each stage, for which the smaller particle size is preferable. Thus, based on the thermodynamic results, we can make the hypothesis that non-volatile elements enrich in ashes in stage 1, semi-volatile elements condense into ashes in stage 2, while volatile elements are not expected to enrich in ashes.

The way that the incinerators **GS** and **F-types** discharge the ash, as explained in **2.2.2**, enabled different types of ashes associated with different temperature and particle size. Generally, **GS** discharged the bottom and riddling ashes, mainly of larger particle sizes (**Table 3-6**), at stage 1. Smaller-sized particles in stage 1 were partially entrained in the flue gas and discharged as the boiler and multi-cyclone dust at stage 2, with semi-volatile elements condensed, leading to a comparable E_f of non-volatile elements while higher enrichment of semi-volatile elements. The **F-types**, on the other hand, discharged all ashes, including ashes in stage 1, as the fly ash only at stage 2. Hence, all elements, except for the volatile elements, enriched in the fly ash. Moreover, no difference in the enrichment is expected in **FB** and **FC**. The above hypothesis agrees well with the experimental data with some exceptions.

To conclude, the enrichment of different groups of elements in ashes is associated with the incinerator type, especially the way they discharge ash. Thermodynamic equilibriums can predict the behavior of elements well with some exceptions. Also, both the temperature and particle size influence the enrichment behavior of elements significantly: lower temperature and smaller particle size enable higher enrichment of semi-volatile elements. The **GS** can combust the sewage sludge; meanwhile, to some extent, it separates heavy metals in the ashes. Therefore, compared with **FB** and **FC**, the incinerator **GS** is favorable for ash recycling and disposal for its separate ash discharge at different units.

3.3.2 Mass balance of elements

3.3.2.1 Step grate stoker

The mass fractions of elements in the input and their recovery rates in the output of the GS are shown in **Figure 3-3**. As mentioned in section **2.2.2**, dewatered sewage sludge was dried with the use of internal recycling water prior to combustion in the GS. The element concentrations including heavy metals (**Table 2-5**) measured in the recycling water were low, and even below the standards for tap water (MHLW) or sewage effluent (Ministry of the Environment). Nonetheless, mass fractions of these elements could have additional inputs into their total mass flow (**Fig. 3-3**). After the drying process, the recovery rates (85–134%) for all of the elements were reasonable. Moreover, the distributions of elements between sludges and water in the output and input were consistent, indicating that the drying process (110–130 °C) did not affect the behavior of the elements.

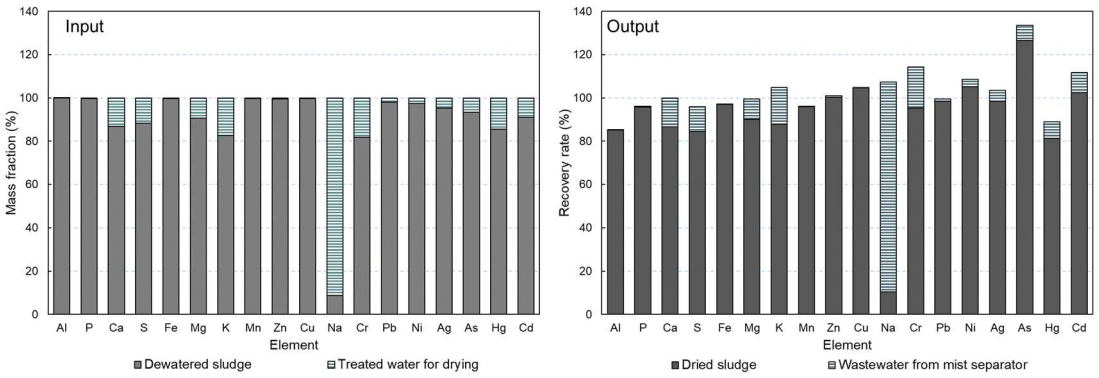

Figure 3-3. The mass fractions and recovery rates for the drying process in the **GS**.

There are four input streams into the **GS** (**Fig. 3-4**). Among them, the dewatered sewage sludge is the primary source of elements such as Al, P, Fe, Mn, Zn, Cu, Pb, and Ni, with their mass fractions > 93%. The treated waters (for drying, WS, and ESP) are the primary sources of Na (97%) as well as Ca, S, Mg, K, Cr, and Cd with mass fractions between 22–38%. Such metal distributions might be linked-to the low solubility of various forms of these elements in the water. The extremely high mass fraction of Na in the treated waters may be associated with its extensive accumulation due to the use of caustic soda in

the desulfurization process.

In the output, most elements showed reasonable overall recovery rates of 77–126%. The only low recovery rates were observed for Hg (57%), Cd (61%), and Pb (68%). The significant inaccuracies in Hg and Cd may be related to underestimating amounts in stack emission (Van de Velden et al., 2008), and the low recovery rates of Pb may be associated with overestimating input of Pb from sludge due to its nonhomogeneity.

Among the eight output streams in the **GS**, the solids (ash and dust) were found to be the main sink for the non-volatile elements (Al, P, Ca, Fe, Mg, K, Mn, Cu, Na, Cr, and Ni) while the wastewater, particularly from the WS, were the main sinks for the volatile elements (S and Hg) (**Fig. 3-4**).

The semi-volatile elements (Zn, Pb, Ag, As, and Cd) showed specific distribution behaviors between ash and wastewater. Compared with the input, where considerable mass fractions (78–99%) were found in the sludge, only 15–52% of these elements were recovered in the total ash in the output. Extremely low fractions appeared for Pb and Cd, for which solid phases were 95% and 78% in the input, but 28% and 15% in the output, respectively. The lower mass fractions in ash indicate that at 250 ℃, not all of the incineration products evolved into the solid phase (Marani et al., 2003). Instead, only a part of the products shifted to the solid phase, and an equal part of gaseous components was absorbed into the water at the WS and ESP, while the remainder was emitted from the stack. Additionally, despite the higher concentrations of semi-volatile elements in the fly ashes (boiler and multi-cyclone dust), they recovered less than 1% of these elements due to the small flow rate (**Table 3-1**) (Zhang et al., 2008). The recovery was much less than that of the bottom and riddling ashes (15–51%). Wastewater discharged 16–40% of these elements. Small fractions (1–8%) of Ag, As, and Cd was found in the flue gas.

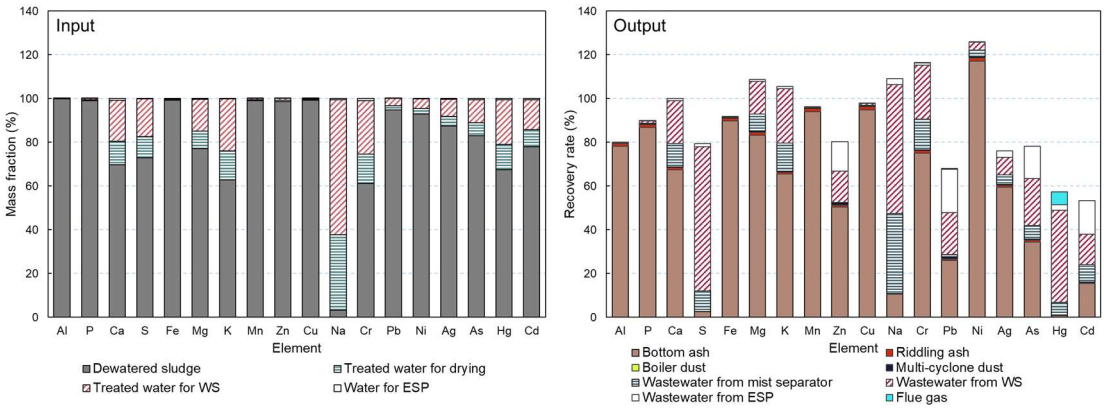

Figure 3-4. The mass fractions and recovery rates for the **GS**. In the output, only Hg in the flue gas was involved in the calculation of recovery rate because concentrations of other elements were under the LOQ.

3.3.2.2 Fluidized bed incinerators

Mass fractions and recovery rates for the F-types are shown in **Figures 3-5** and **3-6**. In the input of **FB** (**Fig. 3-5**), dewatered sewage sludge was the primary source (> 89%) of almost the same elements as in the **GS** (Al, P, Fe, Mn, Zn, Cu, Pb, Ni), with the addition of Hg, while the recycling water provided a considerable fraction of Na (98%). For the other elements, both the sludge and treated water contributed significantly to the mass flow.

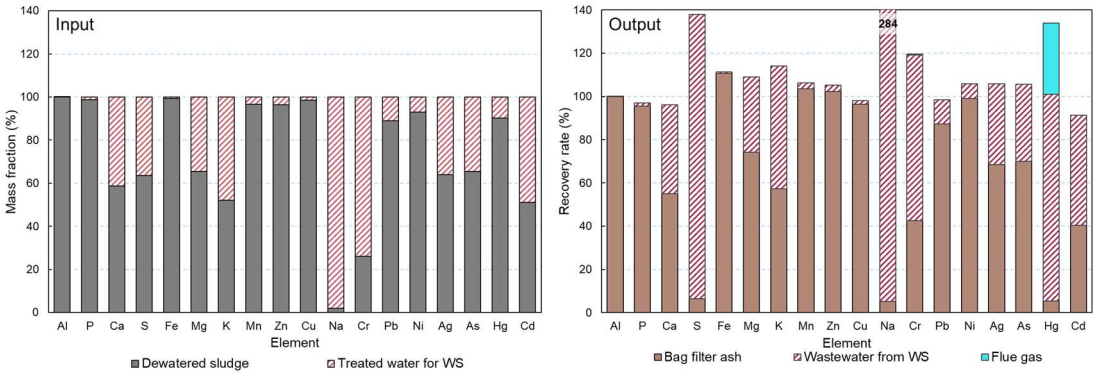

Figure 3-5. The mass fractions and recovery rates for the **FB**. In the output, only Hg in the flue gas was involved in the calculation of recovery rate because concentrations of other elements were under the LOQ.

In the output, all elements showed reasonable recovery rates ranging from 96–138%, except for Na. The extremely high recovery rate for Na (284%) was caused mainly by the use of caustic soda for acid gas (mainly SO_2 and SO_3) removal in the WS. The treated water,

which is used for flue-gas cooling, also contributed an extra input of Na to the ash, resulting in a higher fraction in ash than in the input sludge.

Non-volatile elements, among which Al, P, Fe, Mn, Cu, and Ni were primarily sourced from the sludge, were almost entirely recovered in the bag filter ash (95–111%). Semi-volatile elements (Zn, Pb, Ag, As, and Cd) showed comparable recovery rates (51–96%) in bag filter ash to the mass fraction (40–102%) in the sludge. Inconsiderable amounts of the volatile elements (S and Hg) were recovered in the solid phase (bag filter ash) despite their dominant mass fraction in the sewage sludge. Instead, most of the S (132%) and Hg (96%) was recovered in wastewater from the WS. Moreover, a significant recovery rate of 33% of Hg was detected in the stack emission.

Figure 3-6 shows the mass balance and distribution in **FC**. Since both the incinerator type and the feed sludge of **FC** were the same as **FB** except for the filter unit of the APCDs, the mass fractions in the input to **FC** were almost the same as **FB**. In the output, all elements except for Na showed recovery rates of 75–141%. As in **FB**, the recovery rate of Na in **FC** was very high (287%), and for the same reason. Non-volatile and semi-volatile elements showed a similar distribution to **FB**, with dominant discharges in the filter ash. These results are similar to previously reported studies on fluidized bed incinerators (Elled et al., 2007). Hg, however, scarcely discharged from ash in **FC**, and the fraction in the flue gas was also smaller than that in **FB**. For S (134%), Na (281%), and Hg (83%), the highest recovery rates were found in the wastewater. The extremely high recovery rate for Na in wastewater was associated with the use of caustic soda for acid gas removal, the same as in **FB**.

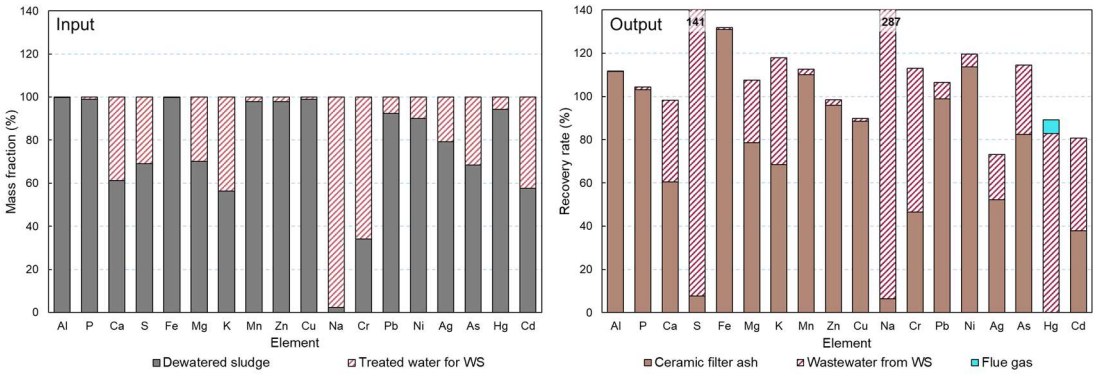

Figure 3-6. The mass fractions and recovery rates for the **FC**. In the output, only Hg in the flue gas was involved in the calculation of recovery rate because concentrations of other elements were under the LOQ.

3.3.2.3 Comparison between the step grate stoker and fluidized bed incinerator

Detailed analyses of the **GS** and the **F-types** showed similar mass fractions in the inputs. The outputs, however, showed different distributions between the **GS** and the **F-types** for semi-volatile elements. These semi-volatile elements are discharged in wastewater rather than in ash in the **GS**, while in the **F-types**, the ashes are the primary sink for the semi-volatile elements. Particular differences were observed for Pb, As, and Cd, for which recovery rates in ashes from the F-types were almost 50% higher than in the **GS**, reaching 87–99%, 70–82%, and 38–40%, respectively.

The different distributions of semi-volatile elements were caused by the distinct differences in ash discharge procedures between the **GS** and the **F-types**. Since the bottom and riddling ashes were already removed at the bottom of the **GS**, the gaseous components could scarcely be absorbed by particles, even though a small amount of new fine particles may form with the decrease of temperature at APCDs. By contrast, in the **F-types**, all ash was entrained in the flue gas, which enabled sufficient contact for the adsorption of gaseous components. Additionally, the smaller particle size of fly ash in the **F-types** compared to the **GS** (**Table 3-6**) also favors adsorption (Y. Li et al., 2017). In addition to adsorption, light metal elements (Al, Ca, K, and Na) create a multilayer external shell that encapsulates heavy metals distributed in discrete pockets toward the core of the particle (Rink et al., 1995). Therefore, the different ash discharge locations in the incinerators significantly

affect the distribution of semi-volatile elements (Lopes et al., 2003). The **GS** favors the separation of semi-volatile elements from the main ash, while the **F-types** tend to discharge non- and semi-volatile elements almost completely in the fly ash.

The volatile elements, especially Hg, are mainly distributed in wastewater in all incinerators (Pudasainee et al., 2013; Takaoka et al., 2012). the **GS** and **FC** showed similar distribution tendencies in wastewater (51–83%), ash (< 1%), and flue gas (6%). However, **FB** showed higher recovery rates in all streams, at 96%, 5%, and 33% for wastewater from the WS, ceramic filter ash, and flue gas, respectively. The higher overall recovery rates may be due to the underestimated input of Hg in sludge and treated water. Besides, the much higher recovery rate in flue gas before with the different species of Hg (Meij et al., 2011; Pudasainee et al., 2013). Due to the short residence time at dust collectors, the combustion components of Hg were a mixture of Hg, HgO, and $HgCl_2$. The fractions of these species are considered responsible for the different distributions in the **GS**, **FB**, and **FC**. However, further information is required for this assumption. S, as discussed in section **3.3.1**, predominantly exists in the gas phase as SO_2 and SO_3, and was therefore chemically absorbed by the caustic soda solutions added at the WS. As a result, S was mostly distributed in wastewater in all three incinerators.

3.3.3 Recycling and disposal of dewatered sewage sludge and incineration ash

Generally, the monocombustion process can efficiently decrease the volume of dewatered sewage sludge waste to about 3.2–3.9% and turn it into ISSA. The generated ISSA is enriched in non-volatile elements, of which P, Mg, and K represent valuable nutrients (**Table 2-7**). However, this ISSA cannot be used as fertilizer due to the presence of heavy metals such as Cr, Pb, Ni, As, and Cd. Moreover, as was previously reported, the P concentrated in ISSA must be transformed into a more biologically available form (Ohtake and Okano, 2015; Ottosen et al., 2013). Considering that the content of P was very high (86,400–94,800 mg/kg) in all ashes, these ISSAs from the **GS** and the **F-types** can be considered a valuable secondary source for P recovery.

Significant differences were found in the concentrations of the aforementioned heavy metals in ashes generated by the **GS** and the **F-types**. In the bottom and riddling ashes of the **GS** (**Table 2-7**), the contents of the heavy metals were well below the standards regulated by the Ministry of Agriculture, Forestry and Fisheries (MAFF), while the concentrations of Pb and Cd exceeded the regulated limits of 100 and 5 mg/kg in dusts (boiler and multi-cyclone), as well as in ashes generated in the **F-types**. The bottom and riddling ashes accounted for 99.7% of the total amount of ash generated in the **GS**, which means that ~99.7% of P have the potential to be recycled as the fertilizer. Our data clearly indicate that incineration of sewage sludge in the **GS** provides ISSA of much lower toxicity than that of the **F-types**. In the same manner, more versatile disposal options can be taken into consideration for the ash generated from the GS. Future practice of sewage sludge incineration should focus on **GS** rather than fluidized bed incinerator technology.

3.4 Summary

During the sewage sludge mono-incineration, non-volatiles were generally distributed in ashes while volatiles were significantly discharged in wastewater. However, the behavior of semi-volatiles depended on the incinerator type: these elements showed similar behavior to non-volatiles in **F-types**, but were less enriched in the bottom and riddling ashes from the **GS**. With lower concentrations of Pb and Cd than regulated limits, the bottom and riddling ashes from the **GS** (99.7% in total amount) can be considered a valuable secondary

source for P recovery. Therefore, the **GS** has an advantage over the **F-types** in terms of the recycling of the ISSA.

The recycling water used for heating and flue gas treatment brought a considerable amount of soluble elements, especially for the Na (97–98%), to the input. Mass balance calculations indicated sufficient recoveries for most elements, being 80–120%, except for Na in F-types, which was 284–287% due to the usage of caustic soda for acid gas absorption.

References

Åmand, L.E., Leckner, B., 2004. Metal emissions from co-combustion of sewage sludge and coal/wood in fluidized bed. Fuel 83, 1803–1821. https://doi.org/10.1016/j.fuel.2004.01.014

Bale, C.W., Bélisle, E., Chartrand, P., Decterov, S.A., Eriksson, G., Gheribi, A.E., Hack, K., Jung, I.H., Kang, Y.B., Melançon, J., Pelton, A.D., Petersen, S., Robelin, C., Sangster, J., Spencer, P., Van Ende, M.A., 2016. Reprint of: FactSage thermochemical software and databases, 2010–2016. Calphad Comput. Coupling Phase Diagrams Thermochem. 55, 1–19. https://doi.org/10.1016/j.calphad.2016.07.004

Balogh, S.J., Nollet, Y.H., 2008. Mercury mass balance at a wastewater treatment plant employing sludge incineration with offgas mercury control. Sci. Total Environ. 9, 125–131. https://doi.org/10.1016/j.scitotenv.2007.08.021

Elled, A.L., Åmand, L.E., Leckner, B., Andersson, B.Å., 2007. The fate of trace elements in fluidised bed combustion of sewage sludge and wood. Fuel 86, 843–852. https://doi.org/10.1016/j.fuel.2006.08.014

Gerstle, R.W., Albrinck, D.N., 1982. Atmospheric emissions of metals from sewage sludge incineration. J. Air Pollut. Control Assoc. 32, 1119–1123. https://doi.org/10.1080/00022470.1982.10465519

Huang, Y., Jin, B., Zhong, Z., Xiao, R., Tang, Z., Ren, H., 2004. Trace elements (Mn, Cr, Pb, Se, Zn, Cd and Hg) in emissions from a pulverized coal boiler. Fuel Process. Technol. 86, 23–32. https://doi.org/10.1016/j.fuproc.2003.10.022

Kasina, M., Kowalski, P.R., Michalik, M., 2017. Seasonal changes in chemical and mineralogical composition of sewage sludge incineration residues and their potential for metallic elements and valuable components recovery. Energy Procedia 125, 34–40. https://doi.org/10.1016/j.egypro.2017.08.049

Lee, S.S., Wilcox, J., 2017. Behavior of mercury emitted from the combustion of coal and dried sewage sludge: The effect of unburned carbon, Cl, Cu and Fe. Fuel 203, 749–756. https://doi.org/10.1016/j.fuel.2017.04.104

Li, Y., Cui, R., Yang, T., Zhai, Z., Li, R., 2017. Distribution characteristics of heavy metals in different size fly ash from a sewage sludge circulating fluidized bed incinerator. Energy and Fuels 31, 2044–2051. https://doi.org/10.1021/acs.energyfuels.6b02676

Lopes, M.H., Abelha, P., Lapa, N., Oliveira, J.S., Cabrita, I., Gulyurtlu, I., 2003. The behaviour of ashes and heavy metals during the co-combustion of sewage sludges in a fluidised bed. Waste Manag. 23, 859–870. https://doi.org/10.1016/S0956-053X(03)00025-4

Marani, D., Braguglia, C.M., Mininni, G., Maccioni, F., 2003. Behaviour of Cd, Cr, Mn, Ni, Pb, and Zn in sewage sludge incineration by fluidised bed furnace : Marani, D. et al. Waste Management, 2003, 23, (2), 117-124. Fuel Energy Abstr. 44, 403.

Meij, R., te Winkel, H., 2007. The emissions of heavy metals and persistent organic pollutants from modern coal-fired power stations. Atmos. Environ. 41, 9262–9272. https://doi.org/10.1016/j.atmosenv.2007.04.042

Nadziakiewicz, J., Kozioł, M., 2003. Co-combustion of sludge with coal. Appl. Energy 75, 239–248. https://doi.org/10.1016/S0306-2619(03)00037-0

Niu, S., Chen, M., Li, Y., Song, J., 2018. Co-combustion characteristics of municipal sewage sludge and bituminous coal. J. Therm. Anal. Calorim. 131, 1821–1834. https://doi.org/10.1007/s10973-017-6716-3

Ohtake, H., Okano, K., 2015. Development and implementation of technologies for recycling phosphorus in secondary resources in Japan. Glob. Environ. Res., 19, 49–65.

Ottosen, L.M., Kirkelund, G.M., Jensen, P.E., 2013. Extracting phosphorous from incinerated sewage sludge ash rich in iron or aluminum. Chemosphere 91, 963–969. https://doi.org/10.1016/j.chemosphere.2013.01.101

Peccia, J., Westerhoff, P., 2015. We should expect more out of our sewage sludge. Environ. Sci. Technol. 49, 8271–8276. https://doi.org/10.1021/acs.est.5b01931

Pilch, B., Grill, D., 1995. Determination of organic and inorganic sulphur byi on chromatography in small quantities of plant material. J. Plant Physiol. 146, 10–14. https://doi.org/10.1016/S0176-1617(11)81960-7

Pudasainee, D., Seo, Y.C., Kim, J.H., Jang, H.N., 2013. Fate and behavior of selected heavy metals with mercury mass distribution in a fluidized bed sewage sludge incinerator. J. Mater. Cycles Waste Manag. 15, 202–209. https://doi.org/10.1007/s10163-013-0115-z

Rink, K.K., Kozinski, J.A., Lighty, J.S., 1995. Biosludge incineration in FBCs: Behavior of ash particles. Combust. Flame 100, 121–130. https://doi.org/10.1016/0010-2180(94)00076-5

Sommers, L.E., Tabatabai, M.A., Nelson, D.W., 1977. Forms of sulfur in sewage sludge 1. J. Environ. Qual. 6(1), 42–46.

Spliethoff, H., Scheurer, W., Hein, K.R.G., 2000. Effect of co-combustion of sewage sludge and biomass on emissions and heavy metals behaviour. Process Saf. Environ. Prot. 78, 33–39. https://doi.org/10.1205/095758200530420

Takaoka, M., Domoto, S., Oshita, K., Takeda, N., Morisawa, S., 2012. Mercury emission from sewage sludge incineration in Japan. J. Mater. Cycles Waste Manag. 14, 113–119. https://doi.org/10.1007/s10163-012-0044-2

Van de Velden, M., Dewil, R., Baeyens, J., Josson, L., Lanssens, P., 2008. The distribution of heavy metals during fluidized bed combustion of sludge (FBSC). J. Hazard. Mater. 151, 96–102. https://doi.org/10.1016/j.jhazmat.2007.05.056

Yang, H., Seo, Y., Kim, J., Park, H., Kang, Y., 1994. Vaporization characteristics of heavy

metal compounds at elevated temperatures. Korean J Chem Eng. 11(4), 232–238.
Yoshida, H., Christensen, T.H., Guildal, T., Scheutz, C., 2015. A comprehensive substance flow analysis of a municipal wastewater and sludge treatment plant. Chemosphere 138, 874–882. https://doi.org/10.1016/j.chemosphere.2013.09.045
Zhang, G., Hai, J., Ren, M., Zhang, S., Cheng, J., Yang, Z., 2013. Emission, mass balance, and distribution characteristics of PCDD/Fs and heavy metals during cocombustion of sewage sludge and coal in power plants. Environ. Sci. Technol. 47, 2123–2130. https://doi.org/10.1021/es304127k
Zhang, H., He, P.J., Shao, L.M., 2008. Fate of heavy metals during municipal solid waste incineration in Shanghai. J. Hazard. Mater. 156, 365–373. https://doi.org/10.1016/j.jhazmat.2007.12.025
Zhao, Z., Wang, R., Wu, J., Yin, Q., Wang, C., 2019. Bottom ash characteristics and pollutant emission during the co-combustion of pulverized coal with high mass-percentage sewage sludge. Energy 171, 809–818. https://doi.org/10.1016/j.energy.2019.01.082

Chapter 4 Mercury speciation and emission in sewage sludge thermal treatment process: mono-incineration and carbonization

4.1 Introduction

Mercury is a toxic pollutant, which is harmful to humans after intake through fish consumption or inhalation (Holmes et al., 2009; Zhang and Wong, 2007). It can be emitted to the atmosphere from both natural and anthropogenic sources (Pacyna et al., 2010). Coal-fired power plants are considered to be the most significant anthropogenic source for mercury emission in most countries (Friedli et al., 2004; Pacyna et al., 2010; Srivastava et al., 2006; Yang et al., 2007). Besides, municipal solid waste and sewage sludge incineration are also essential sources for anthropogenic mercury emission (Takaoka et al., 2012, 2011).

Because of its high volatility and the toxicity of methylmercury (MeHg), special attention was paid to the transfer behavior of Hg from wastewater treatment to sewage sludge incineration. It was reported that mercury emission from municipal sewage might be a primary source for the direct release of total anthropogenic mercury (THg) into aquatic environments in China (Liu et al., 2018). Studies revealed that, in the wastewater treatment process, THg was mostly concentrated in the sewage sludge (Gbondo-tugbawa et al., 2010), while more than 70% of the initial mass of MeHg was degraded (Mao et al., 2016). Volatilization was a minor part of the total amount of Hg at the WWTPs (Gbondo-tugbawa et al., 2010). When combusted, Hg mainly was emitted in the stack gas (Van de Velden et al., 2008).

As already discussed in **Chapter 3**, Hg was mainly discharged from wastewaters generated at the APCDs, especially wastewater from the WS. Only a small amount of Hg was emitted from the stack, and almost no Hg was found in ashes. The distribution of Hg in wastewater, flue gas, and ash is considered to be associated with the different species of Hg. In the flue gas, Hg exists in three forms: oxidized mercury (Hg^{2+}), particulate-bounded

mercury (Hg^p), and elemental mercury (Hg^0) (Galbreath and Zygarlicke, 2000). The APCDs, such as bag filter (BF) , electrostatic precipitator (ESP), and wet flue gas desulfurization (FGD), can remove some Hg^p and Hg^{2+} (Sun et al., 2017), and discharge Hg through wastewaters and ashes. However, Hg^0 often escapes from these devices due to its low water solubility and high vapor pressure (Galbreath and Zygarlicke, 1996; Yang et al., 2007).

On the other hand, sewage sludge carbonization, as a promising method to convert the SS into a storable feedstock and reduce the odor problem, also has the potential risk in emitting Hg. However, so far, Hg emission from the SS carbonization furnace is rarely mentioned.

The emission and speciation of Hg (Hg^0 and Hg^{2+}) in the stack gas is mainly affected by the different APCDs used (Takaoka et al., 2012). Also, the temperature has a significant influence on the speciation of Hg in the flue gas (Grace et al., 2001). However, reports on the revolution of dominant species of Hg at APCDs in sewage sludge thermal treatment processes, especially for carbonization, are rare. Moreover, the thermodynamic calculations on the species of Hg for these processes are less mentioned.

Therefore, the objectives of this chapter are: (1) to specify the dominant species of Hg in the flue gas at the APCDs in sewage sludge incinerator and carbonization furnace; (2) to clarify the relationship between the dominant species of Hg and temperature; (3) to evaluate the adsorptive removal performance of Hg^0 by sorbents. Continuous Hg emission monitors were set up at SS mono-incinerators and carbonization furnace, and the Hg emission profiles in these incinerators were compared. Further, based on the composition of the sewage sludge, the species of Hg generated in the studied furnaces were simulated by the thermodynamic calculation with a wide temperature range of from 100 to 1000 ºC for incinerators and 240–420 ºC for the low-temperature carbonization furnace. The role of the

temperature on the revolution of the dominant species of Hg was evaluated. Further, for the carbonization process, the adsorptive removal of Hg^0 by sorbents was conducted, and the performance of activated carbon and polymer was compared.

4.2 Methodology

4.2.1 Incinerators and carbonization furnace

In order to identify the mercury behavior in the sewage sludge thermal treatment process, mercury emission through the flue gas from one step grate stoker, three fluidized bed incinerators, and one carbonization furnace, were monitored. Among these furnaces, the step grate and two fluidized bed incinerators were already introduced in **chapter 2**. In addition to these incinerators, another fluidized bed incinerator (denoted as **FD**) and a carbonization furnace (**C-F**), was also studied. **Figure 4-1** shows the schematics of these furnaces.

4.2.2 The sampling process

The sampling process at incinerators **GS**, **FB**, and **FC** has already described in **Chapter 3**. Similarly, batch sampling was conducted at **FD** and **C-F**. At **FD**, solid samples, including dewatered sludge and incinerated ash, and water sample as wastewater from WS was collected. At the **C-F**, solid samples included the dewatered sludge, dried sludge, and generated biofuel. For water samples, wastewater from the wet scrubber at the drying unit, wastewater from WS at the APCDs, and wastewater from ESP were collected at **C-F**.

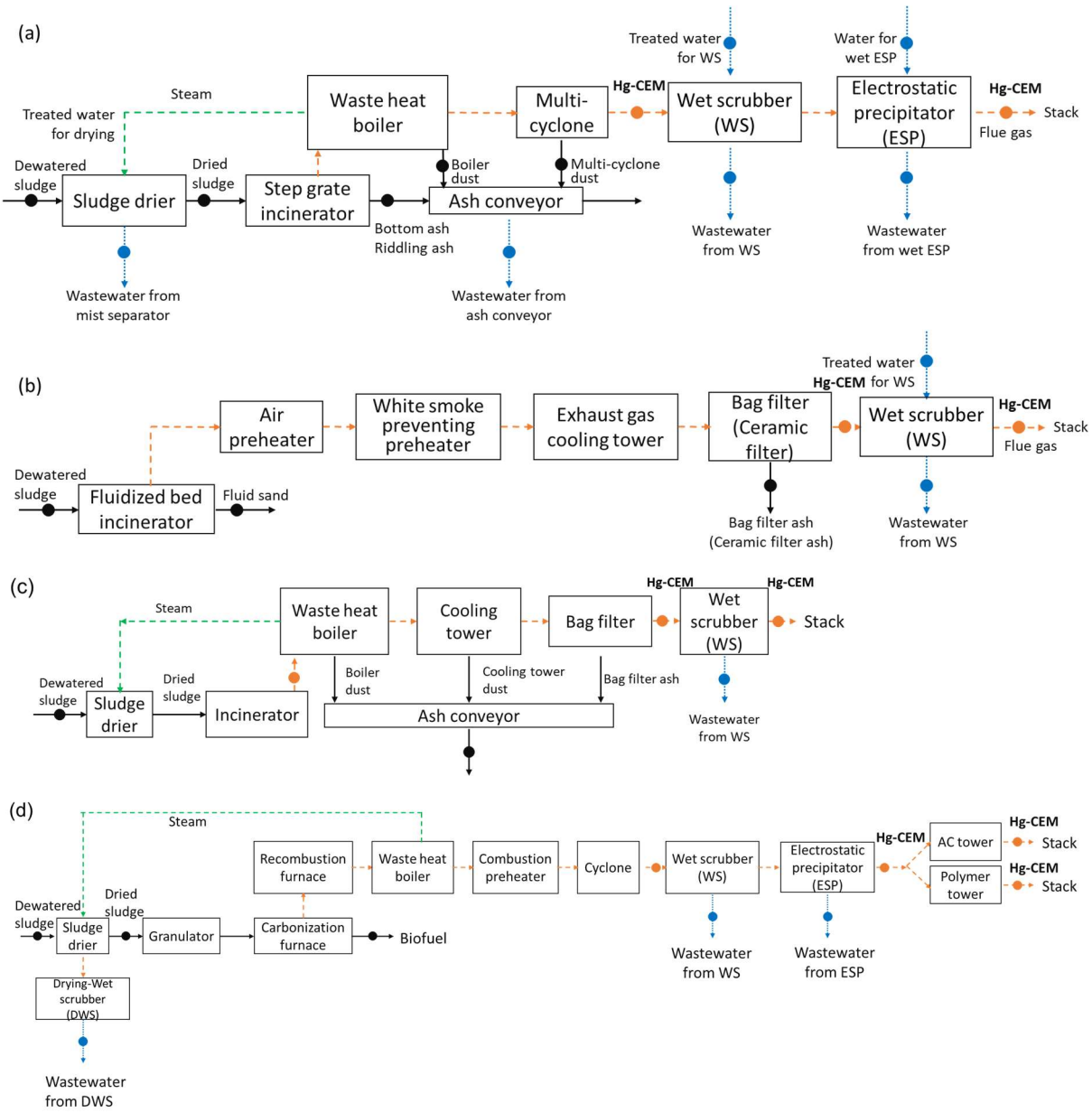

Figure 4-1. Schematics of sample collection from the (a) step grate incinerator (**GS**), (b) fluidized bed incinerators equipped with the bag (**FB**) and ceramic (**FC**) filters, (c) sewage sludge fluidized bed incinerator (**FD**), and (d) carbonization furnace (**C-F**). The green arrow shows the flow of steam. The black, blue, and orange arrows (dots) show the mass flows (sampling points) of solids, water, and flue gas, respectively. Hg-CEM: mercury continuous emission monitor.

Flue gases in **GS**, **FB** and **FC** were manually and sequentially sampled three times at various sampling points, in front of the WS and the stack (**Fig. 4-1**), using impingers, according to the Japanese Industrial Standard (JIS K 0222). The flue gases were passed

through a glass filter and bubbled through a bottle containing 100 mL of 15 wt% H_2O_2 solution and two bottles containing 100 mL of 5.75 w/v % sulfuric acid solution with 0.15 w/v % $KMnO_4$ at all sampling points. The sampling time was approximately 20 min. H_2O_2 solution was used to remove high concentrations of SO_2, and we may expect some oxidized mercury to become absorbed into this solution.

Ontario Hydro Method was used in the sampling of flue gases in **FD** and **C-F**. In this method, a sample is withdrawn from the flue gas stream isokinetically through a probe and filter system, maintained at 120 °C or the flue gas temperature (whichever is greater), followed by a series of impingers in an ice bath. Particle-bound mercury is collected on the quartz fiber filter. Oxidized mercury is collected in impingers containing a chilled 1.0 mol/L KCl solution.

Elemental mercury is collected in subsequent impingers (one impinger containing a chilled 5% HNO_3 and 10% H_2O_2 solution and three impingers with a chilled 10% H_2SO_4 and 4% $KMnO_4$ solution) (Standard, ASTM, 2008).

Besides manual sampling and measurement of the flue gases, speciation mercury continuous emission monitors (Hg-CEM) was also set at the **GS**, **FB**, **FC**, **F-D**, and **C-F**, as shown in **Figure 4-1**.

4.2.3 Analytical methods

Analysis of solid and liquid samples

The solid and liquid samples were measured using the heat-vaporization method with the analyzer MA-2000 (Nippon Instruments Co., Ltd., Japan) soon after sampling. Mercury was collected as a gold amalgam and detected using cold-vapor atomic absorption spectrometry (Löthgren et al., 2007). The detection limit of this analyzer was 0.002 ng.

Manual gaseous mercury measurement

For flue gases, after sampled into the solution with the impinger, the Hg concentration was measured using a frameless reduction vaporization atomic absorption mercury analyzer (RA-4300; Nippon Instruments Co. Ltd., Japan). Stannous chloride ($SnCl_2$) was used as a reducing agent, and the bubbling transformed the mercury ions into mercury vapor, which was directed onto an absorption cell. All the concentrations of Hg in the flue gas were corrected for 12% oxygen concentration.

Mercury continuous emission monitor

The Hg-CEM was developed by Nippon Instruments and the Central Research Insititute of the Electric Power Industry in Japan.

One set of the Hg-CEM consists of a pre-treater of MS-1A and the detector DM-6B (Nippon Instruments)(Takaoka et al., 2012). In the pretreatment process at MS-1A, an aqueous solution of 1 mol/L KCl is used. Flue gas passes through the dust filter at a flow rate of 0.5 L/min and is mixed with the KCl solution in the gas/liquid contact coil, thus oxidized mercury (Hg^{2+}) was transferred into the liquid phase. Then, the gas and solution are separated in the gas/liquid separating tube. The elemental Hg (Hg^0) in the gas phase is washed with 1 mol/L KOH to remove the acid gas, and the excess moisture in the gas is condensed with an electric cooler. After that, the gas that including Hg^0 is fed into the first detection device DM-6B (Hg^0), which is an atomic absorption mercury analyzer. The aqueous solution in the gas/liquid separating tube is directed into another gas/liquid contact coil and then mixed with 1% $SnCl_2$ and 10% H_2SO_4. In this process, the Hg^{2+} in solution is reduced, liberating gaseous Hg^0, which passes through another gas/liquid separating tube before it is fed into the second detection device DM-6B (Hg^{2+}) to quantify the Hg^{2+}. Here, the gas flow rate must be identical to that in line DM-6B (Hg^0).

The other set of the Hg-CEM consists of WLE and EMP-2, also developed by the Nippon Instruments. The WLE is the pretreatment system, in which the flue gas reacts with a tin (II) chloride ($SnCl_2$) solution in the first bottle, then the Hg^{2+} is converted to Hg^0 before flowing into a potassium hydroxide (KOH) solution in the second bottle to remove acid gases. Excess moisture in the gas is condensed with an electric cooler. After that, the Hg^0 is detected in the EMP-2 with an atomic absorption spectrophotometer. The detection limit of this device is 0.1 μg/Nm^3 (Takaoka et al., 2018).

4.2.4 Thermodynamic calculation

As already introduced in **chapter 3**, the thermodynamic calculation was utilized to simulate the effect of temperature on the species of Hg in the furnaces. A wide temperature range of 100–1000℃ was selected for sewage sludge incinerators **GS**, **FB**, **FC**, and **FD**. For carbonization furnace **C-F**, the species of Hg component was estimated at a temperature range of 240–420℃. The experimental data on the composition of the feed sludge was used as the input data for the software *FactSage*. Even though Cl is not the primary element in sludge, it was also involved in the thermodynamic calculations due to its significant influence on the speciation of Hg. The input data for incinerators **GS**, **FB**, and **FC** have already explained in **Chapter 3** (**3.2.2**). The input data for **FD** and **C-F** are shown in **Tables 4-1** and **4-2**, respectively.

Table 4-1. Input data to the FactSage software for **FD**. The combustion components were estimated at a wide temperature range of 100–1000°C, with other conditions consistent with the combustion at 850°C.

Combustion condition							
Temperature 850 ℃							
Pressure 100.78 kPa							
Flow rate (kg/h)							
Sludge (dried and dewatered)				Digestion gas		Combustion air	
Combustible component		Incombustible component					
C	505	H_2O	3636	CO_2	100	N_2	8,198
O	318	SiO_2	205.3	CH_4	79	O_2	2,507
N	77	Al_2O_3	79.7	N_2	19	H_2O	82
H	74.8	P_2O_5	53.3	H_2O	2		
S	18.0	Fe_2O_3	41.6				
		CaO	37.1				
		MgO	11.2				
		Na_2O	5.0				
		K_2O	4.2				
		MnO	0.9				
		Cl	2.32				
		Zn	1.2				
		Cu	0.6				
		Cr	0.2				
		As	0.003				
		Pb	0.02				
		Cd	0.0017				
		Hg	0.0016				
		Se	0.0015				
		CN	0.000029				

Table 4-2. Input data to the FactSage software for **C-F**. The combustion components were estimated at a low-temperature range of 240–420°C, the practical temperature for the low-temperature carbonization process.

Carbonization condition					
Temperature	250~350 ℃				
Pressure	101.325 kPa				
Flow rate (kg/h)					
Dried sludge				Carbonization furnace purge gas	
Combustible component		Incombustible component			
C	409	H_2O	397	N_2	457
O	258	SiO_2	139	H_2O	55
H	57.7	Al_2O_3	84.4	CO_2	64
N	57.6	P_2O_5	76.8	O_2	47
S	15.3	Fe_2O_3	37.0		
		CaO	29.7		
		MgO	15.4		
		K_2O	7.3		
		SO_3	5.8		
		Na_2O	4.8		
		TiO_2	2.7		
		BaO	2.4		
		ZnO	1.3		
		CuO	0.7		
		MnO	0.7		
		Cr_2O_3	0.6		
		V_2O_5	0.2		
		NiO	0.1		
		Cl	1.7		
		Hg	0.0015		

4.2.5 Adsorptive removal of mercury by commercial sorbents in the carbonization furnace

Figure 4-2 shows the schematics for Hg removal tests conducted at the **C-F**. Two kinds of commercial sorbents, modified activated carbon (Shirasagi, MAC, Osaka Gas

Chemicals Co. Ltd.) and Composite polymer (W. L. Gore & Associates, Inc.), were used. These sorbents were set in front of the stack and tested during the same period in parallel (**Fig. 4-1 (d)**).

The AC tower was compiled with 4 layers, and each layer is a cylinder occupied with MAC. The diameter for each layer is 300 mm, and the height is 100 mm. The flue gas flows from the bottom to the top of the AC tower.

The polymer for Hg removal has been recently adopted in coal-fired plants or sewage sludge incinerators in the US as the GORE Mercury Control System (GMCS). This system normally comprises a tower with several layers (**Fig. 4-3**), and an eight-layer tower was adopted in this study. The fixed sorbent can capture elemental and oxidized gas phase mercury from industrial flue gas.

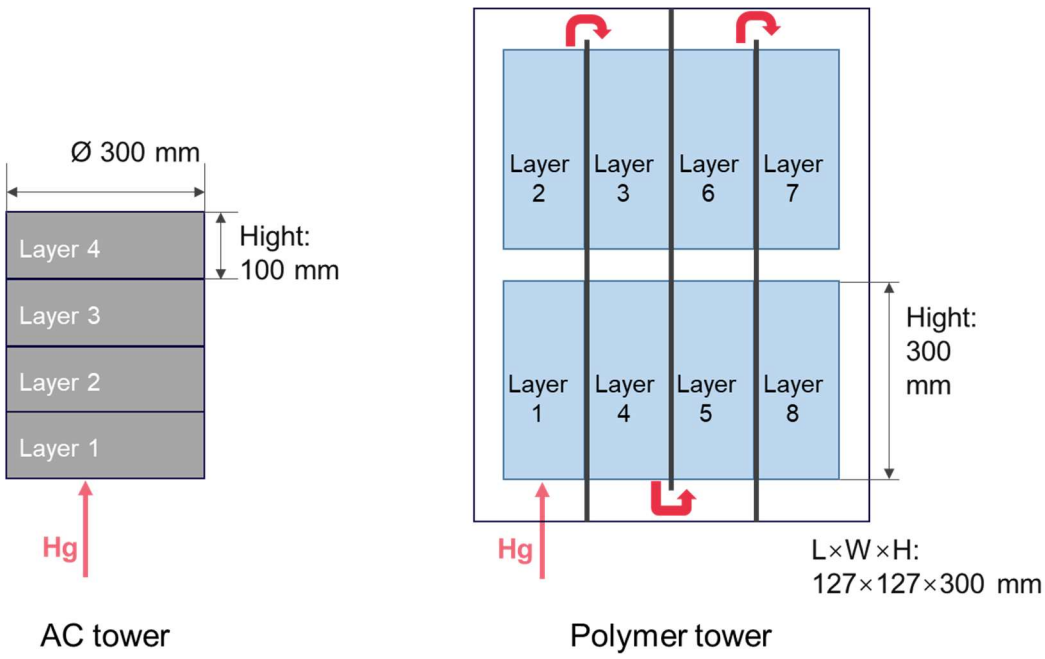

Figure 4-2. Schematic of the adsorption units for AC tower and polymer tower. Flue gas flows from the bottom to the top of the AC and polymer tower.

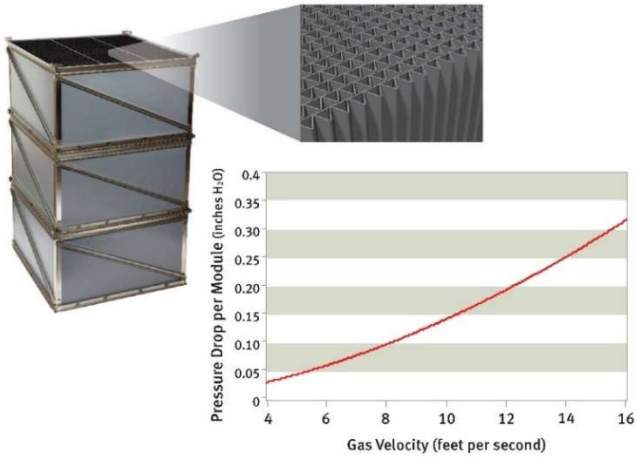

Figure 4-3. The GORE Mercury Control System (GMCS).

4.3 Results and Discussion

4.3.1 Concentration and speciation of mercury in sludge, ash, water, and flue gas

The concentrations of Hg, as well as other elements, in sludge, water, ash, and flue gas in **GS**, **FB**, and **FC** are shown in **Tables 2-4~2-8** in **Chapter 2**, respectively. The concentrations of Hg in all streams as sludge, ash, water, and flue gas in **FD** and **C-F** are summarized in **Tables 4-3** and **4-4** in this chapter, respectively.

Sludge

Incinerators **GS**, **FB**, and **FC** combusted the same sludge. The concentration of Hg was 1.4~2.0 mg/kg-dry (**Table 2-4**) in sludge that fed to **GS**, **FB**, and **FC**. In **FD** and **C-F**, the concentration of Hg was of an identical range of 1.1~1.2 mg/kg-dry (**Tables 4-3** and **4-4**). These measured Hg concentrations were also comparable with previous research conducted in Japan, which was 1.24~1.29 mg/kg-dry (Takaoka et al., 2012).

Ash

In the ISSA, Hg concentrations were 0.1~0.2 mg/kg, 0.5 mg/kg, and 0.02 mg/kg in **GS**, **FB**, and **FC**, respectively. As we already defined the enrichment factor as the ratio of

elemental concentration in ash to that in sludge on a dry basis, the E_f in these ashes were calculated to be 0.06~0.07, 0.4, and 0.01 in ashes from **GS**, **FB**, and **FC**, respectively. In **FD**, the Hg concentration was 0.37 mg/kg in the ISSA, and the E_f in ash was 0.3. Thus, in all the sewage sludge incinerators, **GS**, **FB**, **FC**, and **FD** in this study, Hg concentrations decreased significantly in the ISSA, resulting in low E_f as 0.01~0.4. These enrichment factors were of the same ranges as previous research, which were 0.003~0.2 (Takaoka et al., 2012) and 0.04~0.1 (Pudasainee et al., 2013), under the same calculation as this article. For the **C-F**, Hg concentration also decreased in the generated biofuel, which was 0.05 mg/kg-dry in the biofuel, being 24 folds lower than that in sludge.

Recycling water and wastewater

For water samples, an increase in the Hg concentration in wastewater, primarily from WS, was found in all the incinerators and the carbonization furnace. In **GS**, low concentrations of Hg as 0.003~0.004 mg/L were found in recycling waters (treated water for drying, WS; water for wet ESP), while the concentration increased to 0.01 mg/L in wastewater from WS and ESP (**Table 2-5**). Similarly, in **FB** and **FC**, Hg concentration was 0.0004~0.004 mg/L in the treated water but gained significant increases in the Hg concentrations in wastewater from WS to 0.003~0.01 mg/L. In all these incinerators **GS**, **FB**, and **FC**, Hg was condensed to 3~10 folds in wastewater from WS.

On the other hand, the Hg concentration in treated water was less than 0.0005 mg/L but elevated to 0.089 mg/L and 0.017 mg/L at **FD** and **C-F**, respectively. The Hg concentration in wastewater from WS was condensed to more than 34 folds. Therefore, at the APCDs, the Hg in the flue gas is significantly removed in the WS and discharged in the wastewater from WS. The high removal rate of Hg in the WS is considered to be associated with the speciation of Hg, for which the Hg^{2+} would be more easily to be absorbed in the

water at WS, while the Hg^0 escapes in the flue gas (Yang et al., 2007).

Flue gas

After combustion, the flue gases were directed to the APCDs. As shown in **Table 4-5**, in the inlets to WS, the average THg concentrations were 10.0 μg/Nm^3, 20.3 μg/Nm^3, 40.9 μg/Nm^3, and 77.3 μg/Nm^3 in GS, FB, FC, and FD, respectively. After the treatment at the WS, the THg concentrations in FB, FC, and FD generally decreased to 5.3 μg/Nm^3, 7.9 μg/Nm^3, and 7.6μg/Nm^3, respectively. GS, however, showed an even higher average THg concentration as 11.3 μg/Nm^3 in the inlet of the stack.

The dominant species of Hg in the flue gas evolved after the treatment at the WS. In **GS**, Hg^{2+} was the dominant species of Hg in the inlet of WS, which was 50~84%. However, after the APCDs, which was WS and ESP in **GS**, the dominant species of Hg shifted to Hg^0 (83~96%). Notably, the daily data on 17 December 2016 shows that Hg^{2+} and Hg^0 shared the same fraction as 50% for each in the inlet of WS, but after the WS and ESP, Hg^{2+} turned out to be 96% in the flue gas. This tendency is considered to be caused by the re-emission of Hg from the water in WS (Chang, 2003; Chang and Zhao, 2008; Cheng et al., 2018; Mercedes et al., 2007). Moreover, the re-emission of Hg^0 is possibly associated with the lower Hg removal efficiency in **GS**.

In **FB**, the dominant species of Hg in front of WS was also Hg^{2+} (96~99%). The WS removed more than 75% of the THg in the inlet because of the high solubility of Hg^{2+}. However, in the outlet of WS, a higher concentration of Hg^{2+} than in **GS** was found, which may be caused by the higher O_2 atmosphere in **FB**. **FC** showed a similar tendency as **FB**, with some discrepancies in daily data on 22 January and 23 January 2017 that the outlet concentrations exceeded the inlet. This increase in THg concentration in the outlet is also considered to be caused by the re-emission of Hg from the water in WS (Andersson et al.,

2007).

In **FD**, Hg^{2+} dominantly exists in the inlet of WS as 73 μg/Nm^3 (**Table 4-3**). After the WS, THg was efficiently removed, which is in accordance with the high concentration of Hg in wastewater from WS, as described previously in the recycling water and wastewater section. As a result, the Hg concentration in the flue gas was ~7.5 μg/Nm^3.

Table 4-3. Concentration and speciation of Hg in sewage sludge, ashes, wastewater, and flue gas in **FD**.

	Solid		Water		Flue gas		
	Dewatered sludge	Ashes	Treated water	Wastewater from WS	Outlet of incinerator	Inlet of WS	Stack
Flow rate	t/day		m^3/day		Nm^3/h (dry)		
	201.12	11.02	–	2,650	12,000	12,000	12,000
TS/SS	%		mg/L				
	17.4	99.9	2	1.7			
VTS	%						
	68.5						
c_{THg} (overall)	mg/kg-dry		mg/L		μg/Nm^3		
	1.1	0.37	<0.0005	0.017	5.26	77.28	7.64
c_{Hg} in SS			mg/kg				
			1.8	1900			
					μg/Nm^3		
c_{Hg0} gaseous					4.6	3.9	7.5
c_{Hg2+} gaseous					0.66	73	0.14
c_{Hg} particluate					<0.92	0.38	<0.1

WS: wet scrubber; *TS*: total solids content; *SS*: suspended solids content; *VTS*: volatile total solids content.

Moreover, in all incinerators, the Hg removal performance showed relevance to the Hg concentrations in the inlet. As shown in **Figure 4-4**, with higher Hg concentrations in the inlet of WS, the higher THg removal rates were also found in incinerators **GS**, **FB**, **FC, and FD**. A significant deviation was found at lower inlet THg concentrations of ~10 μg/Nm^3. This deviation may, on the one hand, caused by the relatively higher fraction of the re-emitted Hg^0, which led to the higher THg emission from the stack; on the other hand, the WS used in these incinerators may also affect the THg removal rates.

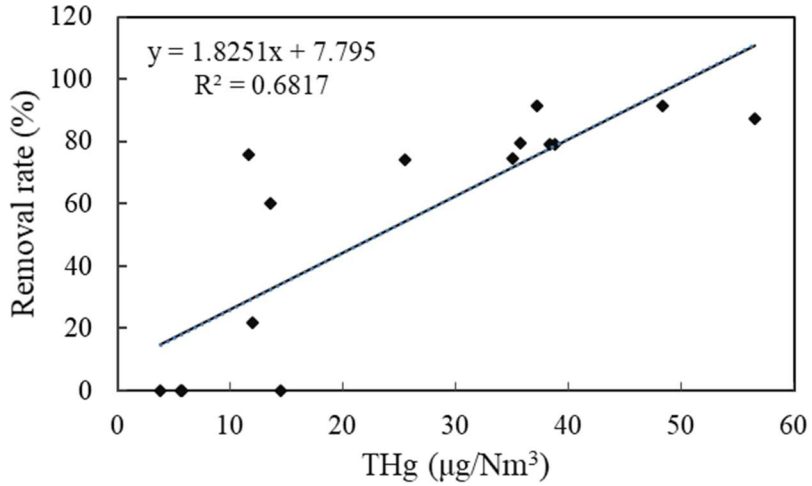

Figure 4-4. The relationship between the removal rate and the THg concentration in the flue gas.

In **C-F**, however, the dominant species of Hg in the inlet of WS was Hg^0 (**Table 4-4**), and this may be caused by the low oxygen content in the carbonization process. Due to the low solubility of the Hg^0, almost no Hg was removed at the WS in **C-F**. Thus, a comparable concentration of Hg in the flue gas as 98.17 μg/Nm^3 to that in the inlet was emitted in the flue gas.

Table 4-4. Concentration and speciation of Hg in sewage sludge, biofuel, wastewater, and flue gas in **C-F**.

	Solid			Water				Flue gas		
	Dewatered sludge	Dried sludge	Biofuel	Treated Water	Wastewater from DWS	Wastewater from WS	Wastewater Synthetic	Inlet of WS	Outlet of WS	Stack
Flow rate	t/day			m^3/day				Nm^3/h (dry)		
	152.2	37.3	20.5	–	1,654	147	2,195	5,400	5,300	5,700
TS/SS	%			mg/L						
	18.2	74.2	95.1	2	5.1	70	250			
c_{THg} (overall)	mg/kg-dry			mg/L				μg/Nm^3		
	1.2	1.3	0.05	<0.0005	<0.0005	0.089	0.0091	108	93.7	98.17
c_{Hg} in SS				mg/kg						
				1.8	0.95	520	15			
								μg/Nm^3		
c_{Hg0} gaseous								79	88	97
c_{Hg2+} gaseous								29	2.3	0.88
c_{Hg} particluate								<0.1	3.4	0.29

WS: wet scrubber; *TS*: total solids content; *SS*: suspended solids content; *VTS*: volatile total solids content.

Table 4-5. Concentration and speciation of Hg in the inlet and outlet of the WS in the flue gas from the **GS**, **FB**, **FC**, and **FD** (incinerator GS: WS+ESP). Some daily data were not available due to mechanical failure and were excluded consequently. Mercury concentration in the stack was monitored separately in species of Hg^0 and Hg^{2+}, and average concentrations within 24 hours of continuous monitoring were shown here.

Incinerator	Date	Inlet of WS			Outlet of WS(ESP)			Removal rate
		THg ($\mu g/Nm^3$)	Hg^0 (%)	Hg^{2+} (%)	THg ($\mu g/Nm^3$)	Hg^0 (%)	Hg^{2+} (%)	
GS	15-Dec-16	3.8	16%	84%	10	90%	10%	–
	16-Dec-16	11.9	20%	80%	9.3	93%	7%	22%
	17-Dec-16	14.5	50%	50%	14.5	96%	4%	0%
	Average	10.0	34%	66%	11.3	93%	7%	–
FC	18-Jan-17	37.2	22%	78%	3.2	19%	81%	91%
	19-Jan-17	48.4	10%	90%	4.1	33%	67%	92%
	20-Jan-17	11.6	11%	89%	2.8	29%	71%	76%
	21-Jan-17	13.6	55%	45%	5.4	29%	71%	60%
	22-Jan-17	5.6	19%	81%	8.4	32%	68%	–
	23-Jan-17	5.7	7%	93%	8.2	47%	53%	–
	Average	20.3	19%	81%	5.3	34%	66%	74%
FB	17-Feb-17	38.8	4%	96%	8.1	89%	11%	79%
	18-Feb-17	38.4	4%	96%	8.1	76%	24%	79%
	19-Feb-17	35.7	3%	97%	7.3	29%	71%	79%
	20-Feb-17	56.5	1%	99%	7.2	14%	86%	87%
	21-Feb-17	35.1	1%	99%	8.9	29%	71%	75%
	Average	40.9	3%	97%	7.9	48%	52%	81%
FD	–	77.3	5%	94%	7.6	98%	2%	90%

4.3.2 Hg emission profiles in mono-incinerators GS, FB, FC, and FD

Figures 4-5~4-8 show the average hourly mass flow of THg in incinerators **GS, FB**, **FC**, and **FD**. Values in the area surrounded by a dotted line have been calculated by addition, subtraction, or both, of measured values. The values surrounded by the solid lines are calculated by the Hg-CEM results and flow rates.

Step grate stoker

Figure 4-5 shows the average hourly mercury mass flow in **GS**. The average hourly mass flow rate of Hg entering the plant was 1.8 g/h, and nearly no mercury loss occurred during the sludge drying process. In the sludge dryer, secondary treated water for drying also brings 0.3 g Hg in hourly. However, after that, 0.2 g Hg was trapped in wastewater from mist separator. Thus, the amount of Hg after the sludge drier almost the same as the feeding sludge.

In the stack, the average concentrations of Hg^0 and Hg^{2+} were 7.2 μg/Nm^3 and 7.3 μg/m^3 at the outlet of multi-cyclone (before wet scrubber) but turned out to be 13.9 μg/m^3 and 0.6 μg/Nm^3 at the inlet of induced draft fan, which is directly in front of the stack (**Table 4-5**). According to the results obtained, APCDs of the step grate incinerator showed poor removal ability of THg in the flue gas. Rather than remove T-Hg, with gas-cooling desulfurized (wet scrubber) and electrostatic precipitator between multi-cyclone and stack, the APCDs, to some extent, converted Hg^{2+} into Hg^0. Thus Hg was mainly emitted into the atmosphere in the form of Hg^0 in the step grate incinerator investigated in this study.

Through the mass balance evaluation, as defined in **Chapter3**, the WS also discharged 42% (1.1 g/h) of Hg, and 8% of THg was emitted from the stack. Based on the CEM results, the THg in the inlet to WS was calculated to be 0.2 g/h, being much lower than the calculated results as 1.9 g/h, and the closure of the overall THg recovery rates across GS was unable to obtain. Since the amount of Hg in the sludge and wastewater from WS showed a relatively small discrepancy, the Hg-CEM results monitored at the outlet of multi-cyclone may be underestimated.

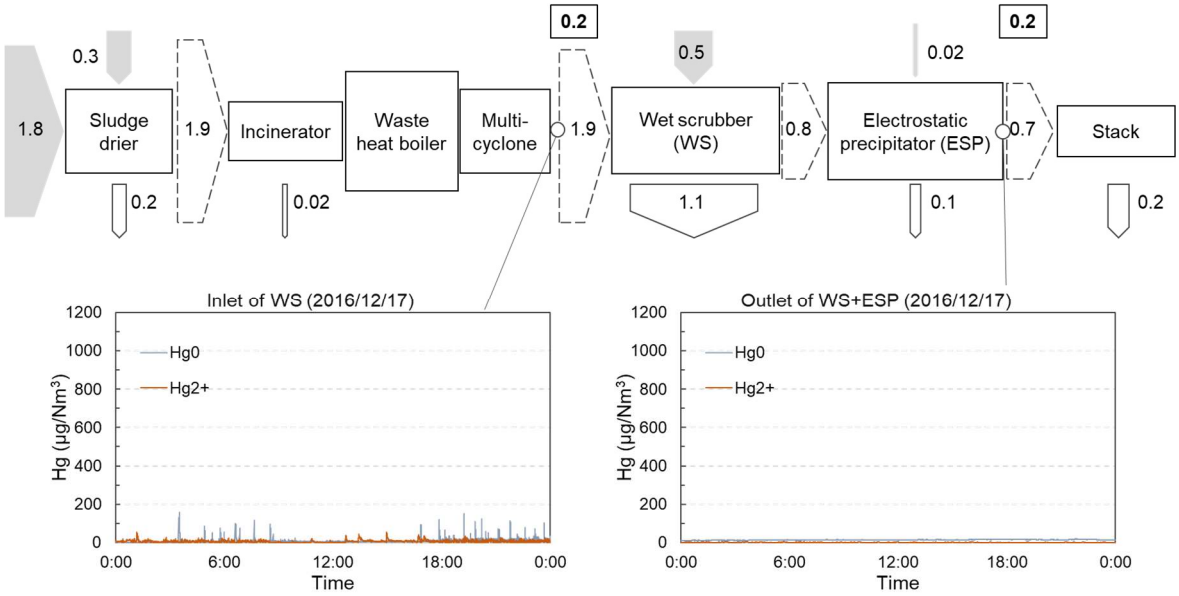

Figure 4-5. The average hourly mass flow of Hg in **GS** (Unit: g/h).

Fluidized bed incinerators

As shown in **Figure 4-6**, in **FB**, the average hourly mass rate of THg from dewatered sludge was 0.6 g and treated water for WS also brought 0.1 g of THg into the whole process. Among the output, 0.04 g/h of THg was discharged in ash hourly, whereas 0.7 g of THg was discharged in wastewater from WS, for which the amount was even more considerable than the input from dewatered sludge. The increase in the amount of THg discharged at WS may be associated with the accumulation of Hg in the WS. Flue gas also emitted 0.2 g THg into the atmosphere, which is 30% of the input from the sludge. Moreover, peaks for Hg emission were found in the outlet of WS, but the timing of these peaks was not consistent with the peaks in the inlet. This phenomenon indicates the possibility of the accumulation and re-emission of Hg at WS in **FB**.

Overall, the total output of THg exceeded the input, thus resulting in a recovery rate of 134%, amongst 100% was discharged through the wastewater from WS. At the WS, the THg in the flue gas calculated based on the CEM results were also comparable to the batch sampling results, and closure in the mass balance was obtained.

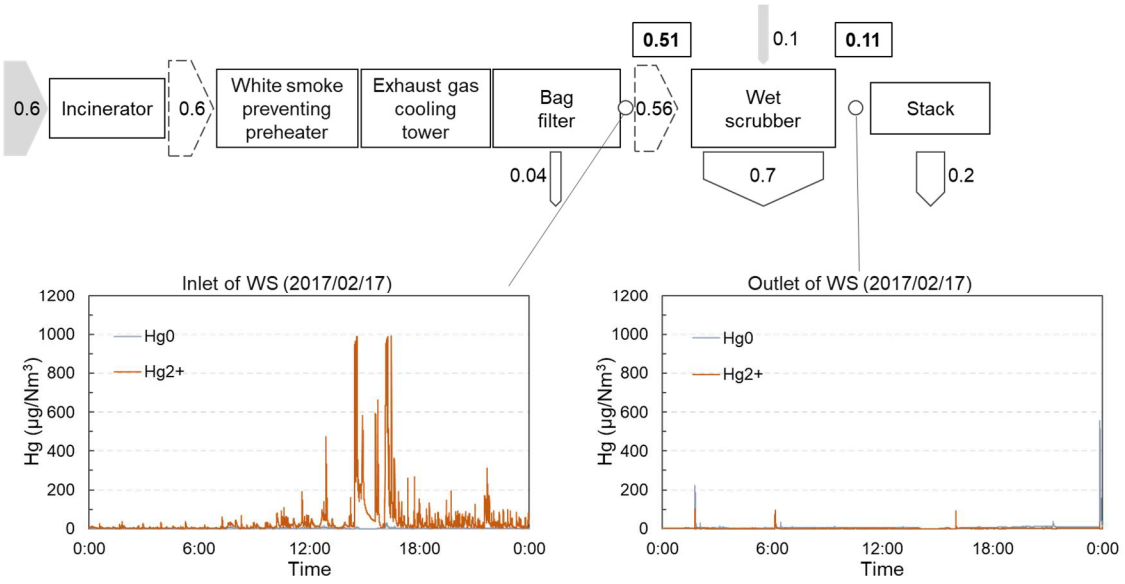

Figure 4-6. The average hourly mass flow of Hg in **FB** (Unit: g/h).

Fluidized bed incinerator **FC (Fig. 4-7)** showed comparable removal rates of mercury as incinerator **FB**. Wastewater from WS also discharged 79% of THg brought in by the sewage sludge and recycling water to WS, while the flue gas discharged 7% of the THg.

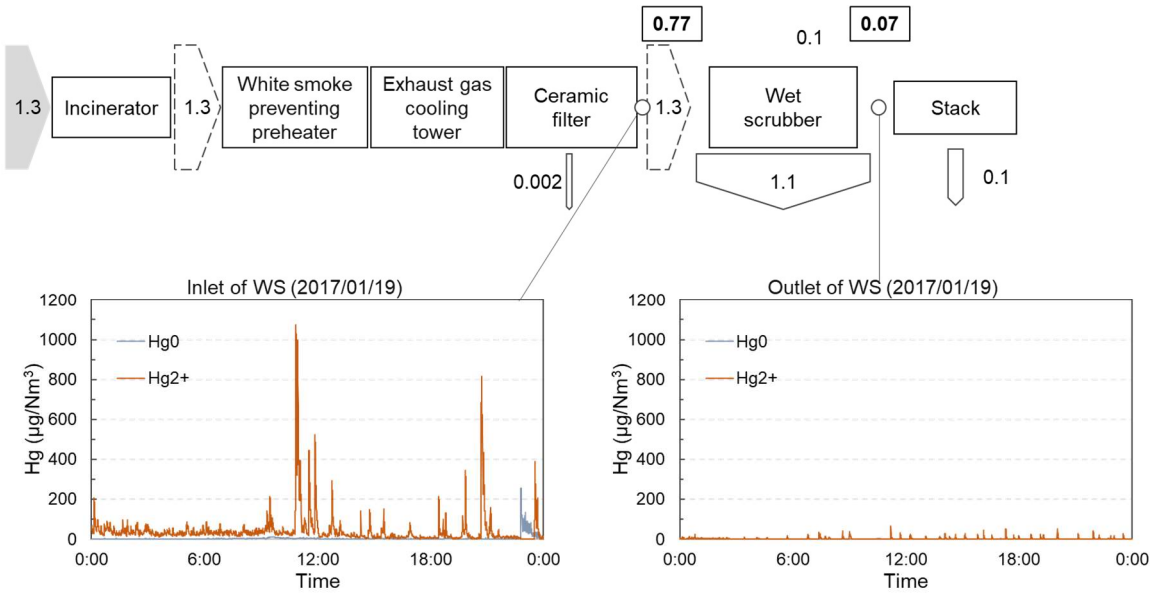

Figure 4-7. The average hourly mass flow of Hg in **FC** (Unit: g/h).

Figure 4-8 shows the average hourly mass flow of Hg in **FD**. The dewatered sludge

brought 1.60 g THg hourly to the incinerator **FD**, and 0.17 g/h was discharged from the ISSA. After that, the remaining THg (1.43 g/h) was entrained in the flue gas and was directed to the WS. At WS, 1.88 g THg was discharged from the wastewater, even exceeded the total input of Hg of 1.60 g/h. The recovery rate, which is defined as the ratio of the amount discharged to the amount brought to the incinerator by sewage sludge, is calculated to be 118% in wastewater from WS. That is to say, almost all of the THg brought to the **FD** was discharged in wastewater from WS in **FD**. The high recovery rates here in WS is associated with the dominant species of Hg, which was Hg^{2+}. The high solubility of Hg^{2+} makes it easier to be removed at WS, as we already discussed in **4.3.1**. After that, about 0.092 g/h was emitted from the stack, with a low recovery rate in this stream as 5.8%.

Therefore, similar to the emission in **FB** and **FC**, the APCDs, especially the WS, can effectively remove the Hg^{2+} by absorption in **FD**. However, the re-emission of Hg^0 by the reduction of Hg^{2+} also raises the concern in Hg emission from sewage sludge mono-incinerators at the WWTPs.

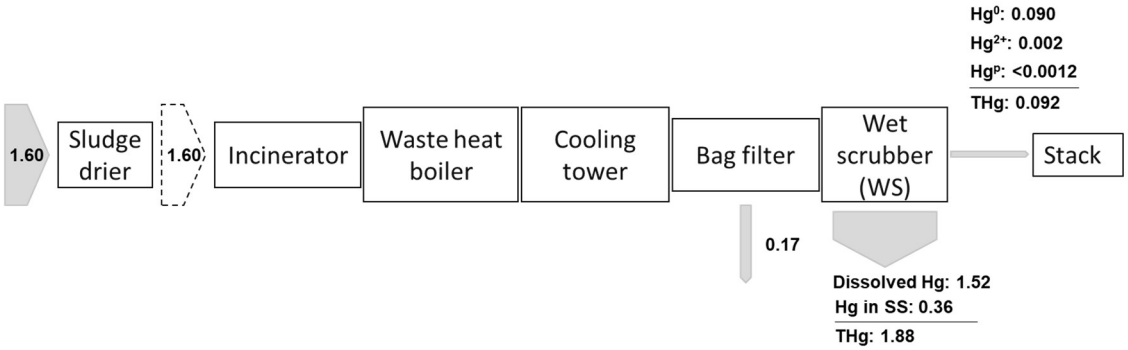

Figure 4-8. The average hourly mass flow of Hg in **FD** (Unit: g/h). *SS*: suspended solids.

To conclude, in sewage sludge incinerators, Hg was almost not concentrated in incineration ash, and most Hg was discharged into the environment through wastewater and flue gas. Since wastewater from wet scrubber was returned to the front of the wastewater treatment process without special Hg treatment, Hg partially kept an internal circulation and accumulating in the system. A small part of THg was emitted into the

atmosphere from the stack, and Hg^0 was dominantly distributed in **GS** and **FD**, contrarily Hg^{2+} occupied an equal or more significant proportion of THg emitted from flue gas in fluidized bed incinerator **FB** and **FC**. Thus, although not primarily emitted to the atmosphere, the THg entered the WWTP was accumulated in wastewater, which may pose potential risks to fish and humans after discharging into waters or the sea.

4.3.3 Hg emission profiles in the carbonization furnace

The hourly flow of Hg in **C-F** is shown in **Fig. 4-9**. From the sewage sludge, 1.39 g of THg was fed to the furnace. During the drying process, less than 0.03 g/h of THg was discharged. Then, 1.50 g/h of THg was found in the dried sludge before feeding to the carbonization furnace. The higher amount in THg than the dewatered sludge is mainly caused by the inhomogeneity of sludge and discrepancies in sampling and measurement. After carbonization, only 0.04 g/h of THg was discharged in the generated biofuel, with a low recovery rate of 2.9%. The remaining THg was entrained in the flue gas and treated at the following APCDs. After the cyclone, 0.59 g/h of THg was detected, and Hg^0 dominantly accounted for 73% of THg in amount. Then, from the WS, ESP, to the stack, the amount of THg in the flue gas was almost the same, with no removal in THg emissions from these units. The dominant species of Hg may cause the extremely low removal efficiencies of THg at WS and ESP as Hg^0, which is hard to be absorbed in water because of its low solubility. However, still, 0.54 g/h of THg was discharged in wastewater from WS, and the mass balance was unable to get a reasonable closure at the WS. The discrepancy here may, on the one hand, be caused by the underestimated THg, especially Hg^{2+} in the flue gas to the WS; on the other hand, it may be related to the re-emission of Hg from the wastewater in WS.

Generally, in **C-F**, the WS and ESP in **C-F** can hardly remove THg due to its dominant

species of Hg as Hg^0. Therefore, a specific Hg^0 removal process should be taken into consideration in Hg emission control in sewage sludge thermal treatment process.

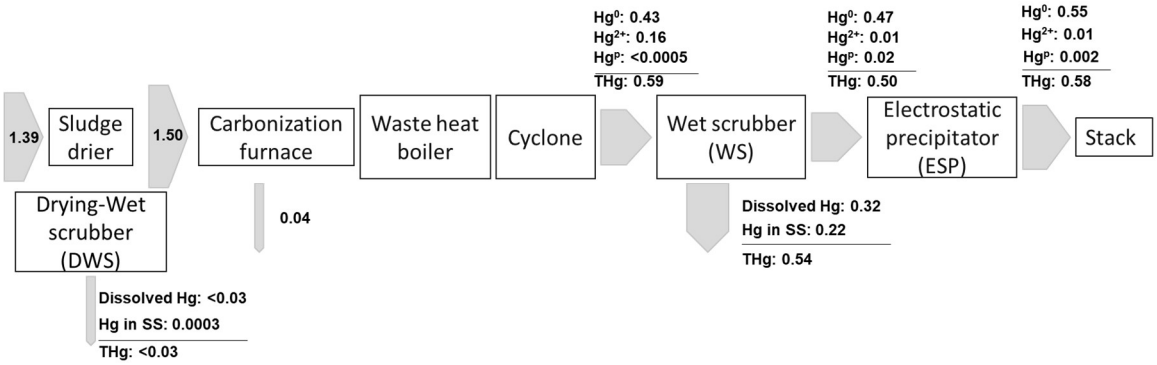

Figure 4-9. The average hourly mass flow of Hg in **C-F** (Unit: g/h). *SS*: suspended solids.

4.3.4 The evolution of Hg species with temperature in sewage sludge incinerators and carbonization furnace

Figure 4-10 shows the thermodynamic calculation results of Hg species in flue gas generated in sewage sludge incinerators **GS**, **FB**, **FC**, and **FD**. For all these incinerators, the primary species of Hg is Hg^0 at temperatures higher than 600 ºC, while the Hg^{2+} dominantly exists when the temperatures decreased to lower than 400 ºC. This tendency is in accordance with the Hg-CEM results in **4.3.1** for **GS** and **FD** that the Hg^{2+} dominantly exists in the flue gas in front of WS, in which the temperature is lower than 400 ºC. At the temperature range of 500~800 ºC, very small fractions of HgO also appeared in **FB**, **FC**, and **FD** as 1~4%, but no HgO is expected to appear at these temperatures in **GS**. The small fractions of HgO in **FB**, **FC**, and **FD** is caused by the oxidation of the excess air used in these fluidized type incinerators.

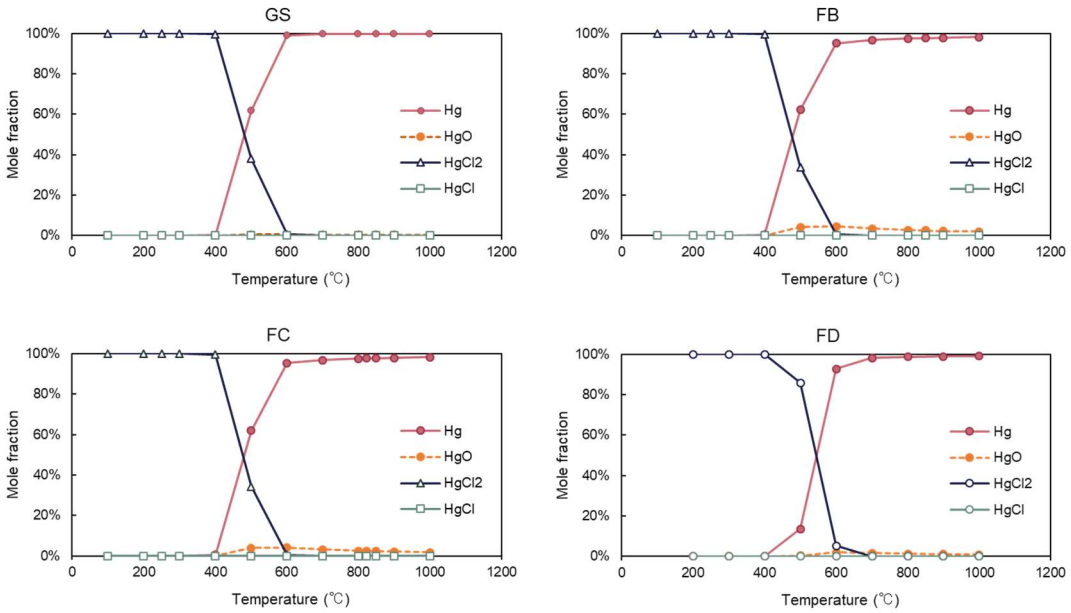

Figure 4-10. Thermodynamic calculation results on the species of Hg in the flue gas in sewage sludge mono-incinerators **GS**, **FB**, **FC**, and **FD**.

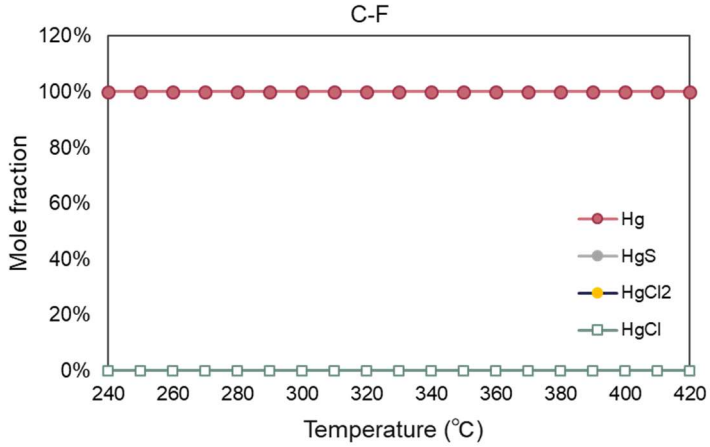

Figure 4-11. Thermodynamic calculation results on the species of Hg in the pyrolysis gas in **C-F**.

The evolution of Hg species in the pyrolysis gas in the carbonization furnace is shown in **Figure 4-11**. From 240 to 420 ºC, the primary Hg species is always Hg^0. The dominant existence of Hg^0 in the carbonization furnace is caused by the reduction atmosphere inside the furnace, in which oxygen is almost not existing; instead, nitrogen was used. The

estimated result compares well with the Hg-CEM results in **4.3.1**, in which the Hg^0 was dominantly detected in the inlet and outlet of WS, as well as in the stack emission.

Besides the speciation, a relevant relationship between the THg concentration in the pyrolysis gas, especially Hg^0, and the temperature was found in **C-F** (**Fig. 4-12**). By extracting the Hg^0 concentration and the temperature data, a linear relationship was discovered (**Fig. 4-13**). Thus, with the increase in temperature between 240 and 340 ºC, the Hg^0 concentration in the flue gas also increases. Since the dominant species of Hg in **C-F** is Hg^0, according to the thermodynamic calculation results (**Fig. 4-11**), the increase of the Hg^0 may be caused by the vapor pressure change with temperature that liberates the Hg^0 adsorbed in the sludge.

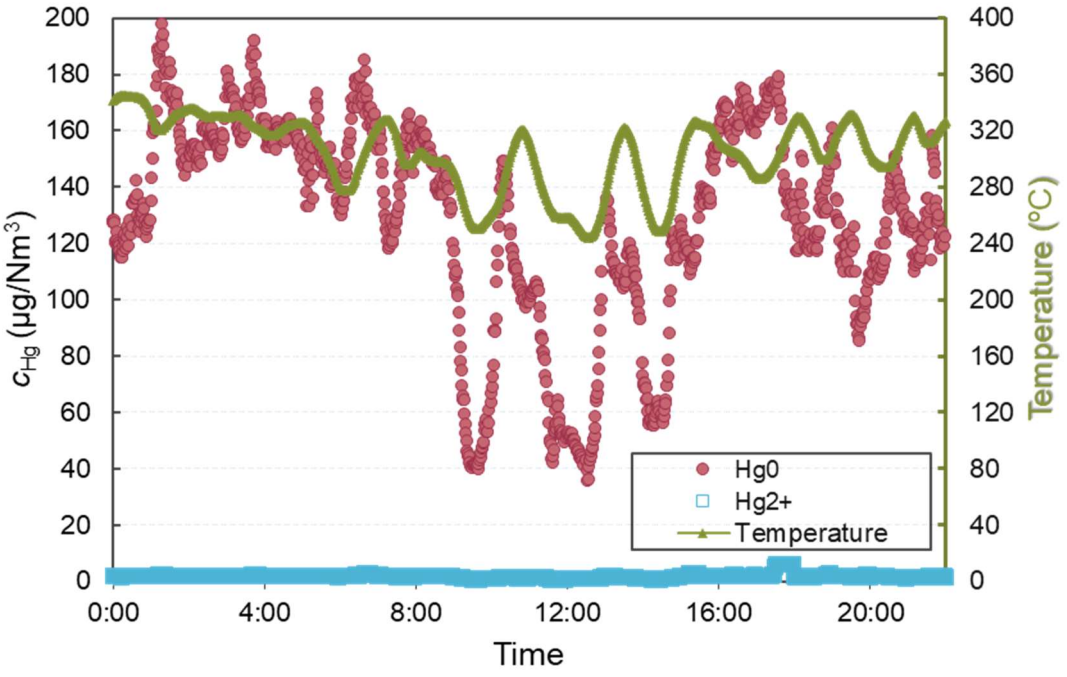

Figure 4-12. Concentrations of Hg^0 and Hg^{2+} in the pyrolysis gas and the temperature in **C-F**.

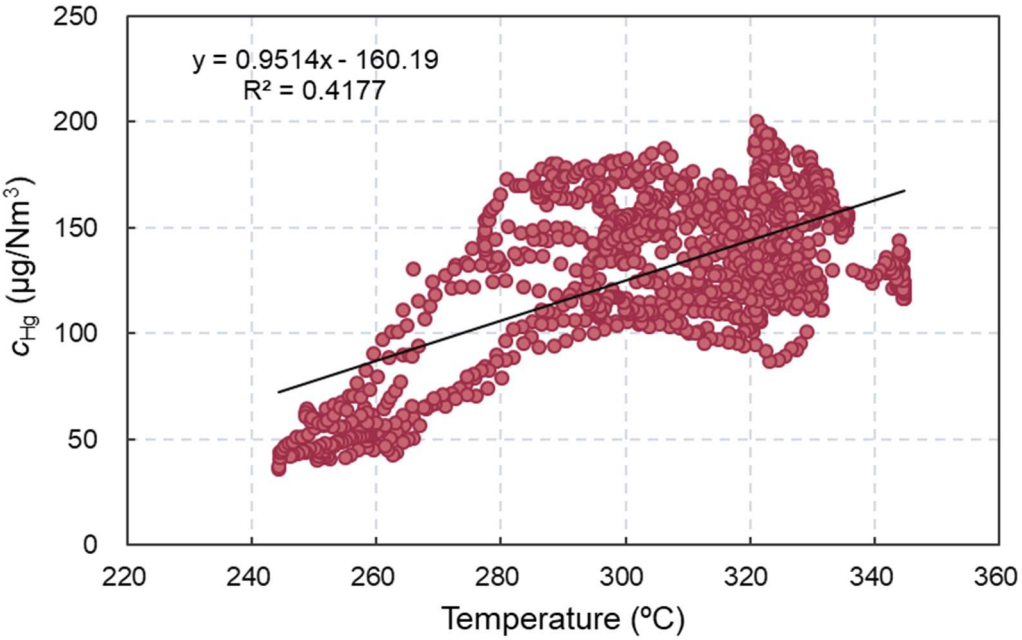

Figure 4-13. Relationship between the Hg^0 concentration in the pyrolysis gas and the temperature in **C-F**.

To conclude, from the thermodynamic calculations, Hg^{2+} was the primary species of Hg in the flue gas in sewage sludge incinerators at temperatures lower than 400 ºC, while Hg^0 dominant exists in the pyrolysis gas in carbonization process due to its reduction atmosphere. These thermodynamic calculation results are in accordance with the experimental data from the Hg-CEM.

4.3.5 The absorptive removal of Hg in sewage sludge carbonization furnace

Since the Hg^0 dominant in the flue gas at the **C-F**, the adsorptive removal of Hg^0 by sorbents was studied using modified activated carbon tower and polymer tower, as explained in **4.2.4**. **Fig. 4-14** shows the concentrations of Hg^0 in the inlet and outlet AC tower at **C-F**. The average Hg concentration in the inlet was 70.6 μg/Nm^3 but decreased to 0.3 μg/Nm^3 in the outlet of the first layer of the AC tower, leading to an average removal rate of Hg^0 by the AC tower as 99.6%. The continuous adsorption test showed a stable Hg^0

removal performance. With excellent Hg^0 removal performance, the MAC is a kind of promising sorbent for Hg^0 control in flue gas.

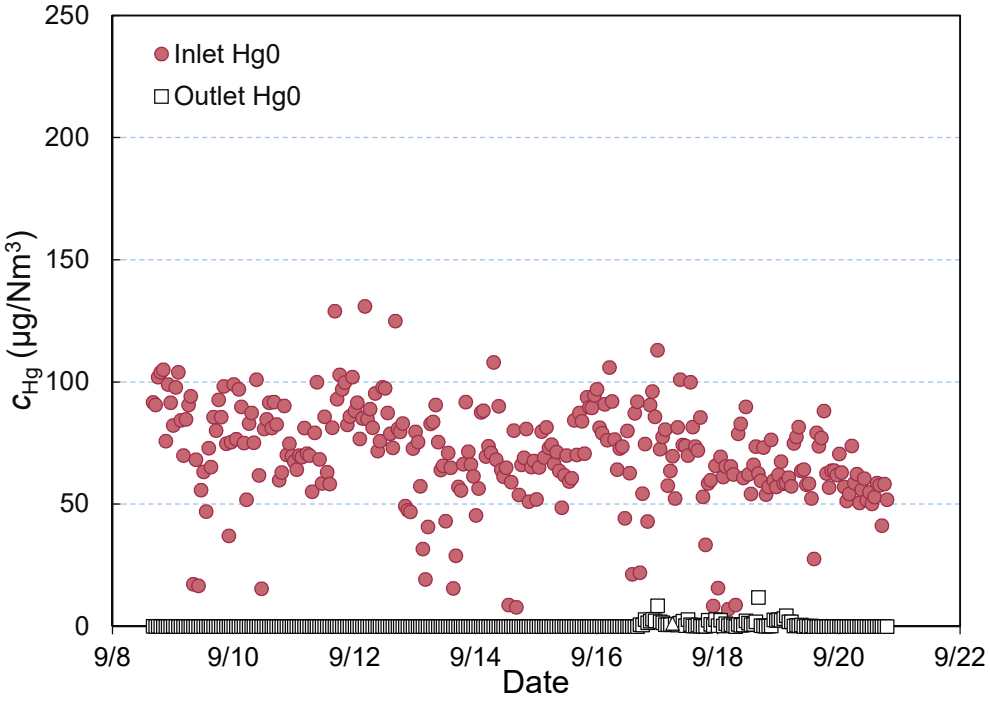

Figure 4-14. The concentrations of Hg^0 in the inlet and outlet of the first layer of the AC tower at **C-F**.

The adsorptive removal performance of Hg^0 by polymer tower is shown in **Fig. 4-15**. The average Hg^0 concentration in the inlet to the polymer tower was 67.5 μg/Nm^3. After the first layer of the polymer, the Hg^0 concentration decreased to about 30 μg/Nm^3, then decrease to 23.3 μg/Nm^{3}and 11.2 μg/Nm^{3}at the second layer and third layer, respectively. After three layers of polymer embedded in the tower, 83.4% of the Hg^0 was effectively removed.

Therefore, both the MAC and polymer tower can remove Hg^0 in the flue gas in the carbonization furnace effectively. Compared with polymer tower, the AC tower provided higher Hg^0 efficiency with only one layer and, consequently, is considered more feasible for Hg^0 removal in the carbonization furnace in this study. However, the disadvantages

were mainly found in its operation on the spot for the AC tower. For example, moisture was found to weaken its performance and the dust blocking also pose difficulties in its utilization and maintenance.

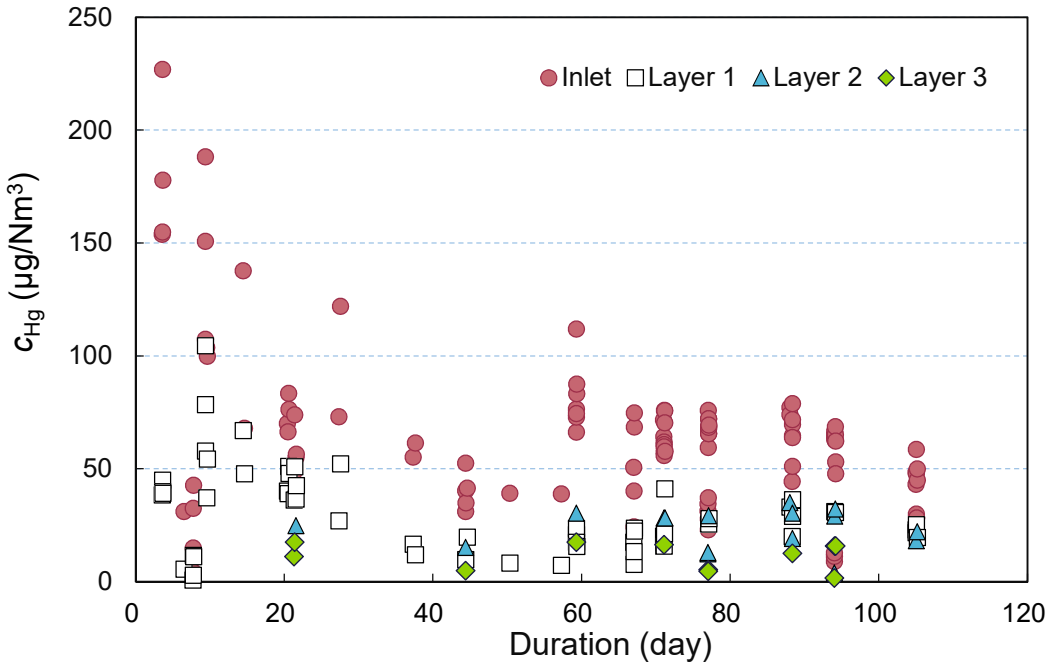

Figure 4-15. The concentrations of Hg^0 in the inlet and outlet of the polymer tower at **C-F.**

4.4 Summary

In this chapter, the continuous Hg emissions in SS mono-incineration and carbonization processes were monitored, and the thermodynamic calculations were conducted in all studied furnaces. In sewage sludge incinerators GS, FB, FC, and FD, despite the different types of incinerators and different sludge used, thermodynamic calculations show that the dominant species of Hg in the flue gas was Hg^{2+} at temperatures lower than 400 ºC. The Hg-CEM also confirmed the dominant existence of Hg^{2+} at the inlet of WS in GS and FD, but FB and FC showed a higher fraction of Hg^{2+} in the outlet of WS. The Hg^{2+} in the flue gas was then removed at the WS, with high recovery rates of Hg in

wastewater from WS in all these incinerators as 61~118%, while the flue gas emitted 6~33% of THg. Moreover, the re-emission of Hg^0 due to the reduction of Hg^{2+} possibly occurred at WS in GS and FB.

In contrary to the sewage sludge incinerators, Hg^0 is the dominant species of Hg in the pyrolysis gas after the carbonization with a low-temperature range of 240~420 ºC. The Hg-CEM results showed stable Hg^0 concentrations in the pyrolysis gas from the inlet of WS to the stack emission. Thus, 42% of Hg was emitted from the stack, with 40% as the Hg^0. The Hg^0 can be effectively removed by the MAC and polymer tower, and MAC is more feasible for its higher removal efficiency as 99.6% than that of polymer (83.4%) in this study, but also has the difficulties in operation.

References

Chang, J.C., Ghorishi, S.B., 2003. Simulation and evaluation of elemental mercury concentration increase in flue gas across a wet scrubber. Environ. Sci. Technol. 37(24), 5763–5766.

Chang, J.C., Zhao, Y., 2008. Pilot plant testing of elemental mercury reemission from a wet scrubber. Energy and Fuels 22(1), 338–342.

Cheng, C.M., Cao, Y., Kai, Z., Pan, W.P., 2013. Co-effects of sulfur dioxide load and oxidation air on mercury re-emission in forced-oxidation limestone flue gas desulfurization wet scrubber. Fuel 106, 505–511.

Díaz-Somoano, M., Unterberger, S., Hein, K.R., 2007. Mercury emission control in coal-fired plants: The role of wet scrubbers. Fuel Process. Technol. 88(3), 259–263.

Friedli, H.R., Radke, L.F., Prescott, R., Li, P., Woo, J.H., Carmichael, G.R., 2004. Mercury in the atmosphere around Japan, Korea, and China as observed during the 2001 ACE-Asia field campaign: Measurements, distributions, sources, and implications. J. Geophys. Res. D Atmos. 109, 1–13. https://doi.org/10.1029/2003JD004244

Galbreath, K.C., Zygarlicke, C.J., 1996. Mercury speciation in coal combustion and gasification flue gases. Environ. Sci. Technol. 30, 2421–2426. https://doi.org/10.1021/es950935t

Galbreath, K.C., Zygarlicke, C.J., 2000. Mercury transformations in coal combustion flue gas. Fuel Process. Technol. 65, 289–310.

Gbondo-tugbawa, S.S., Mcalear, J.A., Driscoll, C.T., Sharpe, C.W., 2010. Total and methyl mercury transformations and mass loadings within a wastewater treatment plant and the impact of the effluent discharge to an alkaline hypereutrophic lake. Water Res. 44, 2863–2875. https://doi.org/10.1016/j.watres.2010.01.028

Grace, J.R., Watkinson, A.P., Herod, A.A., Dugwell, D., 2001. Control of gasi ® er mercury emissions in a hot gas ® lter : the effect of temperature 80.

Holmes, P., James, K.A.F., Levy, L.S., 2009. Is low-level environmental mercury exposure of concern to human health? Sci. Total Environ. 408, 171–182. https://doi.org/10.1016/j.scitotenv.2009.09.043

JIS K 0222, Japanese Industrial Standards Committee (JIS), 1997.The methods of analyzing mercury in waste gas. (in Japanese)

Liu, M., Du, P., Yu, C., He, Y., Zhang, H., Sun, X., Lin, H., Luo, Y., Xie, H., Guo, J., Tong, Y., 2018. Increases of total mercury and methylmercury releases from municipal sewage into environment in China and implications. Environ. Sci. Technol. 52(1), 124–134.

Löthgren, C.J., Takaoka, M., Andersson, S., Allard, B., Korell, J., 2007. Mercury speciation in flue gases after an oxidative acid wet scrubber. Chem. Eng. Technol. 30(1), 131–138.

Mao, Y., Cheng, L., Ma, B., Cai, Y., 2016. The fate of mercury in municipal wastewater treatment plants in China: Significance and implications for environmental cycling. J. Hazard. Mater. 306, 1–7. https://doi.org/10.1016/j.jhazmat.2015.11.058

Pacyna, E.G., Pacyna, J.M., Sundseth, K., Munthe, J., Kindbom, K., Wilson, S., Steenhuisen, F., Maxson, P., 2010. Global emission of mercury to the atmosphere from anthropogenic sources in 2005 and projections to 2020. Atmos. Environ. 44, 2487–2499. https://doi.org/10.1016/j.atmosenv.2009.06.009

Pudasainee, D., Seo, Y.C., Kim, J.H., Jang, H.N., 2013. Fate and behavior of selected heavy metals with mercury mass distribution in a fluidized bed sewage sludge incinerator. J. Mater. Cycles Waste Manage. 15(2), 202–209.

Srivastava, R.K., Hutson, N., Martin, B., Princiotta, F., Staudt, J., 2006. Control of mercury emissions from coal-fired electric utility boilers. Environ. Sci. Technol. 40, 1385–1393. https://doi.org/10.1021/es062639u

Standard, A.S.T.M., 2008. Standard test method for elemental, oxidized, particle-bound, and total mercury in flue gas generated from coal-fired stationary sources (ontario-hydro). Designation: D6784–02.

Sun, P., Zhang, B., Zeng, X., Luo, G., Li, X., Yao, H., Zheng, C., 2017. Deep study on effects of activated carbon ' s oxygen functional groups for elemental mercury adsorption using temperature programmed desorption method. Fuel 200, 100–106. https://doi.org/10.1016/j.fuel.2017.03.031

Takaoka, M., Domoto, S., Oshita, K., Takeda, N., Morisawa, S., 2012. Mercury emission from sewage sludge incineration in Japan. J. Mater. Cycles Waste Manag. 14, 113–119. https://doi.org/10.1007/s10163-012-0044-2

Takaoka, M., Oshita, K., Okada, M., Watanabe, T., Tanida, K., 2018. Uncorrected Proof incinerator and melting furnace Uncorrected Proof 1–9. https://doi.org/10.2166/wst.2018.268

Takaoka, M., Takeda, N., Fujiwara, T., Kurata, M., Kimura, T., 2002. Control of mercury emissions from a municipal solid waste incinerator in Japan. Journal of the Air & Waste Management Association, 52(8), 931–940.

Van de Velden, M., Dewil, R., Baeyens, J., Josson, L., Lanssens, P., 2008. The distribution of heavy metals during fluidized bed combustion of sludge (FBSC). J. Hazard. Mater. 151, 96–102. https://doi.org/10.1016/j.jhazmat.2007.05.056

Yang, H., Xu, Z., Fan, M., Bland, A.E., Judkins, R.R., 2007. Adsorbents for capturing mercury in coal-fired boiler flue gas. J. Hazard. Mater. 146, 1–11. https://doi.org/10.1016/j.jhazmat.2007.04.113

Zhang, L., Wong, M.H., 2007. Environmental mercury contamination in China: Sources and impacts. Environ. Int. 33, 108–121. https://doi.org/10.1016/j.envint.2006.06.022

Chapter 5 Investigation of mercury adsorptive removal using impregnated activated carbon

5.1 Introduction

In 2017, the Minamata Convention (United Nations Environment Programme) entered into force, and is expected to lead to a reduction in the emission and release of Hg (UNEP). To remove Hg^0 from flue gas, virgin and chemically treated activated carbons (ACs) have been studied extensively (Krlshnan et al., 1994; Yang et al., 2007). For example, ACs impregnated with halogens (Y. Chen et al., 2018; Vidic and Siler, 2001) and sulfur (Lee and Park, 2003; Li et al., 2018) are reported to exhibit excellent Hg^0 removal performance (Ghorishi et al., 2002; Suresh Kumar Reddy et al., 2014), and even greater Hg^0 removal efficiency was observed when Cl and S were co-impregnated (Sano et al., 2017). Among the halogen-impregnated ACs, Hg^0 removal efficiency significantly decreases in the following order: I-AC > Br-AC > Cl-AC. Meanwhile, the activation energy barrier associated with HgX formation increases in the following order: HgI < HgBr < HgCl (Rungnim et al., 2016). Another advantage of using an iodine-impregnated sorbent is the lower volatility of HgI_2 (higher boiling point) compared to other mercury halides, which enhances the stability of the spent sorbent (Li et al., 2009). Therefore, iodine-impregnated ACs are promising sorbents for Hg^0 removal.

The mechanisms underlying Hg^0 removal by both virgin and impregnated ACs involve activated sites on the surfaces of the ACs. Oxygen functional groups (OFGs), especially ester groups (C-O) and carbonyl groups (C=O), contribute significantly to mercury removal by providing activated sites for Hg^0 binding (Li et al., 2018, 2002, 2003; Z. Liu et al., 2018; Sun et al., 2017). Furthermore, O_2 also promotes Hg^0 removal by oxidizing Hg^0 (Kong et al., 2011; Z. Liu et al., 2018). For iodine-impregnated ACs such as potassium iodide (KI)-impregnated ACs, molecular iodine (I_2) formed from the oxidation of KI is speculated to participate in the primary mechanism of Hg^0 removal, according to the following proposed reaction: $4\ KI + O_2 = 2\ K_2O + 2\ I_2$ (Li et al., 2009; Tong et al., 2017). However, starch-iodine tests showed that I_2 can barely formed at temperatures lower than 300°C (Li et al.,

2009), and the Gibbs free energy for the proposed reaction has a positive value even at 1,000°C (**Table 5-1**). Hence, the mechanism of Hg^0 adsorption by KI-impregnated sorbents needs further clarification. Moreover, other than results from the starch-iodine test (Li et al., 2009; Zhang et al., 2009) and surface morphology characterization (Lee et al., 2004), there is little evidence regarding the crystalline phase or chemical state of I_2. Therefore, additional investigation regarding the presence of I_2, and the form and chemical state of the iodine impregnated in the ACs, is necessary to clearly elucidate the reaction pathways.

Table 5-1. Thermodynamic results for the equation 2 KI + 1/2 O_2 = I_2 + K_2O. The calculations were conducted with *FactSage* software and the Fact53 database.

T (℃)	△H (kJ)	△S ($J \cdot K^{-1}$)	△G (kJ)
25	294	-97.2	323
105	295	-94.1	331
140	356	45.0	337
200	356	44.2	335
300	355	42.9	330
400	354	41.4	326
500	353	39.6	322
600	351	37.5	318
700	349	35.3	315
800	347	33.8	311
850	347	33.1	309
900	346	32.4	308
1000	344	30.6	305

Furthermore, existing research concerning iodine-impregnated ACs is mostly concerned with KI impregnation; precursors other than KI are scarcely used. Consequently, the influence of the cation element on Hg^0 adsorption performance is rarely discussed.

The purpose of this chapter was to (1) investigate Hg^0 removal performance using iodine-impregnated ACs with different precursors, such as KI, ammonium iodide (NH_4I), potassium iodate (KIO_3), and a co-impregnation of KI followed by $CuSO_4$; (2) explore the mechanism underlying I_2 formation in iodine-impregnated ACs and cation effects; and (3)

propose pathways for Hg^0 removal by the prepared ACs.

Different measurement methods, including Brunauer-Emmett-Teller (BET) specific surface area analysis, X-ray diffraction (XRD), X-ray photoelectron spectroscopy (XPS), and X-ray absorption near-edge structure analysis (XANES), were used to confirm the texture characteristics of the ACs, as well as the species and chemical state of the compounds impregnated in and adsorbed on the ACs. Based on these experimental results, putative pathways for Hg^0 removal by the prepared ACs were proposed and evaluated according to the Gibbs free energy value.

5.2 Methodology

5.2.1 Sorbent preparation

Granular AC based on coconut shells (SHIRASAGI C2c20/48; Osaka Gas Chemicals, Osaka, Japan) was used as the carrier and control sorbent in this study (**Table 5-2**).

The AC samples were dried at 105°C for 12 h before impregnation. The raw AC was impregnated with iodides of different cations—KI and NH_4I—via one-step impregnation to compare the effects of different cations on Hg^0 adsorption performance. The AC was also prepared with KIO_3 using one-step impregnation to analyze the effects of using iodine with different valences. Additionally, co-impregnation with KI and $CuSO_4$ (impregnation with KI followed by impregnation with $CuSO_4$) was conducted in an attempt to precipitate CuI and I_2 into the AC. The impregnation procedures were explained in a previous study (Sano et al., 2017).

Sorbents were denoted as AC-virgin for non-impregnated ACs, and as AC-KI, AC-NH_4I, and AC-KIO_3 for ACs one-step impregnated with KI, NH_4I, and KIO_3, respectively. The co-impregnated AC was denoted as AC-KI+$CuSO_4$.

Table 5-2. Elemental content of raw AC (Sano, A. et al., 2017; Nishimura K. et al., 2004).

Element	S	Cl	P	Ca	Mg	Fe	Ti	Cu	Pb	Mo
mmol/g	0.02	0.05	0.06	0.009	0.01	0.01	0.004	0.0002	0.0006	0.0001

5.2.2 Sorbent characterization

The BET specific surface area (S_{BET}) of the sorbents was determined using nitrogen adsorption at −196°C with an ASAP 2020 analyzer (Micromeritics, Norcross, GA, USA). All sorbents were degassed at 25°C before BET measurements. The average pore size and pore size distribution were determined using the Barrett, Joyner, and Halenda method. The crystal structure of the sorbents was determined using XRD (RINTUltima+/PCQ2; Rigaku, Tokyo, Japan). The Hg L_{III}-edge and I K-edge XANES spectra were collected using a beamline BL01B1 at the SPring-8 synchrotron radiation facility in Hyogo, Japan. Mercury reference components including elemental Hg and solid materials, such as Hg_2Cl_2, $HgCl_2$, HgI, HgI_2, HgO (red), HgO (yellow), HgS (black), HgS (red), Hg_2SO_4, $HgSO_4$, and $Hg_3S_2Cl_2$, were selected based on the precursors used for impregnation and possible products after the adsorption test (Sano et al., 2017). Iodine components (Shimamoto and Takahashi, 2008), including solid materials such as KI, NaI, NH_4I, CuI, CaI_2, HgI, HgI_2, I_2, KIO_3, and $NaIO_3$, triiodide ions (I_3^-) in a KI-I_2 saturated solution (1 mol/L KI solution with 1:1 I_2 added), were used to identify the species of iodine in the ACs. All spectra were collected in transmission mode, except for Hg L_{III}-edge samples, which were recorded in fluorescent mode due to the low concentrations. By applying principal component analysis (PCA) and target transformation, irrelevant reference materials were excluded, and linear combination fitting (LCF) of the XANES data was conducted using relevant reference materials with *ATHENA* software (Ravel and Newville, 2015) to estimate the proportions of all species of Hg or I contained in the samples. The XPS analysis was performed using an ESCA-3200 system (Kratos Analytical Ltd., Manchester, UK). The detection sensitivity of XPS is 0.1 at%. Spectra were collected using Mg Ka radiation at 1,253.6 eV. Data processing was conducted using *COMPRO12* software (COMPRO), and all spectra were calibrated to the C1s peak located at 284.6 eV.

5.2.3 Mercury adsorption experiment

The adsorption tests were conducted using an apparatus that comprised a mercury generator, pre-heater, fixed-bed column, and continuous mercury monitor (**Fig. 5-1**) (Sano

et al., 2017). A dehumidification column and an activated column were placed in front of the air inlet. To avoid adsorption of Hg^0 onto the tube wall, all tubes used in this study were made from Teflon or glass.

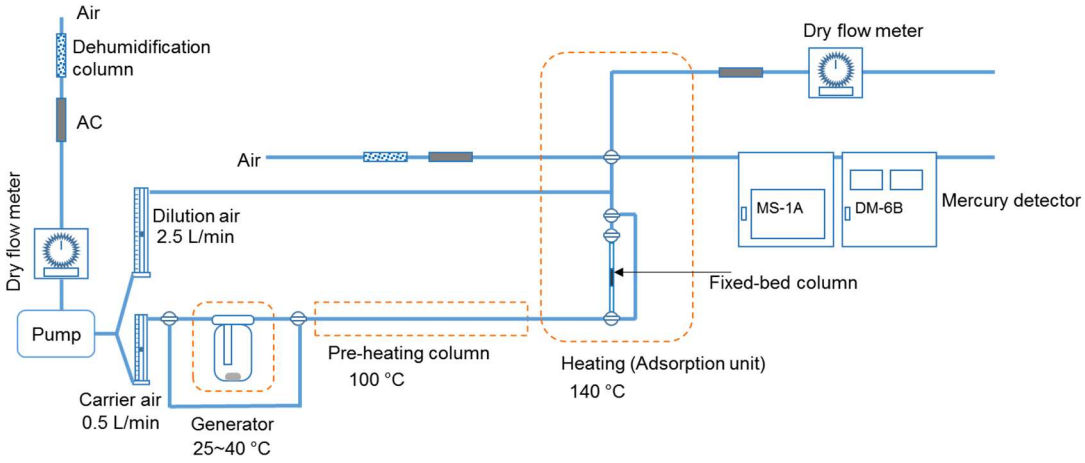

Figure 5-1. Schematic of the elemental mercury adsorption fixed-bed reactor.

The mercury generator consisted of a glass impinger connected to a temperature controller. Metallic mercury was placed at the bottom of the impinger. The dehumidified air flowed at a rate of 0.5 L/min and carried Hg^0 vapor to the adsorption column. After vapor-phase elemental Hg had been generated, the Hg gas was pre-heated to 90°C in a pre-heating column. Then, the Hg^0 gas entered the up-stream fixed-bed column, which was maintained at 140°C with a ribbon heater. The diameter of the fixed-bed column was 10 mm. Glass beads and quartz wool were used to conceal and fix samples inside the column, as well as to homogenize the gas flow and prevent short flow. The Hg^0 concentration was adjusted to approximately 1,500 μg/m^3 to transfer as much Hg^0 as possible to the AC samples. Each sorbent (1.0 g) was exposed to the flowing flue gas simulant at 140°C for 10 h for the impregnated ACs, whereas AC-virgin was only exposed for 3 h because it exhibited an early breakthrough (Sano et al., 2017).

The mercury concentration was detected using continuous mercury monitors, including a pretreatment instrument (MS-1A) and a DM-6B detector (Nippon Instruments Co., Ltd., Tokyo, Japan), which can measure different species of Hg such as Hg^0 and Hg^{2+}. The Hg^0 content was confirmed to be more than 97.9% in the inlets for all tests (**Table 5-**

3); therefore, Hg^{2+} is neglected in the following equation.

The average mercury removal efficiency η_a (%) was calculated as follows:

$$\eta_a = \frac{c_{ina} - c_{outa}}{c_{ina}} \times 100\% \quad (1)$$

where c_{ina} and c_{outa} denote the average Hg^0 concentration ($\mu g/m^3$) at the inlet and outlet of the reactor, respectively.

Table 5-3. The Hg^0 content in the inlet during the adsorption tests.

Sorbent	$c(Hg^0)$ μ g/m^3	$c(Hg^{2+})$ μ g/m^3	Hg^0 content
AC-virgin	1,510	1.4	99.9%
AC-KI	1,130	8.3	99.3%
AC-NH_4I	1,950	13.1	99.3%
AC-KIO_3	1,680	7.6	99.6%
AC-KI+$CuSO_4$	1,640	35.2	97.9%

5.3 Results and Discussion

5.3.1 Mercury adsorption performance of the sorbents

The results of the adsorption tests are summarized in **Figure 5-2**. Because the duration of each adsorption test was only 3 or 10 h, the breakthrough curves and saturated adsorption capacities of the sorbents were not obtained. All impregnated ACs exhibited better Hg^0 removal performance than AC-virgin, and η_a values ranged from 97.2% to 99.9% in the following order: AC-KI+$CuSO_4$ > AC-NH_4I > AC-KIO_3 > AC-KI > AC-virgin. This result demonstrated that co-impregnating with KI and $CuSO_4$ is more efficient for Hg^0 removal than the one-step impregnations used in this study. Moreover, with the same I^- anion, the type of cation precursor used for impregnation (K^+ and NH_4^+) significantly affected the Hg^0 removal rate, with NH_4I being more efficient than KI. Further, the valence of iodine used in this study—i.e., I^{5+} (KIO_3) and I^- (KI)—also affected the Hg^0 removal performance significantly.

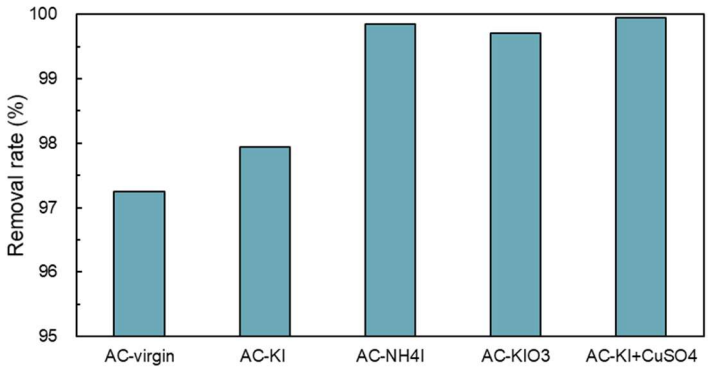

Figure 5-2. The removal rate of Hg^0 for sorbents.

5.3.2 BET surface area analysis (surface morphology)

Table 5-4 summarizes the S_{BET}, pore volume (V_{total}), and pore size (d_{pore}) data. The surface area of AC-virgin was 1,200 m^2/g, which was larger than that reported in other studies (Jang et al., 2017; Li et al., 2018; Sun et al., 2017; Wu et al., 2017; Zhong et al., 2017). After impregnation, the S_{BET} of the ACs decreased, with AC-KI+$CuSO_4$ having the smallest surface area of 1,000 m^2/g, which was 83.3% that of AC-virgin. The decrease in S_{BET} may have been caused by blockage and collapse of internal pores (Z. Liu et al., 2018; Wu et al., 2017; Zeng et al., 2004). Because the average pore size of all impregnated ACs also increased, blockage mainly occurred in micropores, in accordance with a decrease in the volume of the micropores (V_{micro}) (Shao et al., 2016). Moreover, the largest V_{total} was observed for AC-KIO_3, which indicates that both micropores and mesopores had collapsed, perhaps in relation to oxidation by KIO_3. As a result, all pore sizes increased, such that V_{total} also increased.

During Hg^0 removal, micropores can serve as a source of activated sites, and mesopores may function as transmission channels of mercury (Li et al., 2018). Therefore, a decrease in S_{BET} and V_{micro} will negatively affect physical adsorption performance (Wu et al., 2017). However, despite a decrease in S_{BET} and V_{micro}, all impregnated ACs exhibited greater Hg^0 removal efficiency (**Fig. 5-2**). Hence, rather than physical adsorption, chemisorption dominates Hg^0 removal, as reported in previous studies (Sano et al., 2017; Tong et al., 2017; Van Stipdonk et al., 2000; Zhou et al., 2015).

Table 5-4. Brunauer-Emmett-Teller specific surface area (S_{BET}) and microstructure parameters of virgin and impregnated activated carbons (ACs).

Sample	S_{BET} (m^2/g)	V_{micro} (cm^3/g)	V_{total} (cm^3/g)	V_{micro}/V_{total} (%)	d_{pore} (nm)
AC-virgin	1,200	0.43	0.62	68.9	2.36
AC-KI	1,050	0.37	0.58	63.6	3.09
AC-NH_4I	1,110	0.37	0.62	60.1	3.12
AC-KIO_3	1,180	0.40	0.66	60.3	3.15
AC-KI+$CuSO_4$	1,000	0.34	0.55	61.4	3.11

V_{micro}, micropore volume; V_{total}, pore volume; d_{pore}, pore size.

5.3.3 XRD analysis

The results of the XRD analysis of virgin and impregnated ACs are presented in **Figure 5-3**. Two strong and broad peaks for AC-virgin were detected at 2θ = 23.80° and 43.22°. (Wu et al., 2017) The peak at 23.80° can be attributed to amorphous carbon (C) structures, whereas the peak at 43.22° may be due to the *a* axis of the graphite structure (Liu et al., 2010; Okamura et al., 2006). After impregnation, the intensities of these two peaks decreased, indicating that the structure of the ACs was affected by the impregnation.

The crystalline phase of KIO_3 was found in AC-KIO_3 both before and after the adsorption test. After the adsorption test, the intensity of KIO_3 decreased, indicating that KIO_3 had been consumed, possibly in association with Hg^0 removal. The proposed reactions are as follows:

$$3\ Hg\ (g) + KIO_3\ (s) = KI\ (s) + 3\ HgO\ (s) \quad (2)$$

$$\Delta rG^{\ominus}(413\ K) = -134.7\ kJ{\cdot}mol^{-1}$$

$$2\ KIO_3\ (s) + 3\ C\ (s) = 2\ KI\ (s) + 3\ CO_2\ (g) \quad (3)$$

$$\Delta rG^{\ominus}(413\ K) = -1{,}054\ kJ{\cdot}mol^{-1}$$

A faint crystalline phase of CuI was found in AC-KI+$CuSO_4$ before the adsorption test (not marked in **Fig. 5-3**), whereas Cu_2HgI_4 was observed after the adsorption test. We speculate that the reactions proposed in **Eq. (4)** and **(5)** occurred on the surface of the AC during impregnation and adsorption of AC-KI+$CuSO_4$ (Shaffer and Hartmann, 1921;

Ahmad, 2011).

$$2\ CuSO_4\,(aq) + 4\ KI\,(aq) = 2\ CuI\,(s) + I_2\,(s) + 2\ K_2SO_4\,(aq) \quad (4)$$

$$4\ CuI\,(s) + Hg\,(g) = Cu_2HgI_4\,(s) + 2\ Cu\,(s) \quad (5)$$

However, no peaks associated with the crystalline phase of KI, NH_4I, or I_2 were visible for the other sorbents, and could also not be detected using XRD.

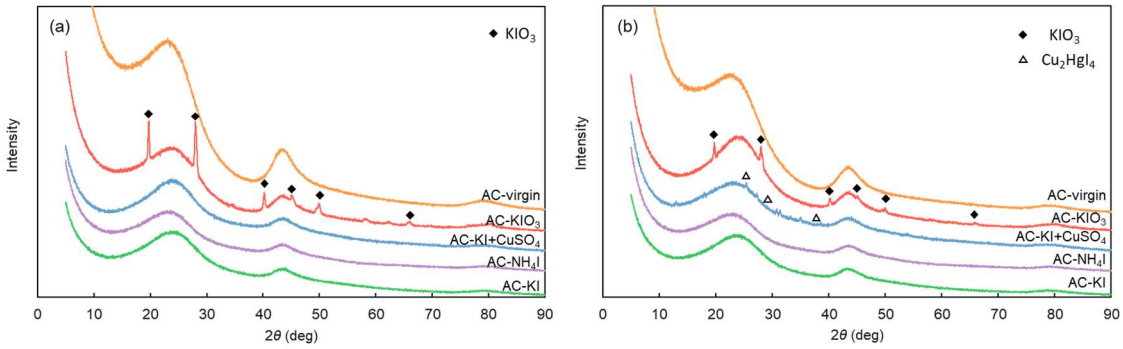

Figure 5-3. X-ray diffraction analysis of virgin and impregnated ACs (a) before and (b) after the adsorption tests.

5.3.4 XPS analysis (surface chemistry of the sorbents)

To confirm the surface chemical composition and chemical states of the sorbents, the XPS wide-scan spectrum was employed initially. Strong peaks for C1s, O1s, and I3d were detected (**Fig. 5-4**); however, peaks ascribed to mercury were not found during the XPS analysis because the concentration of mercury in all samples was less than 0.1 at%, which is the detection sensitivity of XPS. The results revealed that C and oxygen (O) were consumed during the chemisorption of Hg^0 (**Fig. 5-5**). The decrease in C and O on the surfaces of the sorbents indicated that a gaseous phase product—possibly CO_2—may have formed and escaped into the carrier gas during this process (Eichberger and Stieglitz, 1994), in accordance with the XRD results for the sorbent AC-KIO_3 and **Eq. (3)**.

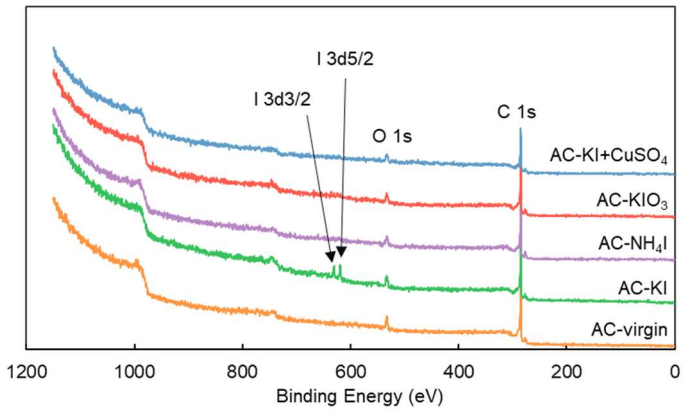

Figure 5-4. Results of XPS wide-scan analysis of the sorbents.

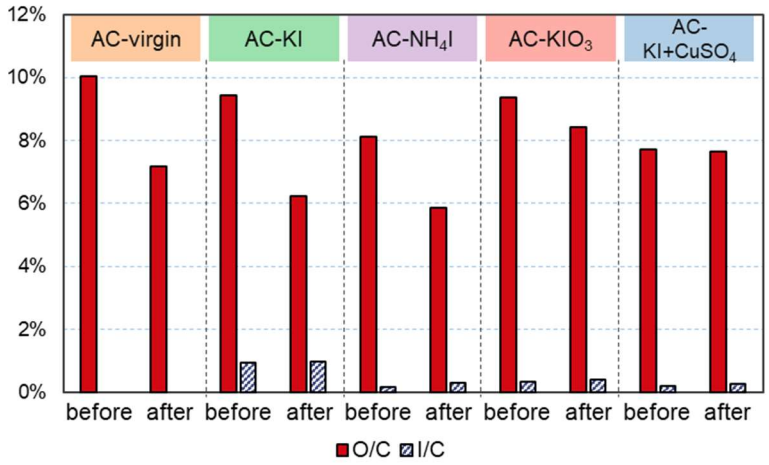

Figure 5-5. Surface elemental composition derived from wide-scan analysis (based on atomic concentration). After adsorption, the ratio of I/C in impregnated ACs increased due to the decrease in the amount of C. Additionally, the O/C ratio decreased for all sorbents except AC-KI+$CuSO_4$, which implies that the amount of O also decreased after adsorption. These results indicate that C and O were consumed during chemisorption of Hg^0. Further, the decreased C and O on the surfaces of the sorbents suggests that a gaseous phase product—possibly CO_2—might have formed and escaped into the carrier gas during this process (Eichberger and Stieglitz, 1994).

The corresponding high-resolution XPS spectra in **Figure 5-6** exhibit the characteristic peaks of C1s, O1s, and I3d for the virgin and impregnated ACs. Because the shapes of the C1s spectra were similar for all sorbents, which featured three typical peaks both before and after the adsorption tests, only the spectra for AC-virgin are shown in **Figure 5-6(a)** (the XPS C1s spectra for the other sorbents are shown in **Fig. 5-7**). The peaks at 284.6, 285.1–285.3, and 287.4–288.7 eV in the deconvoluted C1s XPS spectra (**Fig. 5-**

6(a)) are attributed to C-C/C-H, C-O, and COOH/C(O)-O-C/C=O, respectively (Li et al., 2018, 2015; Zhang et al., 2015). After adsorption, the relative intensity of C-C increased, whereas the relative intensity of OFGs, namely C-O and COOH/C(O)-O-C/C=O, decreased on the surfaces of the sorbents (Li et al., 2018, 2003), as summarized in **Table 5-5**. However, the relative intensity of OFGs increased slightly for AC-KIO_3, possibly due to the consumption of C, as implied by **Eq. (3)**.

The O1s high-resolution spectra for all sorbents except AC-KI+$CuSO_4$ were very similar; therefore, only the spectra for AC-virgin and AC-KI+$CuSO_4$ are shown in **Figure 5-6(b)** and **5-6(c)**, and the spectra for the remaining sorbents are presented in **Figure 5-8**. After fitting, the O1s spectrum can be resolved into two individual component peaks at 530.3–530.5 and 532.7–533.2 eV for all sorbents, except AC-KI+$CuSO_4$, before the adsorption test. The shoulder peaks at 530.3–530.5 eV are attributed to C=O groups, whereas the higher binding energy component is probably due to C-O groups or chemisorbed O, such as COOH carboxylic groups (Altenor et al., 2009; Harijan et al., 2018; Li et al., 2010). After adsorption, the shoulder peak disappeared in all sorbent spectra (**Table 5-6**), indicating that this form of O interacted with other components during the adsorption test at 140°C.

Hence, the XPS C1s and O1s spectra confirmed that OFGs were present on the surfaces of the sorbents. OFGs such as carbonyl and ester groups on the surfaces of the sorbents enhance mercury removal performance by providing activated sites for Hg^0 binding (Li et al., 2003, 2002). From the C1s and O1s spectra (**Tables 5-5** and **5-6**), it appears that OFGs, particularly C=O, were consumed, which is in accordance with the wide-scan results (**Fig. 5-5**). However, the sorbent AC-KI+$CuSO_4$, which has the lowest content among OFGs (**Table 5-5**) and almost no C=O groups (**Fig. 5-6(c)** and **Table 5-6**), exhibited the greatest Hg^0 removal efficiency. This indicates that besides the active sites, such as OFGs, the reaction proposed in **Eq. (5)** also significantly enhanced Hg^0 removal performance for AC-KI+$CuSO_4$. Furthermore, other chemical components, such as O_2 and I_2, may also play essential roles in Hg^0 oxidation (Kong et al., 2011; Li et al., 2009; Tong

et al., 2017).

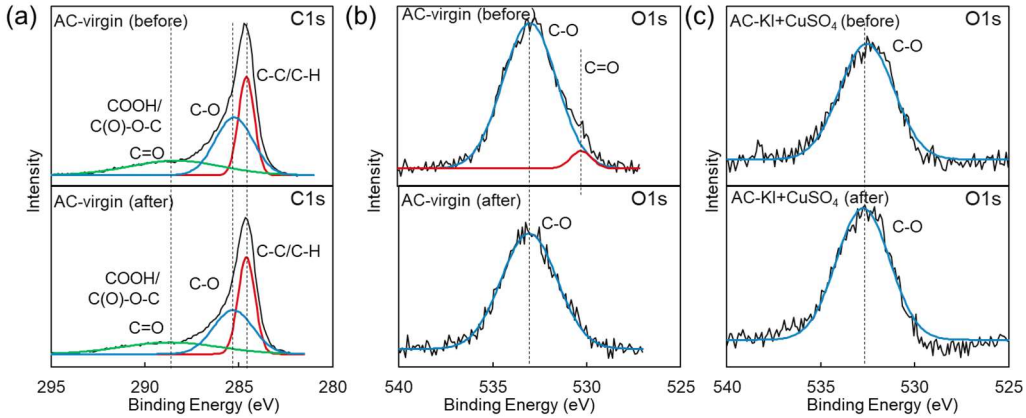

Figure 5-6. High-resolution spectra generated by X-ray photoelectron spectroscopy (XPS) of (a) C1s for AC-virgin, (b) O1s for AC-virgin, and (c) O1s for AC-KI+$CuSO_4$.

Table 5-5. Functional groups of the sorbents before and after the adsorption tests (C1s high-resolution spectra).

		Relative intensity									
		AC-virgin		AC-KI		AC-NH_4I		AC-KIO_3		AC-KI+$CuSO_4$	
Functional group	Binding energy (eV)	before	after	before	after	before	after	before	after	before	after
C-C/C-H	284.6	0.31	0.36	0.35	0.39	0.34	0.38	0.36	0.34	0.37	0.41
C-O	285.1–285.3	0.43	0.39	0.44	0.40	0.38	0.41	0.37	0.44	0.38	0.44
COOH/C(O)-O-C/C=O	287.4–288.7	0.27	0.25	0.21	0.19	0.28	0.22	0.27	0.21	0.24	0.15
Oxygen functional groups		0.69	0.64	0.65	0.59	0.66	0.62	0.64	0.65	0.63	0.59

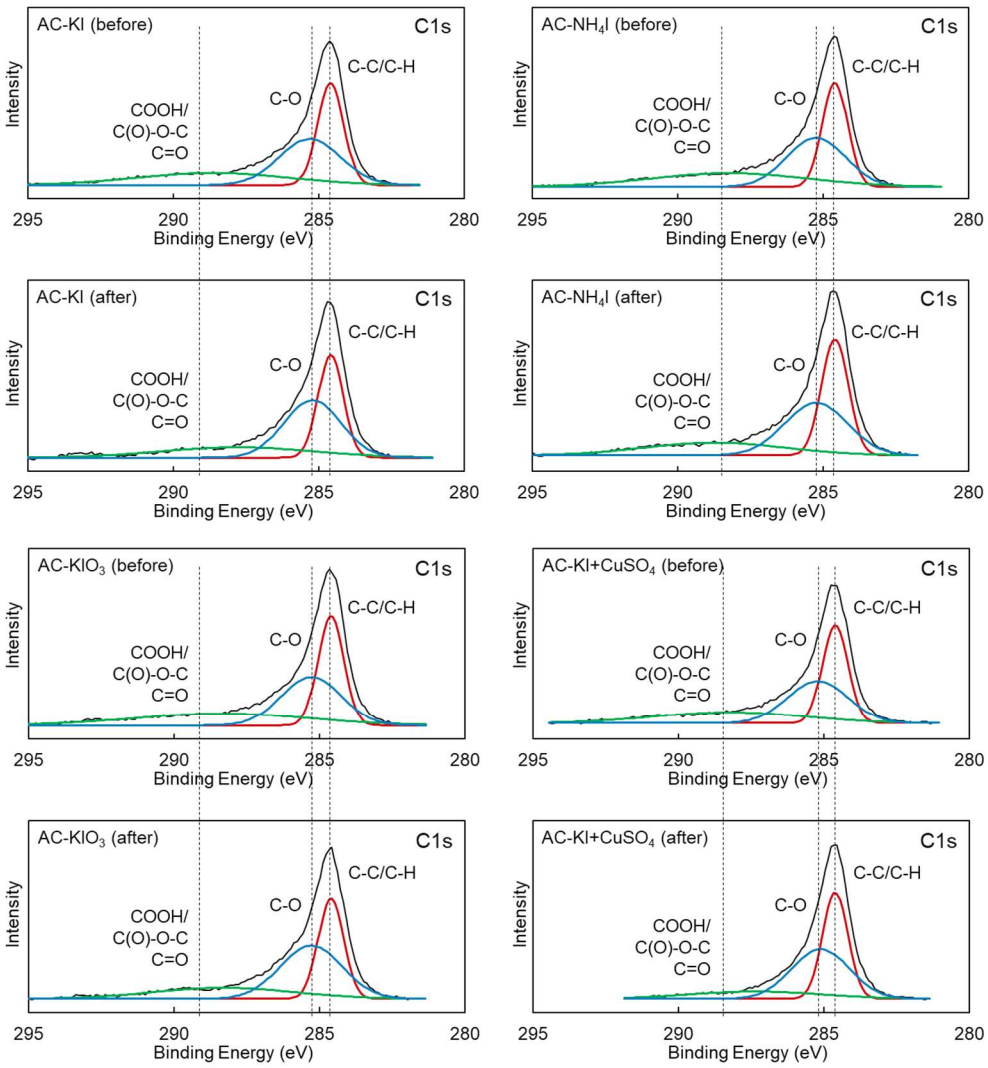

Figure 5-7. XPS high-resolution C1s spectra before and after the adsorption tests.

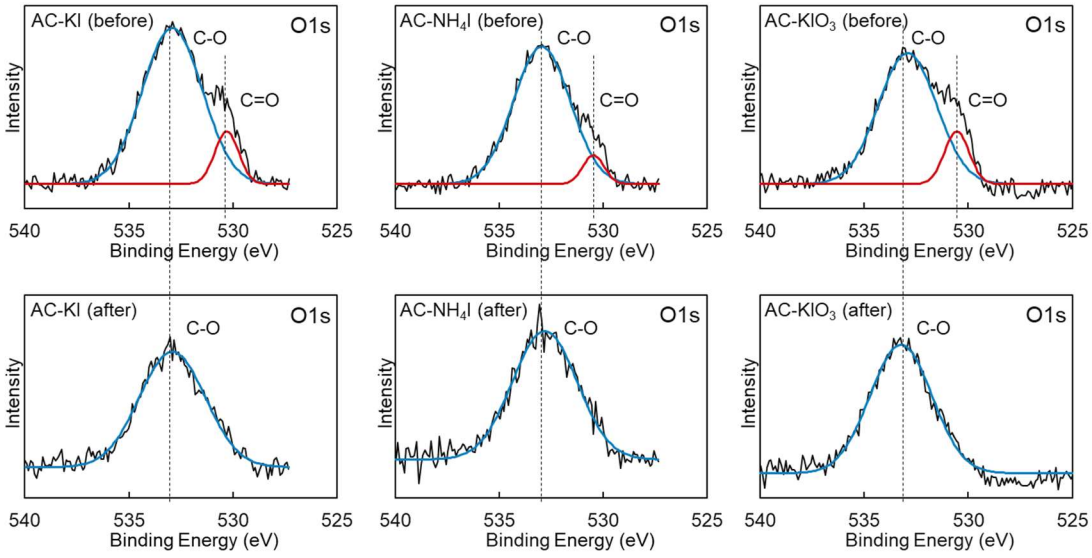

Figure 5-8. XPS high-resolution O1s spectra for sorbents AC-KI, AC-NH_4I, and AC-KIO_3 before and after the adsorption tests.

Table 5-6. Functional groups of the sorbents before and after the adsorption tests (O1s high-resolution spectra).

		Relative intensity									
		AC-virgin		AC-KI		$AC-NH_4I$		$AC-KIO_3$		$AC-KI+CuSO_4$	
Functional group	Binding energy (eV)	before	after	before	after	before	after	before	after	before	after
C=O	530.3–530.5	0.04		0.12		0.07		0.15			
C-O	532.7–533.2	0.96	0.99	0.88	1.00	0.93	0.98	0.85	0.95	1.00	1.00
	537.4–538.6		0.01				0.02		0.05		

To confirm the chemical state of the iodine impregnated in the ACs, I3d high-resolution spectra were recorded. Deconvolution of the I3d spectra revealed that two or four peaks were produced by the impregnated ACs (**Fig. 5-9**). Doublet peaks at 618.8–618.9 and 630.3–630.5eV, which are assigned to $I^- 3d_{5/2}$ and $I^- 3d_{3/2}$ (Han et al., 2019; Zeng et al., 2017; Zhang et al., 2012), respectively, were found for sorbents AC-KI (before adsorption), AC-KI (after), and $AC-KIO_3$ (after), indicating the presence of iodide—possibly KI—in these sorbents.

Doublet peaks at 619.7–620.4 and 631.6–632.4 eV were found for all sorbents except $AC-KIO_3$ (before). These doublet peaks can be ascribed to I_3^- (Zhang et al., 2018) or a carbon-polyiodide compound ($C-I_n^-$) (Barpanda et al., 2007), which might have formed during impregnation and drying. Because the initial precursors contained no I_2, and larger formal polyiodides than I_7^- are unlikely to exist at room temperature (Svensson and Kloo, 2000), the detected chemical state is most likely I_3^-, which can be formed as follows: $I^- + I_2 \rightleftharpoons I_3^-$ (Kralchevska et al., 2016; Thorsmølle et al., 2011). For $AC-NH_4I$ and $AC-KI+CuSO_4$, only doublet peaks representative of I_3^- were found, both before and after the adsorption tests (**Fig. 5-9**). Moreover, both I_3^- and $C-I_n^-$ closely resemble I_2 and are potential I_2 donors (Barpanda et al., 2007), which can enhance the oxidation of Hg^0 (Lee et al., 2004; Li et al., 2009; Z. Liu et al., 2018).

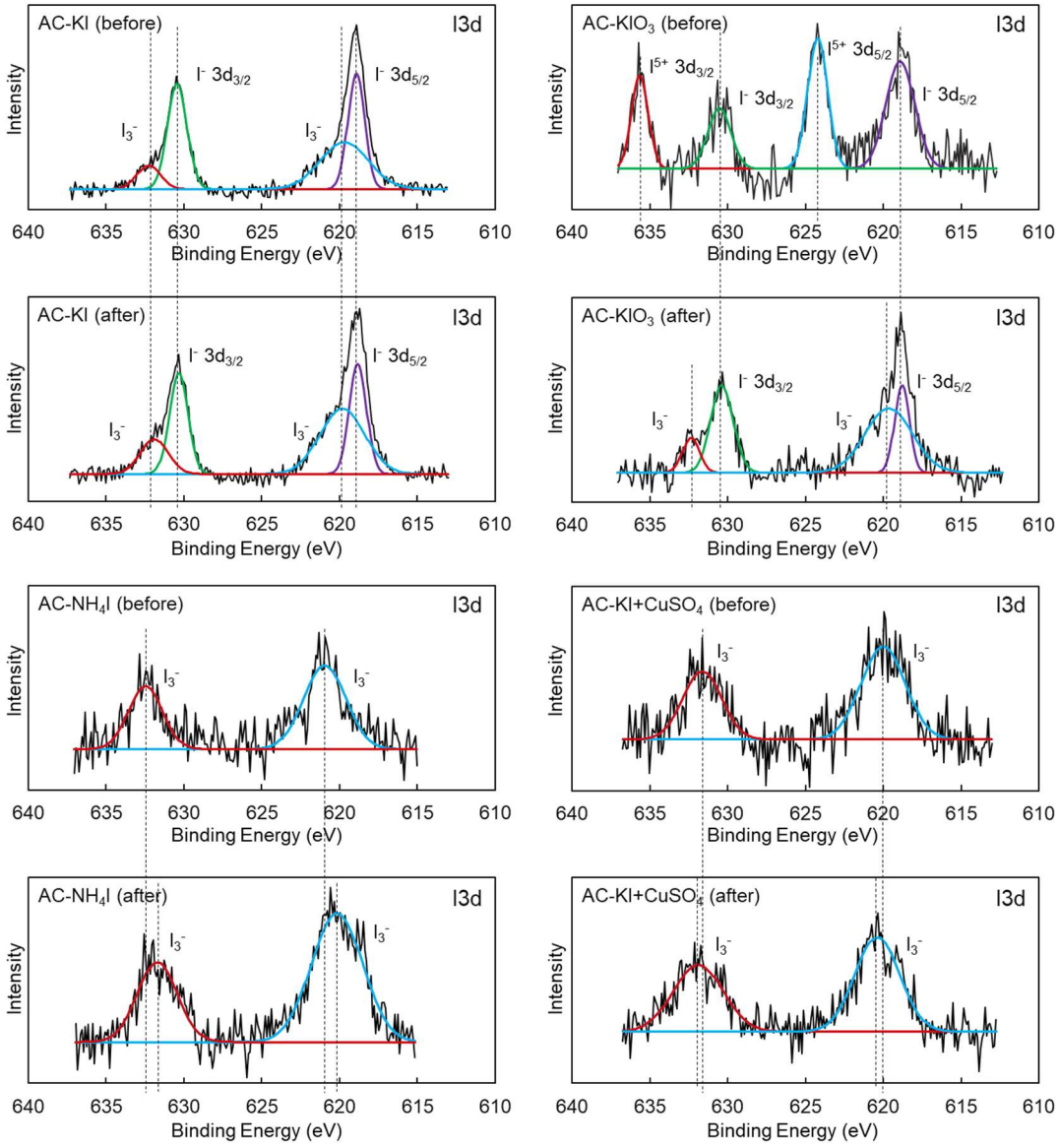

Figure 5-9. XPS high-resolution I3d spectra for iodine impregnated sorbents before and after the adsorption tests.

For the sorbent AC-KIO_3, distinct doublet peaks were found at 624.2 and 635.6 eV. These peaks are assigned to I^{5+} $3d_{5/2}$ and I^{5+} $3d_{3/2}$, indicating that iodate was present on the surface of the AC (Han et al., 2019; Xie et al., 2017). This result demonstrates that I^{5+} and I^- co-existed on the surface of AC-KIO_3 (Xie et al., 2017; Zeng et al., 2017). After adsorption, the peaks associated with I^{5+} $3d_{5/2}$ and I^{5+} $3d_{3/2}$ disappeared, indicating that the iodate on the AC-KIO_3 surface was consumed through interactions with other components. Together with the XRD results, in which the crystalline phase of KIO_3 was also detected after the adsorption test (Section **3.3**), it can be concluded that only KIO_3 on the surface of

AC-KIO_3 was consumed, whereas the KIO_3 inside remained during the adsorption process. Moreover, KI was detected in AC-KIO_3 after adsorption, indicating that it was a reaction product left on the surface of AC-KIO_3 after the processes proposed in **Eq. (2)** and **(3)**.

For all impregnated ACs, no I_2 peaks were detected by XPS. However, the results are not conclusive, as no I_2 was generated in the impregnated ACs. It is possible that I_2 was formed but evaporated into the atmosphere during storage, or that I_2 was not detected by XPS because this modality only analyzes surface chemical states. Thus, the presence or absence of I_2 inside the sorbents should be confirmed using XANES analysis.

5.3.5 XANES analysis

5.3.5.1 Chemical species of iodine in the impregnated ACs

Iodine XANES (I K-edge) analysis was conducted to clarify the chemical species of iodine. **Figure 5-10(a)** and **5-10(b)** show the iodine K-edge XANES spectra for the impregnated ACs. The spectra produced by AC-KI, AC-NH_4I, and AC-KI+$CuSO_4$ were very similar both before and after the adsorption tests. No similarities between the sorbents and their precursors, NH_4I, KI, and CuI, were detected. However, a distinct change in AC-KIO_3 was found after the adsorption test. The sorbent spectra initially had a shape similar to those of KIO_3/$NaIO_3$, and then developed a shape that was intermediate between those of KIO_3/$NaIO_3$ and KI/NaI.

The proportion of each form of iodine was estimated by I K-edge LCF (**Fig. 5-10(c)**); I_2 accounted for approximately 9–16% of all forms of I for AC-KIO_3, AC-NH_4I, and AC-KI+$CuSO_4$ before the adsorption test, which is in agreement with the hypothesis in Section **5.3.4**. Remarkably, the ranking of the I_2 fractions for the iodine-impregnated ACs was consistent with the order of Hg^0 removal efficiency, which was as follows: AC-KI+$CuSO_4$ ≈ AC-NH_4I > AC-KIO_3 > AC-KI. Therefore, I_2 is considered to play an important role in Hg^0 removal by iodine-impregnated ACs (Lee et al., 2004; Li et al., 2009; Z. Liu et al., 2018).

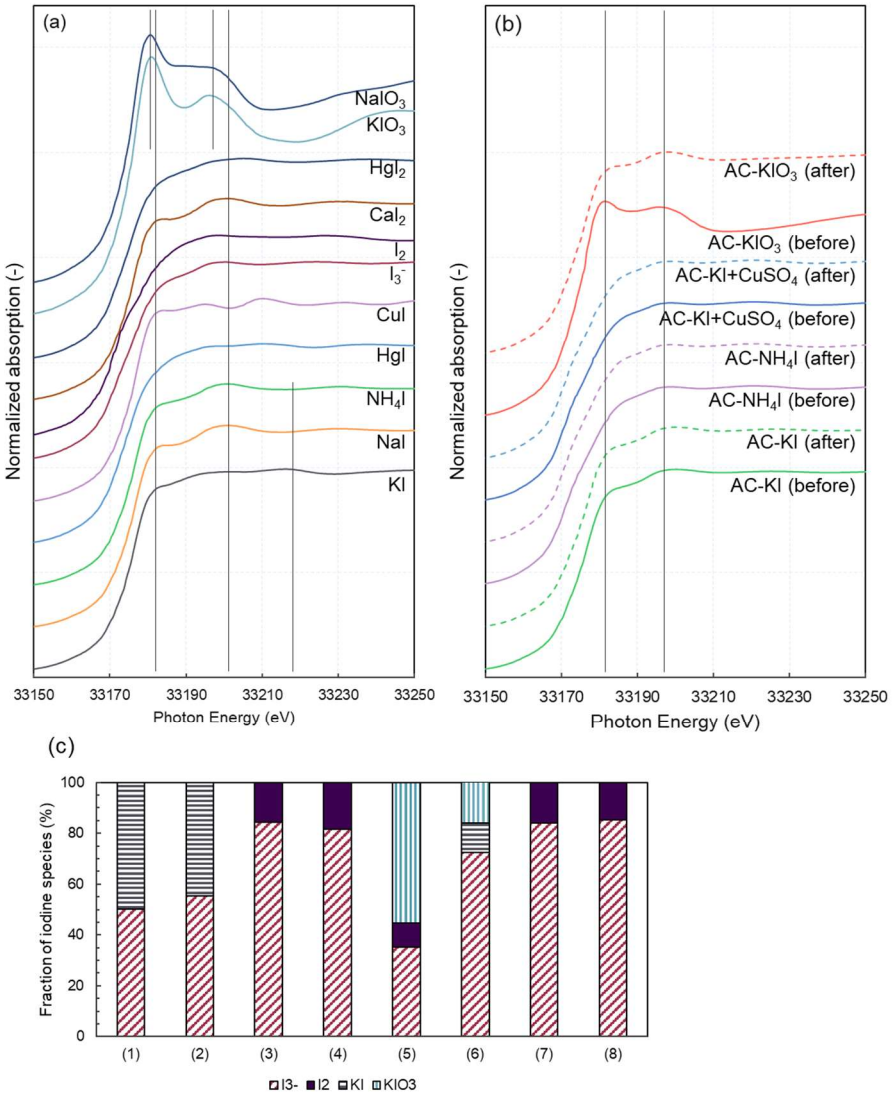

Figure 5-10. Iodine K-edge X-ray absorption near-edge structure (XANES) spectra for (a) solid potassium iodide (KI), solid NaI, solid NH_4I, solid HgI, solid CuI, I_3^- ion, solid I_2, solid CaI_2, solid HgI_2, solid KIO_3, and solid $NaIO_3$; and (b) the impregnated ACs, AC-KI, AC-NH_4I, AC-KIO_3, and AC-KI+$CuSO_4$, before and after the adsorption tests (E0 = 33,172–33,174 eV). (c) The fractions of chemical species of mercury estimated by linear combination fitting (LCF) from iodine K-edge XANES data. (1), AC-KI (before adsorption test); (2), AC-KI (after); (3), AC-NH_4I (before); (4), AC-NH_4I (after); (5), AC-KIO_3 (before); (6), AC-KIO_3 (after); (7), AC-KI+$CuSO_4$ (before); and (8), AC-KI+$CuSO_4$ (after). The range for the LCF is 33,152–33,232 eV.

The formation of I_2 in the impregnated ACs is proposed in **Eq. (6)–(15)**. The formation of I_2 may occur during impregnation, drying, and adsorption. Even though I_2 sublimates at temperatures of more than 113°C, (Li et al., 2009) the pore structure of ACs can adsorb the

iodine vapor during the storage of spent ACs after the adsorption tests due to the decrease in temperature (Zhong et al., 2017).

For AC-KI, it is thermodynamically possible for I_2 to be formed (**Eq. (6)**). However, in this study, no I_2 was detected in AC-KI (**Fig. 5-10(c)**), in contrast to previous predictions (Li et al., 2009; Z. Liu et al., 2018; Tong et al., 2017). For AC-NH_4I, during the impregnation process, NH_4I dissociated and H^+ was released, as shown in **Eq. (7)**. Additionally, **Eq. (8)** can promote the reaction proposed in **Eq. (7)**. As a result, HI was readily formed and adsorbed by the AC (**Eq. (9)**). Then, the HI was oxidized by O; thus, I_2 was formed (**Eq. (10)**).The overall reactions for I_2 generation in AC-NH_4I are summarized in **Eq. (11)**.

For AC-KIO_3, I_2 can be formed according to **Eq. (12)**. The combination of **Eqs. (3)** and **(12)** is shown in **Eqs. (13)** and **(14)**, which are also thermodynamically feasible. For AC-KI+$CuSO_4$, as explained in Section **5.3.3**, **Eq. (4)** can occur quickly, and I_2 was therefore deposited into the pores of AC-KI+$CuSO_4$. Additionally, CuI can also be oxidized by O_2 to generate I_2 (**Eq. (15)**).

For AC-KI

$$4\ KI\ (s) + 3\ O_2\ (g) + 2\ C\ (s) = 2\ K_2CO_3\ (s) + 2\ I_2\ (g) \quad (6)$$

$$\Delta rG^{\ominus}(413\ K) = -772.889\ kJ{\cdot}mol^{-1}$$

For AC-NH_4I

Impregnation process:

$$NH_4^+ + H_2O = NH_3{\cdot}H_2O + H^+ \quad (7)$$

$$NH_3{\cdot}H_2O\ (l) = NH_3\ (g) + H_2O\ (l) \quad (8)$$

$$H^+ + I^- = HI \quad (9)$$

$$4\ HI\ (aq) + O_2\ (g) = 2\ I_2\ (s) + 2\ H_2O\ (l) \quad (10)$$

$$\Delta rG^{\ominus}(298\ K) = -267.99\ kJ{\cdot}mol^{-1}$$

$$4\ NH_4I\ (aq) + O_2\ (g) = 4\ NH_3\ (g) + 2\ I_2\ (s) + 2\ H_2O\ (l) \quad (11)$$

$$\Delta rG^{\ominus}(298\ K) = -16.37\ kJ{\cdot}mol^{-1}$$

For AC-KIO_3

$$4\ KIO_3\ (s) + 5\ C\ (s) = 2\ K_2CO_3\ (s) + 2\ I_2\ (g) + 3\ CO_2\ (g) \quad (12)$$

$$\Delta rG^{\Theta}(413\ K) = -1{,}698.73\ kJ{\cdot}mol^{-1}$$

$$2\ KIO_3\ (s) + 3\ C\ (s) = 2\ KI\ (s) + 3\ CO_2\ (g) \quad (3)$$

$$\Delta rG^{\Theta}(413\ K) = -1{,}054\ kJ{\cdot}mol^{-1}$$

$$KIO_3\ (s) + KI\ (s) + C\ (s) = K_2CO_3\ (s) + I_2\ (g) \quad (13)$$

$$\Delta rG^{\Theta}(413\ K) = -322.365\ kJ{\cdot}mol^{-1}$$

$$3\ KIO_3\ (s) + 4\ C\ (s) = K_2CO_3\ (s) + KI\ (s) + I_2\ (g) + 3\ CO_2\ (g) \quad (14)$$

$$\Delta rG^{\Theta}(413\ K) = -1{,}376.37\ kJ{\cdot}mol^{-1}$$

For AC-KI+$CuSO_4$

$$2\ CuSO_4\ (aq) + 4\ KI\ (aq) = 2\ CuI\ (s) + I_2\ (s) + 2\ K_2SO_4\ (aq) \quad (4)$$

$$2\ CuI\ (s) + O_2\ (s) = 2\ CuO\ (s) + I_2\ (g) \quad (15)$$

$$\Delta rG^{\Theta}(413\ K) = -92.155\ kJ{\cdot}mol^{-1}$$

After the adsorption tests, the fractions of I_2 in AC-NH_4I and AC-KI+$CuSO_4$ remained almost the same, because the amounts of Hg^0 adsorbed by these two ACs were relatively low (almost 100 times lower than the contents of I in these ACs). Thus, the ratios of Hg/I on the surfaces of these ACs were low (**Table 5-7**), and consumption by Hg^0 was not reflected in the LCF results for I. However, an evident decrease in I_2 was found for AC-KIO_3, which might be largely due to the high original Hg/I ratio of approximately 10%.

Table 5-7. Concentrations of Hg and I in each sorbent.

Sorbent	AC-virgin	AC-KI	AC-NH_4I	AC-KIO_3	AC-KI+$CuSO_4$
Hg (mmol/g)	0.0006	0.0011	0.0023	0.0028	0.0023
I (mmol/g)	–	0.47	0.17	0.03	0.2

The LCF results also revealed larger proportions of KI-I_2 (aq) in all impregnated ACs (**Fig. 5-10(c)**). Taken together with the XPS results (**Fig. 5-9**), the form of KI-I_2 (aq) is considered to be I_3^-. Notably, the sorbents with greater Hg^0 removal efficiency, namely AC-KI+$CuSO_4$ and AC-NH_4I, also contained larger fractions of I_3^-. Hence, besides I_2, I_3^-, which may serve as an I_2 donor, could also play an essential role in Hg^0 removal by iodine-impregnated ACs. Moreover, because I_3^- reacts with starch to produce a black-blue color, it is possible that I_3^- was formed and improved Hg^0 removal performance in previous studies (Li et al., 2009; Zhang et al., 2009) that used KI as the impregnation precursor, and applied the starch test for I_2 detection. I_3^- may have formed during impregnation, drying, and adsorption through the following reaction: $I^- + I_2 \rightleftharpoons I_3^-$ (Bexoit et al., 1977; Kralchevska et al., 2016; Thorsmølle et al., 2011). Moreover, the larger proportion of I_3^- found in AC-NH_4I than in AC-KI might have been caused by the higher ion-pair dissociation constant of $NH^{4+}I_3^-$ compared to $K^+I_3^-$ (Milne, 1992).

For AC-KIO_3, the LCF results showed that the proportion of KIO_3 decreased, whereas KI appeared after the adsorption test; this is in agreement with the XRD and XPS results, and also represents evidence of the reactions proposed in **Eq. (2)** and **(3)**.

5.3.5.2 Chemical species of mercury in the spent ACs

Hg L_{III}-edge XANES analysis of sorbents was conducted after the Hg^0 adsorption tests to determine the chemical species of Hg (**Fig. 5-11(a)** and **5-11(b)**). The spectra of HgO (yellow) and HgO (red) exhibited distinct features, i.e., two steep peaks and a valley at ~12,282, 12,298, and 12,306 eV, respectively. However, similar features were not observed across all sorbents. Hence, HgO is likely not the adsorption product in this study. The two references—$HgCl_2$ and $HgSO_4$—produced obvious shoulder peaks at 12,282 eV; this shoulder peak was also produced by AC-virgin, but not by the impregnated ACs. Therefore, $HgCl_2$ and $HgSO_4$ may have been present in AC-virgin but are not considered adsorption products for impregnated ACs.

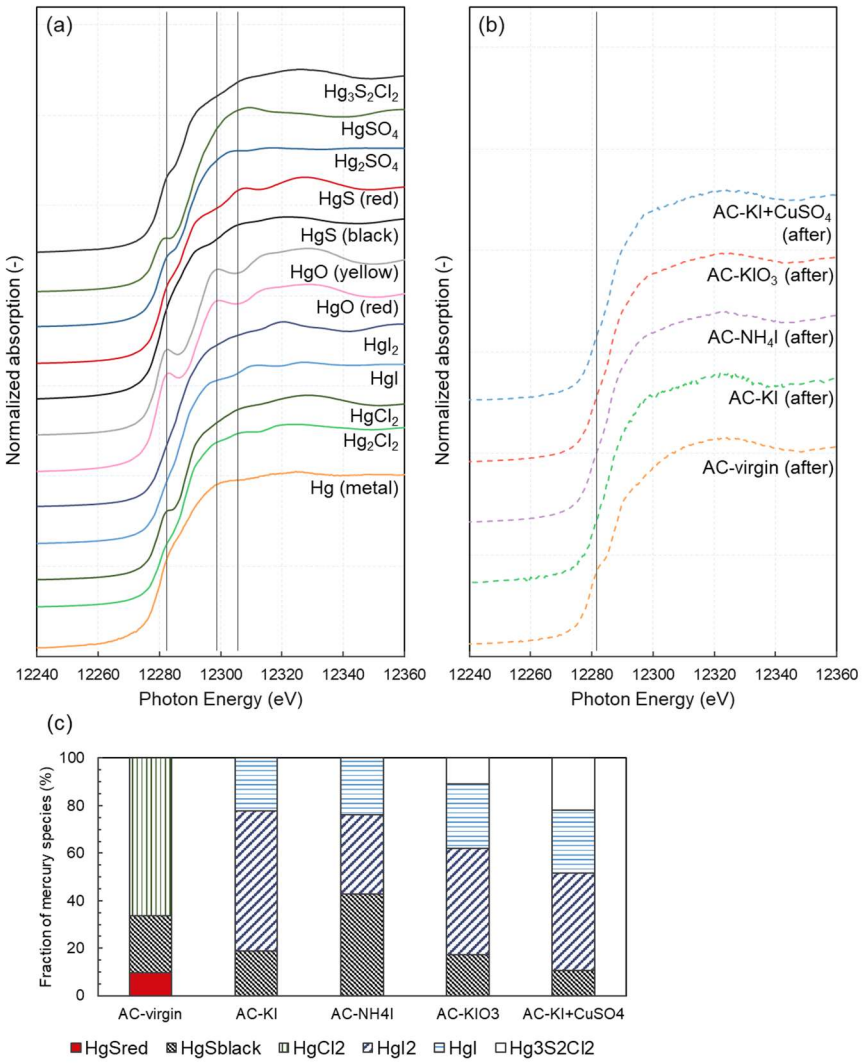

Figure 5-11. Mercury L_{III}-edge XANES spectra for (a) metallic mercury, solid Hg_2Cl_2, solid $HgCl_2$, solid HgI_2, solid HgI, solid HgO (yellow), solid HgS (black), solid $Hg_2S_2Cl_2$, solid Hg_2SO_4, and solid $HgSO_4$; and (b) AC-virgin and impregnated ACs—AC-KI, AC-NH_4I, AC-KIO_3, and AC-KI+$CuSO_4$—both before and after adsorption tests (E0 = 12,284 eV). (c) The fractions of chemical species of mercury estimated via LCF from mercury L_{III}-edge XANES data. The range for the LCF is 12,264–12,344 eV.

The shapes of the spectra for other reference materials and spent ACs are very similar (X. Li et al., 2012); therefore, LCF was conducted after PCA and target transformation to confirm the species and ratios of Hg in the spent sorbents. The LCF results (**Fig. 5-11(c)**) revealed that there was no elemental Hg in any sorbent (Sano et al., 2017), whereas there was a significant fraction of HgS in all sorbents. Besides HgS, the main species of Hg found in AC-virgin was $HgCl_2$. These results indicate that all sorbents, even AC-virgin, adsorbed

Hg^0 via chemisorption. Moreover, the impurities of S and Cl in AC-virgin (**Table 5-2**) also played essential roles in Hg^0 removal by the ACs, which reacted with Hg^0 and fixed Hg in the forms of HgS and $HgCl_2$ (**Fig. 5-11(c)**). Putative pathways for HgS and $HgCl_2$ formation have already been proposed in previous research (Sano et al., 2017), in which O_2 in the carrier gas and C in ACs also participated in the chemisorption process.

The main species of Hg in the impregnated ACs in this study were HgI_2 and HgI, with a higher proportion of HgI_2 than HgI. Possible reactions leading to the formation of HgI and HgI_2 are proposed in **Eqs. (16)–(19)** (Li et al., 2009; Z. Liu et al., 2018; Tong et al., 2017). In impregnated ACs, HgI is more easily formed (**Eq. (16)**) than HgCl due to the lower activation energy barrier (Rungnim et al., 2016). Then, HgI can be further oxidized into HgI_2, as proposed in **Eq. (17)**. HgI_2 can also be formed via the oxidation of Hg^0 by I_2 (**Eq. (18)**) (Li et al., 2009). Furthermore, HgI_2 is more stable than $HgCl_2$ (**Eq.(19)**) (Li et al., 2009), which is in accordance with the result that, rather than $HgCl_2$, HgI_2 dominated in iodine-impregnated ACs. A significant fraction of $Hg_3S_2Cl_2$ was found in AC-KIO_3 and AC-KI+$CuSO_4$, and the proposed pathway explaining this outcome is as follows: α-HgS → α-$Hg_3S_2Cl_2$ → Hg_2Cl_2 (Radepont et al., 2015). Additionally, $Hg_3S_2Cl_2$ might also have formed during storage after the adsorption test.

HgI (Z. Liu et al., 2018):

$$Hg\ (g) + 1/2\ I_2\ (s) = HgI\ (s) \quad (16)$$

$$\Delta rG^{\ominus}(413\ K) = -76.191\ kJ{\cdot}mol^{-1}$$

HgI_2 (Li et al., 2009; Z. Liu et al., 2018):

$$2\ HgI\ (s) + I_2\ (s) = 2\ HgI_2\ (s) \quad (17)$$

$$\Delta rG^{\ominus}(413\ K) = -96.969\ kJ{\cdot}mol^{-1}$$

$$Hg\ (g) + I_2\ (s) = HgI_2\ (s) \quad (18)$$

$$\Delta rG^{\ominus}(413\ K) = -124.676\ kJ{\cdot}mol^{-1}$$

$$HgCl_2\ (s) + 2\ KI\ (s) = HgI_2\ (s) + 2\ KCl\ (s) \quad (19)$$

$$\Delta rG^{\ominus}(413\ K) = -92.77\ kJ{\cdot}mol^{-1}$$

Iodine-impregnated ACs have long been considered excellent sorbents for Hg^0 removal, and the underlying mechanism is widely assumed to be the generation of I_2. However, evidence for the presence of I_2 is limited to the starch test and morphological characterization. In this study, even though XRD and XPS could not be used to observe the crystalline or chemical state of I_2, the XANES analysis successfully demonstrated that I_2 was generated inside the impregnated ACs. Moreover, both the XPS and XANES results revealed the presence of I_3^-, where both I_2 and I_3^- are considered to enhance Hg^0 removal efficiency. Future research should focus on the stability and regeneration of the spent sorbents.

5.4 Summary

In this study, we introduced iodine precursors, which are KI, NH_4I, KIO_3, and KI followed by $CuSO_4$, into the activated carbon by the impregnation supporting method. Adsorption tests were conducted with an up-flow fixed-bed column at 140 °C, using the air as the carrier gas. All sorbents showed excellent removal efficiencies of Hg^0 of 97.2–99.9%. The XANES results show no metal Hg^0 in all sorbents, including the virgin AC, indicating that the chemisorption dominant in the Hg^0 removal by the ACs in this study. Based on the XPS analysis, the C and O in the ACs, as well as the O_2 in the carrier gas, are considered to participate in the chemical reactions responsible for the Hg^0 removal. Besides activated sites such as C=O and C-O, O_2 and I_2/I_3^- promoted the chemisorption significantly. Sorbents of AC-NH_4I and AC-KI+$CuSO_4$ showed extremely high Hg^0 removal efficiencies as 99.9%, with a high inlet concentration as 1,500 $\mu g/m^3$. The extremely high removal efficiencies are by large associated with the high I_3^- and I_2 fractions of iodine impregnated to these sorbents.

References

Ahmad, A., 2011. Phase transition study in a [Cu2HgI4:0.2AgI] mixed composite system doped with K2SO4. Ionics. 2011, 17, 759–766. https://doi.org/10.1007/s11581-011-0608-5

Altenor, S., Carene, B., Emmanuel, E., Lambert, J., Ehrhardt, J.J., Gaspard, S., 2009. Adsorption studies of methylene blue and phenol onto vetiver roots activated carbon prepared by chemical activation. J. Hazard. Mater. 165, 1029–1039. https://doi.org/10.1016/j.jhazmat.2008.10.133

Barpanda, P., Fanchini, G., Amatucci, G.G., 2007. The physical and electrochemical characterization of vapor phase iodated activated carbons. Electrochim. Acta 52, 7136–7147. https://doi.org/10.1016/j.electacta.2007.05.051

Bexoit, L., Wilson, F., Wilson, F., 1977. Studies on the iodidetriiodide equilibrium. Can. J. Chem. 55, 792–797.

Chen, Y., Guo, X., Wu, F., Huang, Y., Yin, Z., 2018. Applied Surface Science Experimental and theoretical studies for the mechanism of mercury oxidation over chlorine and cupric impregnated activated carbon. Appl. Surf. Sci. 458, 790–799. https://doi.org/10.1016/j.apsusc.2018.07.167

Common Data Processing System (COMPRO) (15 January, 2020 accessed) http://www.sasj.jp/COMPRO/

Eichberger, M. and Stieglitz, L., 1994. The influence of different types of activated carbons on the formation of polychlorinated compounds in de-novo-syntheses. Organohalogen Compd. 20, 385–390.

Ghorishi, S.B., Keeney, R.M., Serre, S.D., Gullett, B.K., Jozewicz, W.S., 2002. Development of a Cl-impregnated activated carbon for entrained-flow capture of elemental mercury. Environ. Sci. Technol. 36, 4454–4459. https://doi.org/10.1021/es0255608

Han, S., Um, W., Kim, W.S., 2019. Development of bismuth-functionalized graphene oxide to remove radioactive iodine. Dalt. Trans. 48, 478–485. https://doi.org/10.1039/C8DT03745K

Harijan, D.K.L., Chandra, V., Yoon, T., Kim, K.S., 2018. Radioactive iodine capture and storage from water using magnetite nanoparticles encapsulated in polypyrrole. J. Hazard. Mater. 344, 576–584. https://doi.org/10.1016/j.jhazmat.2017.10.065

Jang, H.N., Back, S.K., Sung, J.H., Jeong, B.M., Kang, Y.S., Lee, C.K., Jurng, J., Seo, Y.C., 2017. Adsorption and kinetics of elemental mercury vapor on activated carbons impregnated with potassium iodide, hydrogen chloride, and sulfur. Korean J. Chem. Eng. 34(3), 806–813.

Kong, F., Qiu, J., Liu, H., Zhao, R., Ai, Z., 2011. Catalytic oxidation of gas-phase elemental

mercury by nano-Fe2O3. J. Environ. Sci. 23, 699–704. https://doi.org/10.1016/S1001-0742(10)60438-X

Kralchevska, R.P., Sharma, V.K., Machala, L., Zboril, R., 2016. Ferrates (FeVI, FeV, and FeIV) oxidation of iodide: Formation of triiodide. Chemosphere 144, 1156–1161.

Krishnan, S.V., Gullett, B.K., Jozewicz, W., 1994. Sorption of elemental mercury by activated carbons. Environ. Sci. Technol. 28(8), 1506–1512.

Lee, S.H., Park, Y.O., 2003. Gas-phase mercury removal by carbon-based sorbents. Fuel Process. Technol. 84, 197–206. https://doi.org/10.1016/S0378-3820(03)00055-9

Lee, S.J., Seo, Y.C., Jurng, J., Lee, T.G., 2004. Removal of gas-phase elemental mercury by iodine- and chlorine-impregnated activated carbons. Atmos. Environ. 38, 4887–4893. https://doi.org/10.1016/j.atmosenv.2004.05.043

Li, L., Liu, E., Li, J., Yang, Y., Shen, H., Huang, Z., Xiang, X., Li, W., 2010. A doped activated carbon prepared from polyaniline for high performance supercapacitors. J. Power Sources 195, 1516–1521. https://doi.org/10.1016/j.jpowsour.2009.09.016

Li, N., Wei, H., Duan, Y., Tang, H., Zhao, S., Hu, P., Ren, S., 2018. Experimental study on mercury adsorption and adsorbent regeneration of sulfur-loaded activated carbon. Energy and Fuels 32(10), 11023–11029.

Li, X., Lee, J., Heald, S., 2012. XAFS characterization of mercury captured on cupric chloride-impregnated sorbents. Fuel 93, 618–624. https://doi.org/10.1016/j.fuel.2011.11.013

Li, Y., Daukoru, M., Suriyawong, A., Biswas, P., 2009. Mercury emissions control in coal combustion systems using potassium iodide: Bench-scale and pilot-scale studies. Energy and Fuels 23, 236–243. https://doi.org/10.1021/ef800656v

Li, Y.H., Lee, C.W., Gullett, B.K., 2003. Importance of activated carbon's oxygen surface functional groups on elemental mercury adsorption. Fuel 82, 451–457. https://doi.org/10.1016/S0016-2361(02)00307-1

Li, Y.H., Lee, C.W., Gullett, B.K., 2002. The effect of activated carbon surface moisture on low temperature mercury adsorption. Carbon 40(1), 65–72.

Li, Z., Yu, H., Bian, T., Zhao, Y., Zhou, C., Shang, L., Liu, Y., Wu, L.Z., Tung, C.H., Zhang, T., 2015. Highly luminescent nitrogen-doped carbon quantum dots as effective fluorescent probes for mercuric and iodide ions. J. Mater. Chem. C 3, 1922–1928. https://doi.org/10.1039/c4tc02756f

Liu, X.Y., Huang, M., Ma, H.L., Zhang, Z.Q., Gao, J.M., Zhu, Y.L., Han, X.J., Guo, X.Y., 2010. Preparation of a carbon-based solid acid catalyst by sulfonating activated carbon in a chemical reduction process. Molecules 15, 7188–7196. https://doi.org/10.3390/molecules15107188

Liu, Z., Yang, W., Xu, W., Liu, Y., 2018. Removal of elemental mercury by bio-chars derived from seaweed impregnated with potassium iodine. Chem. Eng. J. 339, 468–

478. https://doi.org/10.1016/j.cej.2018.01.148

Milne, J., 1992. A Raman spectroscopic study of the effect of ion-pairing on the structure of the triiodide and tribromide ions. Spectrochim Acta A 48, 533-542.

Nishimura K., Takaoka, M., Takeda, N., 2004. Effect of chemical properties of carbon on de novo synthesis of PCDD/PCDF, in: Proceedings of the Annual Conference of the Japan Society of Waste Management Experts, 901–903 (in Japanese).

Okamura, M., Takagaki, A., Toda, M., Kondo, J.N., Domen, K., Tatsumi, T., Hara, M., Hayashi, S., 2006. Acid-catalyzed reactions on flexible polycyclic aromatic carbon in amorphous carbon. Chem. Mater. 18, 3039–3045. https://doi.org/10.1021/cm0605623

Radepont, M., Coquinot, Y., Janssens, K., Ezrati, J.J., De Nolf, W., Cotte, M., 2015. Thermodynamic and experimental study of the degradation of the red pigment mercury sulfide. J. Anal. At. Spectrom. 30, 599–612. https://doi.org/10.1039/c4ja00372a

Ravel B., Newville M., 2015. ATHENA, ARTEMIS, HEPHAESTUS: data analysis for X-ray absorption spectroscopy using IFEFFIT. J. Synchrotron Rad. 12, 537–541 doi:10.1107/S0909049505012719

Rungnim, C., Promarak, V., Hannongbua, S., Kungwan, N., Namuangruk, S., 2016. Complete reaction mechanisms of mercury oxidation on halogenated activated carbon. J. Hazard. Mater. 310, 253–260. https://doi.org/10.1016/j.jhazmat.2016.02.033

Saha, A., Abram, D.N., Kuhl, K.P., Paradis, J., Crawford, J.L., Sasmaz, E., Chang, R., Jaramillo, T.F, Wilcox, J., 2013. An X-ray photoelectron spectroscopy study of surface changes on brominated and sulfur-treated activated carbon sorbents during mercury capture: performance of pellet versus fiber sorbents. Environ. Sci. Technol. 47(23), 13695-13701.

Sano, A., Takaoka, M., Shiota, K., 2017. Vapor-phase elemental mercury adsorption by activated carbon co-impregnated with sulfur and chlorine. Chem. Eng. J. 315, 598–607. https://doi.org/10.1016/j.cej.2017.01.035

Shaffer, P.A., Hartmann, A.F., 1921. The iodometric determination of copper and its use in sugar analysis. Jour. Biol. Chem 45, 349-390.

Shao, H., Liu, X., Zhou, Z., Zhao, B., Chen, Z., Xu, M., 2016. Elemental mercury removal using a novel KI modified bentonite supported by starch sorbent. Chem. Eng. J. 291, 306–316. https://doi.org/10.1016/j.cej.2016.01.090

Shimamoto, Y.S., Takahashi, Y., 2008. Superiority of K-edge XANES over L III-edge XANES in the Speciation of Iodine in Natural Soils. Analytical Sciences 24, 405–409.

Sun, P., Zhang, B., Zeng, X., Luo, G., Li, X., Yao, H., Zheng, C., 2017. Deep study on effects of activated carbon ' s oxygen functional groups for elemental mercury adsorption using temperature programmed desorption method. Fuel 200, 100–106. https://doi.org/10.1016/j.fuel.2017.03.031

Suresh Kumar Reddy, K., Al Shoaibi, A., Srinivasakannan, C., 2014. Elemental mercury adsorption on sulfur-impregnated porous carbon-A review. Environ. Technol. (United Kingdom) 35, 18–26. https://doi.org/10.1080/21622515.2013.804589

Svensson, P.H.; Kloo, L., 2000. A vibrational spectroscopic, structural and quantum chemical study of the triiodide ion. J. Chem. Soc., Dalton Trans. 14, 2449–2455.

Thorsmølle, V.K., Rothenberger, G., Topgaard, D., Brauer, J.C., Kuang, D.B., Zakeeruddin, S.M., Lindman, B., Grätzel, M., Moser, J.E., 2011. Extraordinarily Efficient Conduction in a Redox-Active Ionic Liquid. ChemPhysChem, 12(1), 145–149.

Tong, L., Yue, T., Zuo, P., Zhang, X., Wang, C., Gao, J., Wang, K., 2017. Effect of characteristics of KI-impregnated activated carbon and flue gas components on Hg 0 removal. Fuel 197, 1–7. https://doi.org/10.1016/j.fuel.2016.12.083

UN environment programme, Minamata Convention on mercury. (Accessed on 26 December 2019) http://www.mercuryconvention.org/Convention/Text/tabid/3426/language/en-US/Default.aspx

Van Stipdonk, M.J., Santiago, V., Schweikert, E.A., Chusuei, C.C., Goodman, D.W., 2000. Secondary ion emission from keV energy atomic and polyatomic projectile impacts on sodium iodate. Int. J. Mass Spectrom. 197, 149–161. https://doi.org/10.1016/s1387-3806(99)00255-9

Vidic, R. D., Siler, D. P., 2001. Vapor-phase elemental mercury adsorption by activated carbon impregnated with chloride and chelating agents. Carbon 39, 3–14.

Wu, J., Zhao, Z., Huang, T., Sheng, P., Zhang, J., Tian, H., Zhao, X., Zhao, L., He, P., Ren, J., Gao, K., 2017. Removal of elemental mercury by Ce-Mn co-modi fi ed activated carbon catalyst. Catal. Commun. 93, 62–66. https://doi.org/10.1016/j.catcom.2017.01.016

Xie, J., Cao, Y., Jia, D., Li, Y., Wang, K., Xu, H., 2017. In situ solid-state fabrication of hybrid AgCl/AgI/AgIO 3 with improved UV-to-visible photocatalytic performance. Sci. Rep. 7, 1–11. https://doi.org/10.1038/s41598-017-12625-8

Yang, H., Xu, Z., Fan, M., Bland, A.E., Judkins, R.R., 2007. Adsorbents for capturing mercury in coal-fired boiler flue gas. J. Hazard. Mater. 146, 1–11. https://doi.org/10.1016/j.jhazmat.2007.04.113

Zeng, C., Huang, H., Dong, F., Ye, L., Zhang, T., Zhang, Y., Guo, Y., Liu, C., Hu, Y., 2017. Dual redox couples Ag/Ag+ and I−/(IO3)− self-sacrificed transformation for realizing multiplex hierarchical architectures with universally powerful photocatalytic performance. Appl. Catal. B Environ. 200, 620–632. https://doi.org/10.1016/j.apcatb.2016.07.029

Zhang, A., Xiang, J., Sun, L., Hu, S., Li, P., Shi, J., Fu, P., Su, S., 2009. Preparation, characterization, and application of modified chitosan sorbents for elemental mercury

removal. Ind. Eng. Chem. Res. 48, 4980–4989. https://doi.org/10.1021/ie9000629

Zhang, B., Xu, P., Qiu, Y., Yu, Q., Ma, J., Wu, H., Luo, G., Xu, M., Yao, H., 2015. Increasing oxygen functional groups of activated carbon with non-thermal plasma to enhance mercury removal efficiency for flue gases. Chem. Eng. J. 263, 1–8. https://doi.org/10.1016/j.cej.2014.10.090

Zeng, H., Jin, F., Guo, J., 2004. Removal of elemental mercury from coal combustion flue gas by chloride-impregnated activated carbon. Fuel 83(1), 143–146.

Zhang, J., Xing, A., Jia, B., Liu, X., 2018. Synthesis of conductive polyaniline nanofibers in one step by protonic acid and iodine doping. High Perform. Polym. https://doi.org/10.1177/0954008318806979

Zhang, Q., Gao, T., Andino, J.M. and Li, Y., 2012. Copper and iodine co-modified TiO2 nanoparticles for improved activity of CO2 photoreduction with water vapor. Appl. Catal., B 123, 257–264.

Zhong, L., Li, W., Zhang, Y., Norris, P., Cao, Y., Pan, W., 2017. Kinetic studies of mercury adsorption in activated carbon modified by iodine steam vapor deposition method. Fuel 188, 343–351. https://doi.org/10.1016/j.fuel.2016.10.048

Zhou, Q., Duan, Y., Hong, Y., Zhu, C., She, M., Zhang, J., Wei, H., 2015. Experimental and kinetic studies of gas-phase mercury adsorption by raw and bromine modi fi ed activated carbon. Fuel Process. Technol. 134, 325–332. https://doi.org/10.1016/j.fuproc.2014.12.052

Chapter 6 Conclusions and future perspectives

6.1 Conclusions

This dissertation surveys the behavior of elements, especially heavy metals such as Hg, during the SS thermal treatment process. The contents of this dissertation are summarized as follows:

Chapter 1

The first chapter is a general introduction to this dissertation. This chapter firstly surveyed the status of the SS generation in Japan and introduced conventional SS treatment and disposal methods. Since the thermal treatment methods are more widely used in Japan, further literature review on the SS incineration and carbonization was conducted. After that, gaseous Hg removal technologies were introduced to solve the Hg emission problem arise in SS thermal treatment. At last, the objectives and structure of this dissertation were explained.

Chapter 2

In the SS incineration process, after combustion, elements in SS are distributed in different streams as ash, wastewater, and flue gas. The concentration of elements in each stream is associated with their final recycling and disposal. In order to provide such elemental concentrations in SS incineration, a WWTP that has both the step grate stoker and fluidized bed incinerators located in western Japan was selected and monitored. Results show that, after combustion, concentrations of most elements were elevated to ~5-fold in the ISSA (e.g., P, K), some soluble elements accumulated in the recycling water (e.g., Na), and only Hg showed detectible concentrations in the flue gas. Moreover, different enrichment tendencies of heavy metals were found between the GS and F-types: the GS discharged the main ashes (bottom ash and riddling ash) with lower concentrations of heavy metals than the dust generated at the APCDs in GS, as well as the fly ash discharged in the

F-types.

Chapter 3

In order to clarify the different behavior of elements in each stream (especially the ISSA) that caused by the incinerator types, a comprehensive comparison of the distribution and mass balance of elements across the GS and F-types were conducted. Enrichment factor (E_f) was defined to evaluate the enrichment behavior of elements in the various ISSA, and mass fraction and recovery rate was defined to discuss the contribution of each stream in the mass balance. All target elements were classified into three groups as the non-volatile (Al, P, Ca, Fe, Mg, K, Mn, Cu, Na, Cr, and Ni), semi-volatile (Zn, Pb, Ag, As, and Cd), and volatile (S and Hg), for further discussion. Moreover, Thermodynamic calculations were also introduced to the discussion and explanation in this chapter.

Experimental results demonstrated higher E_f for semi-volatile elements in the boiler and multi-cyclone dust than the bottom and riddling ashes in GS, while similar enrichment of these semi-volatiles to non-volatiles was found in ashes from F-types. The distinct ash removal procedures may be the reason for this different enrichment behavior between GS and F-types: GS discharges the bottom and riddling ashes at the bottom of the incinerator at 850 °C and only generates a very small fraction (~0.3%) of boiler and multi-cyclone dust at APCDs at ~250 °C; F-types remove all particulate matters at the bag or ceramic filters and generate only fly ash at ~250 °C. Thermodynamic calculations indicated gaseous combustion components for Pb, Ag, As, and Cd at 850 °C, but the dominant phase of the combustion components shifted to the solid at 250 °C due to the secondary reactions among combustion components. Thus, the experimental results and thermodynamic calculations revealed that the GS can, to some extent, separates semi-volatile elements from the main ash.

Mass balance results showed good closures for most elements. The significant accumulation of Na was found in recycling water, and S and Hg were also discharged primarily in the wastewater in all incinerators. Significant emissions from the flue gas were

only found for Hg.

At last, the possibility of the recycling of the ISSA as fertilizer was discussed. The GS has an advantage over the F-types in terms of the recycling of the ISSA because it discharges a large amount of bottom and riddling ashes with lower concentrations of heavy metals.

Chapter 4

In order to clarify the Hg emission profiles in SS thermal treatment process, besides GS, FB, and FC, another fluidized bed incinerator (FD) and a carbonization furnace (C-F) were monitored with speciation continuous Hg emission monitors (Hg-CEM). Tests on the adsorptive removal of Hg^0 by commercial sorbents in carbonization was also conducted.

Results showed different dominant species of Hg in the SS thermal treatment process. In the incineration, Hg^{2+} is the dominant species in the flue gas before WS, but after the WS, the fraction of Hg^0 increased in the flue gas. In the carbonization, however, Hg^0 was always dominantly existed in the flue gas, both before and after the WS. These tendencies were consistent with the thermodynamic results for the Hg species in the flue gas in incineration and carbonization, respectively.

Commercial sorbents were effective in Hg^0 removal. The MAC showed higher removal efficiency than the polymer, but more problems were found in the operation and maintenance.

Chapter 5

This chapter further investigated the adsorptive removal of Hg^0 using iodine-impregnated AC. The purposes of this chapter are to develop high-performance iodine-impregnated ACs with precursors other than KI and to investigate the mechnisms for Hg^0 adsorption by prepared ACs. Different measurement methods, including BET specific surface area analysis, XRD, XPS, and XANES, were used to confirm the texture characteristics of the ACs, as well as the species and chemical state of the compounds

impregnated in and adsorbed on the ACs. Based on these experimental results, putative pathways for Hg^0 removal by the prepared ACs were proposed and evaluated according to the Gibbs free energy value.

Adsorption tests showed higher Hg^0 removal efficiencies by the iodine-impregnated ACs than the virgin one. Since the impregnated ACs had smaller BET specific surface area, the chemisorption dominant in the Hg^0 by the impregnated ACs. From XRD and XPS results, we made the hypothesis that the C in AC also participated in reactions during the adsorption, and CO_2 may be one of the reaction products. Both the XPS and XANES identified the triiodide (I_3^-) in impregnated ACs, and the XANES also identified I_2. Moreover, both the ranking of the I_2 and I_3^- fractions for the iodine-impregnated ACs was consistent with the order of Hg^0 removal efficiency.

Since the dominant species of Hg in impregnated ACs after adsorption was HgI_2, I_2 is considered the mechanism for Hg^0 removal through the reaction: $Hg\ (g) + I_2\ (s) = HgI_2\ (s)$. I_3^- plays an important role in the Hg^0 removal as the I_2 donor: $I_3^- \rightleftharpoons I^- + I_2$.

6.2 Future perspectives

The behavior and control of mercury in the sewage sludge thermal treatment process were discussed in this study. Further studies are proposed as follows:

(1) This study revealed the Hg emission in SS thermal treatment process as mono-incineration and carbonization. In mono-incineration, the APCDs, especially the WS, can remove Hg^{2+} effectively. However, Hg^0 often escaped due to its low solubility, and re-emission of Hg^0 may occur at the WS. In carbonization, Hg^0 was also dominant in the flue gas. Therefore, further studies on the Hg removal in SS thermal treatment is necessary, and the Hg control in flue gas should pay more attention to the Hg^0 removal technologies.

(2) Wastewater from WS was the primary sink for soluble elements, e.g., Hg, Na, and S, in

SS mono-incineration. Since this wastewater is usually sent back to the wastewater treatment process, rather than immobilized, soluble elements are actually diluted and kept circulating and accumulating in the WWTPs. However, the potential risk that the accumulation would pose to the incineration process and natural waters after the discharge remains unclear. Therefore, investigations on such problems should also be taken into consideration, and further studies on the separate treatment of wastewater from WS is recommended.

(3) Since the ISSA is a less significant sink for Hg, two Hg control strategies in SS thermal treatment process can be proposed by focusing on the wastewater and flue gas: 1. Use the existing WS adopted at the incinerators to remove the Hg^{2+} from the flue gas, and further treat the dissolved Hg^{2+} in the wastewater from WS separately. Then, remove the Hg^0 in the flue gas with a sorbent tower; 2. Make use of the re-emission at WS to transfer Hg^{2+} to Hg^0, then treat Hg^0 with sorbents.

(4) The comprehensive investigation of the two main types of sewage sludge mono-incinerators revealed that step grate stoker is more feasible for sewage sludge combustion in terms of recycling of the ISSA. Based on these results, further studies on the utilizing of the ISSA, especially for the nutrients, e.g., P recovery, are recommended.

(5) This study reveals that iodine impregnated ACs can remove Hg^0 effectively. However, due to the short duration, the adsorption capacities of prepared ACs were not obtained. Additional adsorption tests until the breakthrough point should be accomplished to evaluate the performance of the prepared sorbents comprehensively.

(6) Due to the high cost of the AC, the regeneration of the spent ACs is recommended. Proper methods for the regeneration of the spent ACs should be discussed based on the results from this study, for which Hg^0 is chemisorbed by the iodine impregnated ACs. At last, the saturated ACs are hazardous waste that needs proper stabilization and disposal. Technologies for the final disposal of these ACs also need further study.